On ikaite crystallization

Dissertation zur Erlangung des Doktorgrades
an der Fakultät für Geowissenschaften
der Ludwig-Maximilians-Universität München

vorgelegt von

Samuel Benedikt Strohm

München, 21. Januar 2025

Erstgutachter: Prof. Dr. Guntram Jordan

Zweitgutachterin: Prof. Dr. Elena V. Sturm

Tag der mündlichen Prüfung: 24. Juni 2025

Contents

Preface

First and foremost, I would like to sincerely thank those who made the realization of my scientific work possible. It was a real pleasure to work with so many courteous and dedicated people over the past few years.

I want to thank my supervisor, Prof. Dr. Guntram Jordan, for giving me the opportunity to be part of this research project. I am extremely grateful for his enduring support and excellent guidance throughout the last years. It was a great pleasure to work with him as a PhD student. *Lieber Guntram, vielen herzlichen Dank!*

A special thanks to Prof. Dr. Elena Sturm for her willingness to conduct a second review for this work.

Furthermore, I am grateful for the outstanding cooperation with Dr. Giuseppe Saldi and PD Dr. Vasileios Mavromatis at Géosciences Environnement Toulouse. The fruitful exchange contributed substantially to the present research work. Many thanks!

A special thanks to Sebastian Inckemann, Kun Gao, Sebastian Berghofer and Juliane Buhl for their valuable assistance with lab work. Many thanks to Christian Kaiser, Dr. Marie-Louise Lemloh and PD Dr. Michael Schweikert for providing cryo scanning electron microscopy analyses.

Likewise, I am grateful to my colleagues at the Sektion Kristallographie and the Mineralogische Staatssammlung for the pleasant atmosphere and the excellent collaboration. Special thanks to Prof. Dr. Wolfgang Schmahl and Prof. Dr. Sandro Jahn for the support of my research work.

Furthermore, I would also like to thank the Deutsche Forschungsgemeinschaft DFG (JO301/6-1,2) and the Deutsche Akademische Austauschdienst DAAD (Projekt-ID: 57560933) for their financial support.

Lastly, I want to express my deep gratitude to my family and friends for their continued support and encouragement. *Von ganzem Herzen: Danke!*

Abstract

The crystallization of ikaite ($CaCO_3 \cdot 6H_2O$) instead of less soluble calcium carbonate polymorphs has important implications for formation pathways of calcium carbonate minerals, carbon dynamics in polar regions of Earth or paleoclimatic reconstructions. However, the crystallization of ikaite is far from fully understood. Although several conditions that promote the formation of ikaite have been identified, the occurrence of ikaite remains unclear, as fundamental kinetic aspects of the crystallization of ikaite remain largely unexplored to date. In order to contribute to a better understanding of the occurrence of ikaite, this doctoral thesis investigated the crystallization of ikaite by unraveling key aspects of nucleation, growth and persistence using experimental approaches.

As mineral surfaces are potentially effective for heterogeneous nucleation, the formation of ikaite was investigated in the presence of quartz and mica substrates at 0 °C. The study showed that mineral surfaces are an important formation parameter, which can promote the nucleation of ikaite: At supersaturations with respect to ikaite $\Omega_{ikaite} \geq 15$, ikaite was formed irrespective of the presence of these mineral substrates. At $\Omega_{ikaite} < 15$, in contrast, ikaite precipitated only in the presence of the mineral substrates, while precipitation experiments in absence of these surfaces revealed the formation of the anhydrous $CaCO_3$ minerals vaterite and calcite. Thus, the promotion of ikaite nucleation by quartz and mica prevented competing precipitation of anhydrous $CaCO_3$ minerals and led to ikaite formation within a supersaturation range, which was much wider than under pseudohomogeneous conditions.

Furthermore, induction periods measured in both supersaturation regimes enabled the determination of the interfacial energy of ikaite nucleation. Using classical nucleation theory, the interpretation of induction periods from ikaite-forming precipitation experiments ($\Omega_{ikaite} \geq 8$) yielded an effective interfacial energy of nuclei of 15 ± 3 mJ/m². This interfacial energy of ikaite nuclei is significantly lower than values reported for anhydrous $CaCO_3$ phases and, therefore, may support the hypothesis of a low energy formation pathway of ikaite via an ordering of aqueous ion pair complexes without extensive dehydration. Moreover, such a formation mechanism is corroborated by the results of the study of ikaite growth kinetics in phosphate containing solutions at 1 °C. Applying the empirical equation $R = k(\Omega - 1)^n$, measured growth rates yielded a rate constant k = 0.10 ± 0.03 µmol/m²/s and a reaction order n = 0.8 ± 0.3. This reaction order implies a transport- or adsorption-controlled growth mechanism which supports the formation of ikaite involving the assemblage of aqueous ion pair complexes.

Apart from this finding, the experimental growth rates of ikaite provided no sign that ikaite growth is retarded by the presence of phosphate. A potential depletion of aqueous phosphate due to incorporation into ikaite was not detected. Thus, it must be assumed that carbonate anions in ikaite are not substantially substituted by phosphate, which supports the key role of phosphate as an inhibitor of anhydrous $CaCO_3$ mineralization and as a powerful promotor of ikaite formation.

Without such an inactivation of anhydrous $CaCO_3$ mineralization, the occurrence of ikaite was generally transient in precipitation experiments at different solution temperatures (0–20 °C). The persistence of ikaite decreased from 28 h at 0 °C to less than 4 min at 20 °C due to concomitant nucleation of less soluble vaterite and calcite. This concomitant multiphase nucleation indicated a limited applicability of Ostwald's rule of stages. Applying classical nucleation theory, an adequate fit of nucleation rates was obtained for T = 0 °C with a kinetic pre-factor A of ikaite being at least 3 orders of magnitude larger than A of vaterite and calcite. Such a kinetic advantage of ikaite potentially originates from the specific nucleation mechanism without dehydration.

Furthermore, the ephemeral occurrence of ikaite between 0 and 20 °C supports that nucleation of ikaite is not limited to near-freezing environments per se. However, low temperatures are important for a prolonged persistence of ikaite. In order to ensure the persistence of ikaite, an inactivation of competing precipitation, for example by inhibitors, might be indispensable. An inhibition ensuring persistence of ikaite, though, most likely becomes more complex to achieve with temperature.

In summary, the studies showed that the fundamental crystallization kinetics of ikaite differs significantly from anhydrous $CaCO_3$ minerals. The specific formation mechanism of ikaite involving the assemblage of aqueous ion pair complexes might be essential for the crystallization. The investigations also revealed that mineral surfaces have a substantial effect on ikaite formation and play a more important role for the nucleation of ikaite in manifold environments of Earth than previously assumed. Furthermore, the relation between temperature and ephemerality of ikaite was shown for the first time in detail. The observed ephemerality indicated that the extent of ikaite persistence decreases significantly with temperature. Therefore, pseudomorphs after ikaite (*glendonites*) very likely may serve as reliable proxies of low temperatures in most cases.

1 Introduction

1.1 Calcium carbonate crystallization

Crystallization of calcium carbonate ($CaCO_3$) minerals is a ubiquitous process. Huge amounts of $CaCO_3$ minerals crystallize from abundant biotic and abiotic sources in manifold environments of Earth. Particularly the extensive precipitation in sea water has led to a massive occurrence of $CaCO_3$ minerals on the Earth's surface (Morse et al., 2007). This omnipresence of $CaCO_3$ minerals has a tremendous impact on chemistry of marine systems due to large-scale mineral-fluid interactions (Morse et al., 2007). In this regard, calcium carbonate crystallization, in combination with weathering, contributes to a substantial carbon exchange, which is considered as an important part of the ocean ecosystem and, moreover, of the global carbon cycle (Millero, 2013; Ridgwell and Zeebe, 2005). Therefore, important implications for the ocean ecosystem can be derived from the response of $CaCO_3$ minerals to changes in the marine carbonate system, such as the increased uptake of atmospheric CO_2 due to rising anthropogenic emissions (e.g. Caldeira and Wickett, 2003; Doney et al., 2009; Guinotte and Fabry, 2008).

Furthermore, the crystallization of $CaCO_3$ minerals is a key concern in various industrial applications. The deposition of calcium carbonate minerals often appears as an undesirable process (*scale formation*) that causes technical and costly harms (MacAdam and Parsons, 2004). Thus, the inhibition of the mineralization of calcium carbonate is an important operational challenge in a wide range of industrial applications such as oil and gas production (Kamal et al., 2018) or water heating and cooling systems (Karabelas, 2002; Kavitha et al., 2011). Conversely, the occurrence of calcium carbonate minerals also provides important technical and economic benefits. In manufacturing, readily available calcium carbonates are used as a feedstock for a variety of purposes. These purposes include the extensive use as a raw material for the production of construction materials (Jimoh et al., 2018) or the application as fillers in plastics, paints, ceramics, pharmaceutics, etc. (Brečević and Kralj, 2007).

The great ecological and societal relevance of the formation of calcium carbonate minerals has led to a considerable interest in their multifaceted crystallization processes. Although thermodynamic considerations provide distinct stability conditions of the limited number of known calcium carbonate minerals (e.g. Chaka, 2018; Marland, 1975), the highly complex crystallization kinetics causes a broad distribution of the actual occurrence depending on the formation environment (Morse et al., 2007). Hence, a fundamental understanding of the kinetics of the crystallization is essential to predict the appearance of different $CaCO_3$ minerals and to improve models of complex natural and applied systems that involve the mineralization of calcium carbonate.

1.2 The highly hydrous calcium carbonate mineral ikaite

To date, six different forms of calcium carbonate crystals are known (Zou et al., 2019). These include the three anhydrous $CaCO_3$ polymorphs calcite, aragonite and vaterite and the three hydrous forms hemihydrate ($CaCO_3 \cdot ½H_2O$), monohydrocalcite ($CaCO_3 \cdot 1H_2O$) and ikaite ($CaCO_3 \cdot 6H_2O$) (Zou et al., 2019). Furthermore, solid calcium carbonate appears as an amorphous phase (amorphous calcium carbonate, ACC), which most likely involves different identities due to the incorporation of varying amounts of water (e.g. Addadi et al., 2003; Cartwright et al., 2012; Lázár et al., 2023; Zou et al., 2018).

Among these calcium carbonate phases, the mineral ikaite stands out due to its highly hydrous nature. The occurrence of ikaite is less frequent relative to abundant anhydrous $CaCO_3$ polymorphs. Furthermore, the crystallization of ikaite generally leads to a fragile metastable phase at the Earth's surface (Marland, 1975). Nevertheless, substantial amounts of ikaite occur in low temperature environments of Earth ($T \leq 9$ °C) and provide a significant impact on ecological systems (e.g. Geilfus et al., 2016; Huggett et al., 2005; Stockmann et al., 2022). For instance, the formation and dissolution of ikaite in (near-)freezing environments has important implications for the polar carbon cycle (e.g. Delille et al., 2014; Dieckmann et al., 2010; Geilfus et al., 2013; Geilfus et al., 2016; Jones et al., 2023a, 2023b; Rysgaard et al., 2012, 2013, 2014): The precipitation of ikaite from sea ice brines may induce seasonal partitioning of alkalinity and thus contributes to polar carbon dynamics in surface oceanic water (Dieckmann et al., 2008; Jones et al., 2023b; Rysgaard et al., 2007). Moreover, the appearance and disappearance of ikaite in sea ice might also contribute to CO_2 fluxes at the air-ice and the ice-water interface (Dieckmann et al., 2008; Fransson et al., 2011; Jones et al., 2023b; Rysgaard et al., 2007). In this context, model calculations suggested that these CO_2 fluxes potentially may be an effective sea-ice driven carbon pump that might be capable of sequestering CO_2 to the ocean (Rysgaard et al., 2007).

In addition to carbon dynamics, nutrient dynamics in polar surface oceanic water might be associated with the formation of ikaite in sea ice. The growth of ikaite within sea ice might lead to a significant depletion of aqueous phosphate due to incorporation, which may support the enrichment of phosphate in sea ice relative to surface oceanic water (Hu et al., 2014; Jones et al., 2023b). Such a contribution could provide an important abiotic process for seasonal nutrient cycling in polar regions of Earth that complements the impact on polar nutrient dynamics by microbial activity (Jones et al., 2023b).

Apart from these dynamics, ikaite has been considered as an important transient intermediate or precursor phase for the crystallization of less soluble calcium carbonate minerals. As ikaite usually appears as a metastable phase that readily decomposes into less hydrous $CaCO_3$ minerals in aqueous solutions (e.g. Besselink et al., 2017; Ito, 1996; Purgstaller et al., 2017; Stockmann et al., 2022), formation pathways of anhydrous $CaCO_3$ minerals may proceed along the formation of ikaite. Nevertheless, the appearance of ikaite in the course of the crystallization of less soluble $CaCO_3$ minerals has hardly been investigated so far, although

studies on the nucleation and growth of calcium carbonate minerals in recent decades have indicated that formation pathways can be manifold and may involve different intermediates (e.g. Cartwright et al., 2012; De Yoreo et al., 2015). Furthermore, numerous findings of the appearance of ikaite (see chapter 1.3) indicate that the contribution of ikaite to formation pathways has potentially been underestimated to date.

Likewise, the paleoclimatic significance of ikaite might be considerable, but remains poorly constrained yet. The occurrence of ikaite has usually been reported at low temperature environments. Therefore, it has been suggested that ikaite is a powerful indicator of near-freezing temperatures of water and may be a useful paleoclimatic proxy to reconstruct temperature conditions (e.g. Shearman and Smith, 1985; Suess et al., 1982; Swainson and Hammond, 2001). However, studies on the appearance of ikaite in nature and in laboratory syntheses provide an ambiguous picture of the temperature-dependent occurrence of ikaite, as the appearance of ikaite has not been observed exclusively at temperatures close to the freezing point of water (Purgstaller et al., 2017; Rogov et al., 2023; Stockmann et al., 2018; Tollefsen et al., 2020). Hence, further studies on the temperature dependence of the persistence of ikaite are inevitable in order to gain a profound understanding of the applicability of ikaite as an indicator of low temperature environments.

1.3 Occurrence of ikaite

While the appearance of ikaite in laboratory syntheses was already reported in the 19th century by Pelouze (1865), the natural occurrence of ikaite was unknown at that time. Also later, when the formation of calcium carbonate hexahydrate was achieved in further laboratory syntheses at near-freezing temperatures of water (Hume and Topley, 1926; Johnston et al., 1916; Krauss and Schriever, 1930; MacKenzie, 1923), the natural occurrence remained unrecognized. It took until 1963 for the mineral to be determined for the first time in a natural environment, namely in the Ikka fjord (Greenland), which gave rise to the mineral name *ikaite* (Pauly, 1963).

The precipitation of ikaite in the Ikka fjord is triggered by mixing of solutions due to subaquatic seeping spring water (Bischoff et al., 1993b; Stockmann et al., 2022; Tollefsen et al., 2019). Conditions that enable the precipitation of ikaite in nature, however, are not exclusive to Ikka fjord. Rather, it has become clear that growth sites of ikaite are manifold. These growth sites include different saline lakes (Bischoff et al., 1993a, 1993b; Council and Bennett, 1993; Oehlerich et al., 2013; Shearman and Smith, 1985), cold saline springs (Ito, 1996; Omelon et al., 2001), or unique settings like a concrete river basement (Boch et al., 2015), steel-slag leachate (Bastianini et al., 2024) or a tree wound (Garvie, 2022).

Furthermore, the precipitation of ikaite has been corroborated by widely distributed occurrences of pseudomorphs after ikaite (glendonites) (e.g. Kennedy, 2022; Morales et al., 2017; Peckmann, 2017; Rogov et al., 2021; Selleck et al., 2007; Swainson and Hammond, 2001; Vickers et al., 2022; Wang et al., 2017). Especially in boreal regions of the Northern Hemisphere,

these pseudomorphs appear frequently (Kennedy, 2022). The formation of ikaite as precursor mineral of glendonites has usually been associated with sedimentary environments, where precipitation has been suggested to be triggered by a release of bicarbonate resulting from sulfate reduction (Qu et al., 2017), methane release (Schubert et al., 1997), or authigenic diagenetic decomposition (Suess et al., 1982). In addition to glendonites, the above-mentioned findings of ikaite in Arctic and Antarctic sea ice (see chapter 1.2) further indicate a widespread formation (Dieckmann et al., 2008; Dieckmann et al., 2010; Fischer et al., 2013; Geilfus et al., 2013).

1.4 The fragile structure of ikaite

The low stability of ikaite relative to its less hydrous $CaCO_3$ polymorphs can be ascribed to the highly structured binding of water through a weak hydrogen bond network (Chaka, 2018). Unlike anhydrous $CaCO_3$ minerals, Ca^{2+} ions in ikaite crystals are eightfold coordinated by two oxygens of the CO_3^{2-} anion and by six oxygens of water molecules which gives a coordination of isolated bidentate contact $CaCO_3^0$ ion pairs enveloped by water molecules (Fig. 1, inset) (Chaka, 2018; Demichelis et al., 2014). These $CaCO_3^0$ ion pairs are arranged in rows, where the calcium, carbon and one oxygen of the carbonate group are located in the ab-plane of the lattice (Fig.1) (Demichelis et al., 2014). The surrounding water molecules connect the $CaCO_3^0$ ion pairs with each other due to the formation of a complex hydrogen bond network (Demichelis et al., 2014). In this network, all hydrogens of water molecules act as donors of hydrogen bonds, while acceptors are two-thirds of the oxygen of water molecules and all oxygens of the carbonates, i.e. twice the bidentate contact oxygen of the carbonate and four times the third oxygen, which is not coordinated by the Ca^{2+} ion (Demichelis et al., 2014).

Crystallographic data from single crystal X-ray structure analysis of a natural sample of ikaite at 248 K by Hesse et al. (1983) were in agreement with structural data of synthetic ikaite specimen (Dickens and Brown, 1970). The refined lattice parameters of the monoclinic (C2/c) unit-cell of ikaite (weighted R_w = 0.028) are a = 8.792(2) Å, b = 8.310(2) Å, c = 11.021(2) Å, β = 110.53(5)° (Hesse et al., 1983). For the bond length of the mean C–O distance of the planar carbonate group, a value of 1.286(1) Å was reported, which agrees with mean values of previously reported bond lengths in carbonate groups (Hesse et al., 1983). The bond length of bidentate Ca–O contact of the $CaCO_3^0$ ion pairs was specified with 2.442(2) Å, while the Ca–O distances to the oxygens of six water molecules were 2.387(1) Å (2x), 2.544(1) Å (2x), and 2.516(1) Å (2x) (Hesse et al., 1983). O–H distances within water molecules range from bond lengths of 0.728(19) Å to 0.825(17) Å, whereas hydrogen bonds provide lengths between 1.922(18) Å and 2.184(19) Å for O···H. These bond lengths led to distances of 2.709(1)–2.906(1) Å between different oxygens of water (Hesse et al., 1983).

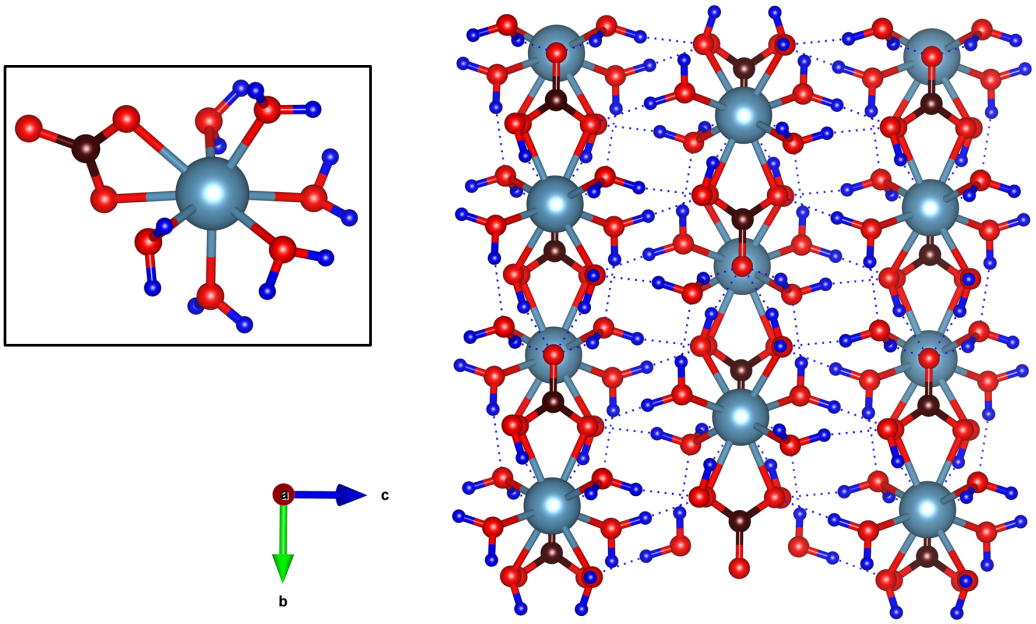

Figure 1. Projections of the crystal structure of ikaite (light blue: calcium, brown: carbon, red: oxygen, dark blue: hydrogen). Inset shows the hydrated $CaCO_3^0$ ion pair in ikaite: Ca^{2+} ions are eightfold coordinated by two oxygen of one CO_3^{2-} group and by six oxygen of water molecules. The large section of the ikaite structure shows the arrangement of calcium, carbon and one oxygen of the carbonate group in rows in the ab-plane which are interlinked by extensive hydrogen bonding (dotted lines).

1.5 Decomposition of ikaite

The extensive hydration of the structure of ikaite is essential for the stabilization of $CaCO_3^0$ ion pair complexes, however, the hydrogen bond network merely provides a fragile crystal structure (Chaka, 2018; Demichelis et al., 2014). Even minor changes of physicochemical conditions can induce the dehydration and subsequent decomposition of ikaite into less hydrous calcium carbonate phases (Buchardt et al., 2001; Chaka, 2018; Demichelis et al., 2014; Marland, 1975; Stockmann et al., 2022; Tang et al., 2009; Tollefsen et al., 2020; Vickers et al., 2022). Furthermore, the persistence of ikaite can be limited through the competing formation of anhydrous $CaCO_3$ minerals, as simultaneous precipitation might lead to undersaturation of ikaite. This becomes more pronounced with increasing temperatures because of the inversely correlating solubility behaviours of ikaite and anhydrous $CaCO_3$ minerals (e.g. Clarkson et al., 1992; Rodríguez-Ruiz et al., 2014).

Although from a perspective of structural controls, the conversion of ikaite into vaterite might be favourable (Tang et al., 2009), the temperature-induced transformation of ikaite is not limited to the conversion into vaterite. The transformation of ikaite into aragonite (Purgstaller et al., 2017), monohydrocalcite (Stockmann et al., 2022) and calcite (Besselink et al., 2017; Purgstaller et al., 2017) in aqueous solution has also been reported. Most likely, the product

phase selectivity of the transformations of ikaite is considerably affected by composition of aqueous solution. It has been shown, for instance, that the formation of calcite and aragonite after ikaite depends on the aqueous Mg^{2+}/Ca^{2+} ratio (Purgstaller et al., 2017).

In contrast to the transformations in aqueous solution, only the formation of vaterite or calcite after ikaite has been obtained under air exposure (Purgstaller et al., 2017; Sánchez-Pastor et al., 2016). For these conversions, a dissolution-precipitation reaction at the crystal-liquid interface that originates from surface moisture or release of structural water has been proposed (Purgstaller et al., 2017; Sánchez-Pastor et al., 2016). This mechanism coincides with that suggested for the transformation of ikaite in aqueous solution, however, it remains open whether the dehydration of ikaite in aqueous solution provides a similar crystal-liquid interface as in air (Besselink et al., 2017; Purgstaller et al., 2017). A different crystal-liquid interface has been suggested for transformations of ikaite under vacuum or in polar organic solvents (Lázár et al., 2023; Zou et al., 2018). Under these conditions, accelerated dehydration may inhibit the dissolution-precipitation reaction and ikaite transforms into ACC due to partial release of structural water (Lázár et al., 2023; Zou et al., 2018).

1.6 Crystallization of ikaite

1.6.1 The complex formation conditions of ikaite

The stabilization of ikaite is largely unknown yet. However, it has been shown that specific conditions are capable of promoting the formation of ikaite. In this context, natural occurrences and laboratory syntheses of ikaite have indicated that the conditions that support the formation of ikaite include near-freezing temperatures (e.g. Bischoff et al., 1993a; Boch et al., 2015; Buchardt et al., 1997; Clarkson et al., 1992). This finding has been associated with the prograde solubility of ikaite that contrasts the retrograde solubility of less hydrous $CaCO_3$ minerals (Bischoff et al., 1993a; Clarkson et al., 1992).

Furthermore, inhibitors that suppress competing nucleation and growth of anhydrous $CaCO_3$ minerals but do not interfere equally with the formation of ikaite have been found to be highly effective in supporting the formation of ikaite (Bischoff et al., 1993b; Clarkson et al., 1992; Hu et al., 2015; Purgstaller et al., 2017; Stockmann et al., 2018; Tollefsen et al., 2018). In natural environments, particularly Mg^{2+} and phosphate ions (Bischoff et al., 1993a; Lin and Singer, 2006; Morse et al., 2007; Tadier et al., 2017) are known inhibitors that suppress the nucleation and growth of anhydrous $CaCO_3$ minerals. Even minor amounts of phosphate (< 1 µM) can selectively retard the formation of anhydrous $CaCO_3$ minerals (Lin and Singer, 2006; Tadier et al., 2017) and thus promote the precipitation of ikaite. Similarly, the presence of ionic aqueous Mg species, which are abundant in sea water, may support the formation and persistence of ikaite due to growth retardation of calcite (e.g. Buchardt et al., 1997; Stockmann et al., 2018; Tollefsen et al., 2018).

Likewise, alkaline conditions may promote the formation of ikaite. This was derived from laboratory precipitation experiments (Hu et al., 2015) and was also implied by the impact of microbial biofilms on ikaite precipitates in nature (Trampe et al., 2016). However, as the pH of solution increases, the supersaturation with respect to all calcium carbonate minerals increases. Therefore, ikaite is not favoured per se. Instead, the cause for the promotion of ikaite formation by high pH is assumed to be the increased activity of the $CaCO_3^0$ ion pair (Chaka, 2018). Increased activity of the $CaCO_3^0$ ion pair may support the formation of six-fold coordinated hydrated $CaCO_3^0$ ion pair complexes, which most likely play a key role for the crystallization of ikaite (Chaka, 2018).

1.6.2 Nucleation of ikaite

The nucleation of ikaite most likely deviates significantly from known formation pathways of anhydrous $CaCO_3$ polymorphs (Chaka, 2018). Due to the highly hydrated nature of ikaite, the above-mentioned key role of the aqueous $CaCO_3^0$ ion pair complex was suggested for the nucleation of ikaite (Buchardt et al., 2001; Chaka, 2018; Stockmann et al., 2018). This was corroborated by density functional theory (DFT) calculations which obtained that the nucleation of ikaite could proceed via a low energy pathway of crystallization through the arrangement of aqueous $CaCO_3^0$ ion pair complexes in solution (Chaka, 2018). Electrostatic forces might provide a sufficient driving force for the arrangement of $CaCO_3^0 \cdot 6H_2O$ complexes in clusters, similarly to the alignment of the crystal structure of ikaite (Chaka, 2018). Consequently, extensive dehydration of complexes prior to incorporation is not required.

A separate kinetic model that describes the nucleation via such unique formation mechanism is largely lacking to date. Nevertheless, an acceptable approximation of the nucleation kinetics might be given by classical nucleation theory (CNT, e.g. Kashchiev, 2000; Sangwal, 2007). Although in the macroscopical consideration of classical nucleation theory (CNT), single steps of nucleation can generally be insufficiently captured, previous studies have shown that CNT-based calculations can provide a useful approximation of the overall nucleation kinetics for the formation of various minerals from aqueous solution. These include anhydrous $CaCO_3$ polymorphs (e.g. De Yoreo et al., 2013; Söhnel and Mullin, 1978; Verdoes et al., 1992) as well as phases involving potentially more complex nucleation steps (e.g. van Driessche et al., 2019).

For the model considerations by CNT, it is essential to distinguish between homogeneous (volume) and heterogeneous nucleation, as the presence of active foreign surfaces tremendously modifies the free energy of nucleation (Kashchiev, 2000; Kashchiev and van Rosmalen, 2003). Particularly in natural environments, impurities (e.g. foreign particles or surfaces) are usually widespread and may provide active sites for heterogeneous nucleation (Kashchiev, 2000). This heterogeneous type of nucleation is frequently favoured over homogeneous nucleation because bonds between molecules in nuclei and substrates provide

stronger bond strengths than solvation, which leads to a lower enthalpic contribution to free energy (De Yoreo et al., 2013). Therefore, the energy required to form an interface in the heterogeneous case is lower than in absence of effective foreign surfaces (De Yoreo et al., 2013). As interfacial energy has a tremendous impact on the activation barrier of nucleation, even slightly reduced interfacial energies may favour heterogeneous over homogeneous nucleation (De Yoreo et al., 2013).

In nature, mineral surfaces are ubiquitous and thus provide widespread potential effective surfaces for heterogeneous nucleation. For the crystallization of calcium carbonate minerals, it has been shown that foreign minerals are capable of supporting nucleation: The nucleation of calcite and vaterite on foreign mineral substrates of quartz or mica, for example, indicated significantly reduced interfacial energies relative to the homogeneous nucleation of calcite or vaterite, respectively (Li et al., 2014). Therefore, it must be assumed that foreign mineral surfaces can support essentially the nucleation of anhydrous $CaCO_3$ minerals in natural environments. For ikaite, however, it remains unknown so far, whether mineral surfaces similarly support the nucleation of ikaite by reducing interfacial energies. Although studies on the growth of ikaite in presence of calcite substrates (Marland, 1975) and on the precipitation of ikaite on substrates of functionalized polymers (Dalas, 1992; Malkaj et al., 2002) imply that foreign surfaces might be effective for the nucleation of ikaite, the impact of the omnipresence of foreign mineral surfaces in nature on the nucleation of ikaite remains largely unknown to date.

1.6.3 Crystal growth and persistence of ikaite

Analogous to the proposed unique nucleation mechanism of ikaite, it can be suggested that the growth of ikaite proceeds via the incorporation of hydrous $CaCO_3^0$ ion pairs without massive dehydration. However, the growth kinetics has not been extensively studied yet. So far, growth rates of ikaite have only been determined in one laboratory study on the precipitation of ikaite from highly saline seawater-derived brines at sub-zero temperatures (Papadimitriou et al., 2014). The results of this study implied the rapid formation of ikaite in sea ice, but implications for the growth mechanism of ikaite in diverse natural settings remained ambiguous.

The investigation of the growth kinetics of ikaite is challenging due to the largely unknown conditions that ensure sufficient persistence of ikaite for extensive growth. Although various studies have identified solution conditions which support the precipitation of ikaite (see chapter 1.6.1), comparatively few findings have been reported on the factors that increase the persistence of ikaite and, thus, enable extensive growth. Furthermore, the ephemeral appearance of ikaite resulting from the limited persistence of ikaite has important implications for the crystallization of calcium carbonate minerals in multi-phase precipitating systems. In this context, the formation of metastable ikaite, for instance, has been associated with the empirical approach of Ostwald's rule of stages (ORS, Chaka, 2018; Rodríguez-Ruiz et al., 2014). From the perspective of ORS, the phase that nucleates first is not inevitably the most

thermodynamically stable one, but a metastable one which subsequently transforms into the next stable phase (Ostwald, 1897). Therefore, the nucleation and growth of ikaite prior to less hydrous $CaCO_3$ minerals might be in agreement with ORS. However, the applicability of ORS depends essentially on kinetic arguments (e.g. De Yoreo, 2022; Navrotsky, 2004), which are poorly constrained for ikaite to date. Hence, further investigations of ikaite formation and persistence may help to evaluate the capability of ORS for providing an explanation of the ephemeral appearance of ikaite.

2 Scope of this thesis

2.1 Aim of this thesis

The crystallization kinetics of ikaite remains largely unexplored to date. Furthermore, knowledge from the formation kinetics of anhydrous $CaCO_3$ minerals can hardly be transferred to ikaite, as the crystallization kinetics of ikaite and anhydrous $CaCO_3$ minerals most likely differs significantly. Therefore, key aspects of ikaite formation, such as the formation mechanism or the impact of surfaces on nucleation, e.g. by foreign mineral surfaces, remain ambiguous. Likewise, the transient nature of ikaite and, thus, the controls of ikaite persistence are far from understood. This lack of knowledge of the formation and persistence of ikaite impedes estimations of the contribution of ikaite precipitation to polar carbon dynamics and frequently leaves the role of the appearance of ikaite in the context of crystallization pathways of more stable $CaCO_3$ polymorphs unclear. Furthermore, the use of ikaite as a powerful paleoclimatic proxy indicating near-freezing temperatures, remains challenging, as there is no scientific consensus about the temperature-dependent persistence of ikaite so far.

This doctoral thesis aims to contribute to a better understanding of the crystallization of ikaite by unraveling key aspects in the nucleation, growth and persistence of ikaite. To this end, investigations of the nucleation kinetics of ikaite in presence and absence of foreign mineral surfaces intend to reveal the impact of mineral surfaces on the nucleation of ikaite and to find out whether the formation mechanism of ikaite coincides with the classical picture of nucleation. Studies on ikaite growth in the presence of phosphate aim to complement the investigations of the nucleation kinetics and to explore the effect of potential phosphate coprecipitation on the formation of ikaite and its environment. Together with investigations of ikaite persistence, it is also intended to figure out the role of inactivation of anhydrous $CaCO_3$ minerals for the extensive formation of ikaite. Furthermore, investigations of the persistence aim to contribute to a better understanding of the occurrence of ikaite instead of less soluble $CaCO_3$ minerals. In this context, a more thorough understanding of the role of ikaite as a potential precursor of less hydrous $CaCO_3$ minerals at different temperatures is targeted. This might, for example, help to gain new insights into the applicability of Ostwald's rule of stages or the role of glendonites as low temperature indicators.

2.2 Author contributions

The three studies reported in this doctoral thesis were published as separate articles in scientific journals after peer review:

Chapter 4.1 was published as

Strohm S.B., Inckemann S.E., Gao K., Schweikert M., Lemloh M.-L., Schmahl W.W., Jordan G., 2022. On the nucleation of ikaite ($CaCO_3x6H_2O$) – A comparative study in the presence and absence of mineral surfaces. Chemical Geology 611, 121089.

SBS and GJ designed the study. SBS, SEI, and KG performed the precipitation experiments and the subsequent analyses. M-LL, MS provided the analysis by cryo scanning electron microscopy. SBS processed the experimental data and drafted the manuscript. All authors discussed the results and contributed to the final manuscript.

Chapter 4.2 was published as

Strohm, S.B., Saldi, G.D., Mavromatis, V., Schmahl, W.W., Jordan, G., 2023. A Study on Ikaite Growth in the Presence of Phosphate. Aquatic Geochemistry 29 (4), 219–233.

SBS, GDS and GJ contributed to the design of the presented study. SBS conducted the growth experiments. SBS and GDS performed the analyses of aqueous solutions and precipitates. SBS evaluated the data and wrote the manuscript. All authors contributed to the discussion of the results and the final version of the manuscript.

Chapter 4.3 was published as

Strohm S.B., Berghofer S.A., Kaiser C., Jordan G., 2024. On the Ephemeral Occurrence of Ikaite in Aqueous Solutions between 0 and 20 °C. ACS Earth and Space Chemistry 8 (9), 1725-1736.

SBS, and GJ designed the study. SBS and SAB conducted the CMBR experiments and performed the solution/solid analyses. CK carried out the analysis by cryo scanning electron microscopy. SBS evaluated the data and drafted the manuscript. All authors discussed the results and contributed to the final manuscript.

3 Methods

Nucleation of ikaite was studied with experiments in a cryo-mixed-batch reactor (CMBR, see chapter 3.1). Using CMBR experiments, both heterogeneous and pseudohomogeneous nucleation of ikaite were investigated in order to reveal the impact of mineral surfaces on nucleation and to determine the interfacial energy of ikaite nuclei. Likewise, this approach was used to study the persistence of ikaite. Cryo-mixed-flow reactor (CMFR) experiments were conducted to determine ikaite growth rates (see chapter 3.2). Analysis of solutions from CMFR enabled the calculation of growth rates and the detection of depletion of constituents. Both the CMBR and the CMFR approach were complemented by analyses of precipitates (see chapter 3.3) as well as aqueous geochemical calculations (see chapter 3.4).

3.1 Cryo-mixed-batch reactor experiments

3.1.1 Experimental setup and procedure

Precipitation and monitoring

Cryo-mixed-batch reactors were used for precipitation experiments. The experimental setup of CMBR consists of a glass reactor vessel (total volume: 250 ml) containing a $CaCl_2$ solution adjusted to an ionic strength of 0.1 M by the addition of NaCl solution (1 M) and to a pH of 10 by adding NaOH solution (1M). All solutions were prepared by dissolving analytical-grade chemicals in deionized water with a resistivity of 18.2 MΩ cm.

Inside the reactor, rigorous stirring of a PFTE coated stirring bar ensures homogeneous solution conditions. In order to maintain constant temperature conditions (±0.1 °C), the glass reactor was submerged in a thermostatic water bath (Lauda alpha RA 8). The solution pH and Ca^{2+} concentration was monitored throughout the experiment using ion selective electrodes sensitive toward the hydrogen ion (calibrated with NIST certified pH 4.01, 7.13 and 10.32 buffer solutions at 0 °C) and the Ca^{2+} ion, respectively (Fig. 2). These measurements were conducted with a multiparameter benchtop meter (HANNA instruments HI 5222).

Precipitation of calcium carbonate mineral(s) was initialized by the rapid addition of $NaHCO_3$/Na_2CO_3 solution in the CMBR, which led to a constant volume of the reactive solution of 200 ml. Continuous stirring inside the reactor by the magnetic stirrer allowed mixing of solutions in less than 5 seconds. Stirring was maintained throughout the entire runtime.

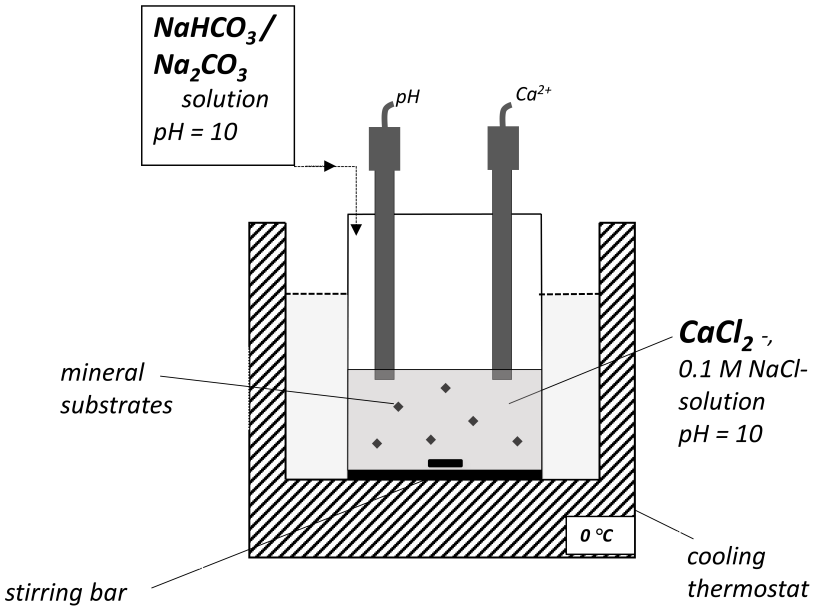

Figure 2. Experimental set up of a cryo-mixed-batch reactor (CMBR) experiment (from Strohm et al., 2022).

Upon the end of each CMBR precipitation experiment, the solids were removed from the solution within less than 30 seconds by vacuum filtration and immediately rinsed with ethanol or acetone (T = −18 °C). Solid samples were stored in a freezer (*T* = −18 °C) for further solid analyses as described in chapter 3.3. Furthermore, filtered solutions were collected for measurements of total alkalinity and aqueous Ca concentration. These analyses were applied to solutions that were retrieved after run times of at least 40 minutes, as these samples provide a sufficiently decreased reactivity required for ex-situ analyses. Both total alkalinity and aqueous Ca concentration were analysed by potentiometric end point titrations using an automatic titrator (SI Instruments TitroLine 7000). Total alkalinity was analysed using a standard glass electrode calibrated with NIST certified pH 4.01, 7.01 and 10.01 buffer solutions at room temperature and a 0.01 M HCl standard solution (detection limit: 2 x 10^{-5} M). Aqueous Ca concentrations were determined by complexometric titration using 0.01 M Na_2-EDTA (ethylenediaminetetraacetic acid) standard solution and a Ca^{2+} ion selective electrode (Ca^{2+}-ISE, detection limit: 2 x 10^{-5} M).

CMBR experiments in presence of mineral substrates

Runs of precipitation experiments as described above were performed in the presence and absence of mineral substrates (quartz, mica) with experimental run times between < 30 s and 40 minutes (see chapter 4.1). Quartz crystals were added to the reactor in one series of experiments and mica in a second series prior to triggering precipitation by the rapid addition of $NaHCO_3$/Na_2CO_3 solution. In a third series aiming at pseudohomogeneous ikaite formation, no substrate crystals were added. For each condition, experiments were performed in triplicate (Table 2, chapter 4.1.2). Quartz substrates were prepared by grinding quartz powder from

Fluka. Mica substrates (Ziegler Minerals, Germany, particle size < 45 µm, chemical composition: SiO_2: 46 %, Al_2O_3: 32 %, K_2O: 11 %, Fe_2O_3 < 5 %, Na_2O_3: 0.3 %, MgO: 0.2 %, TiO_2: 0.6 %) were used without grinding. The powders were washed and decanted with deionized water (18.2 MΩ cm) repeatedly. Specific surface areas of 0.21 m^2/g for quartz and 3.97 m^2/g for mica substrates were obtained using krypton gas adsorption following standard BET procedures.

CMBR experiments at different solution temperatures

Apart from nucleation experiments in the presence and absence of mineral surfaces at 0 °C, pseudohomogeneous precipitation experiments were conducted at T = 0, 5, 10, 15 and 20 °C, with temperatures maintained within a range of ±0.1°C by the thermostatic water bath (see chapter 4.3). Compositions of initial solutions in CMBR experiments are listed in Table 1. A series of experiments with five different run times (r_1–r_5) was carried out for each temperature: run time r_1) less than 30 seconds after mixing; r_2) $1 \leq t \leq 4$ min after mixing, when a temporary slow-down of pH decrease was observed; r_3) t = 8 minutes after mixing; r_4) t = 40 minutes, when the pH-decrease was significantly retarded; r_5) after 24 hours. Once the designated run time had been reached, the experiments were terminated, and the reactor contents were sampled. For this, precipitates were separated from the solutions within 30 seconds and instantaneously rinsed with acetone to remove adhering aqueous solution (T of acetone corresponded to the solution temperature), before acetone with a temperature of –18 °C was used in a second rinse.

Table 1. Compositions of initial solutions in cryo-mixed-batch reactor experiments.

	Solution composition			**Solution speciation[a]**					**Saturation state[a]**		
T [°C]	$CaCl_2$ [mM]	$NaHCO_3$ [mM]	Na_2CO_3 [mM]	$a_{Ca^{2+}}$ [mM]	$a_{CO_3^{2-}}$ [mM]	$a_{CaCO_3^0}$ [mM]	$a_{Ca^{2+}}/a_{CO_3^{2-}}$	pH (modelled)	Ω_{ikaite}	$\Omega_{calcite}$	$\Omega_{vaterite}$
0	7.00	3.50	3.50	2.07	0.56	1.50	3.7	10.01	18	288	65
5	8.70	4.50	4.50	2.39	0.65	2.21	3.7	9.89	18	389	91
10	11.0	6.00	6.00	2.74	0.75	3.31	3.7	9.79	18	550	132
15	14.5	8.25	8.25	3.22	0.88	5.06	3.7	9.65	18	794	195
20	18.5	10.9	10.9	3.66	0.99	7.24	3.7	9.53	18	1096	269

[a] Solution speciation and saturation were calculated using PHREEQC (Parkhurst and Appelo, 2013).

3.1.2 Determination and interpretation of induction periods

The induction period of precipitation t_{ind} defines the time interval that elapses from the moment of supersaturating a solution to the time at which precipitation is detected by solution monitoring (Gómez-Morales et al., 1996; Söhnel and Mullin, 1988). For the precipitation of calcium carbonate minerals in CMBR experiments, t_{ind} can be defined as the duration from the addition of carbonate to the Ca^{2+} solution until the growth of detectable nuclei that cause a detectable change of the pH or Ca^{2+} signal (Fig. 3).

In order to determine t_{ind}, the inflection of the first derivative of a polynomial fit of our experimental data was used in CMBR experiments. Induction periods determined by pH monitoring generally agreed well with t_{ind} indicated by Ca^{2+} measurements. However, pH monitoring provided more precise data compared to Ca^{2+} measurements due to experimental conditions including free pH drift at 0 °C. Hence, t_{ind}-data from pH monitoring were used for the determination of all induction periods.

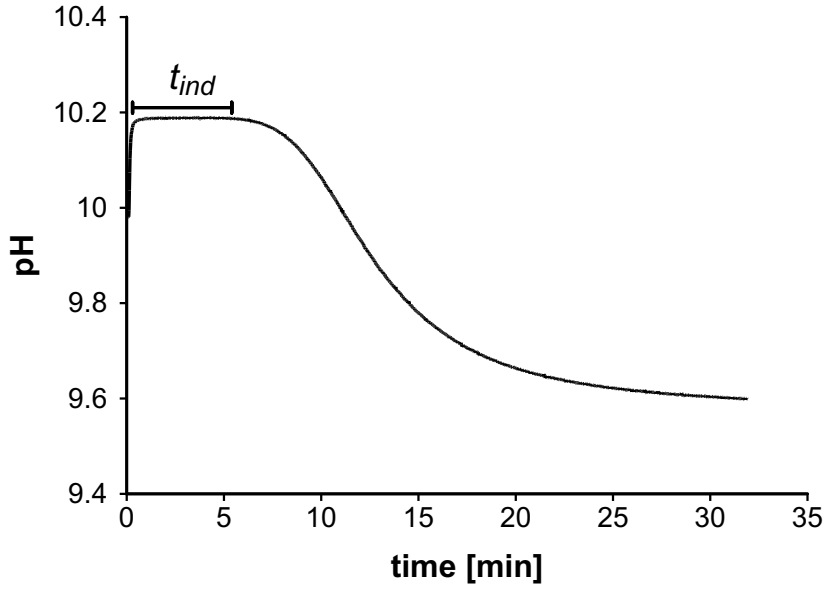

Figure 3. pH versus time plot for a CMBR experiment with a solution of $\Omega_{\text{ikaite}} = 5$ at $T = 0$ °C. The decrease of pH is induced by the precipitation of the carbonate phase (ikaite) and determines the induction period t_{ind} (from Strohm et al., 2022).

The detectable induction period t_{ind} involves the time required for the formation of a stable nucleus t_n from the metastable parent solution and the time elapsed for the growth of nuclei to a detectable size t_g (Söhnel and Mullin, 1988):

$$t_{ind} = t_n + t_g \tag{3.1}$$

Because t_n and t_g cannot be isolated in precipitation experiments (Mullin, 2001), it is convenient to interpret the sum of the two as a measure of the nucleation process (t_{ind}). For

this, both t_n and t_g require assumptions, such as a steady-state size distribution of nuclei, irrespective of supersaturation, and the applicability of the growth kinetics derived from microcrystals to newly formed nuclei (Mullin, 2001; Söhnel and Mullin, 1988). Furthermore, the interpretation of any induction periods generally requires standardized conditions, as t_{ind} depends on the latency and resolution of the particular experimental method and, thus, does not provide a fundamental property of the system (Kashchiev, 2000).

Given standardized conditions including constant volume V, temperature T, and initial supersaturation Ω of the parent phase and under the assumption of linear growth of nuclei in regular shape, the induction period t_{ind} can be defined for individual systems (Kashchiev et al., 1991; Söhnel and Mullin, 1988). Two limiting cases can be distinguished, which are considered as mononuclear (MN) and polynuclear (PN) mechanism (e.g. Kashchiev et al., 1991; Kashchiev, 2000; Sangwal, 2007; Söhnel and Mullin, 1988).

The MN mechanism applies to the case that the formation of the first stable nucleus terminates the presence of a metastable solution (Kashchiev and van Rosmalen, 2003; Sangwal, 2007). In the MN approach, the probability of the formation of a single nucleus P_1 within time t for a constant nucleation rate J is (Kashchiev et al., 1991; Toschev et al., 1972):

$$P_1(t) = 1 - \exp(-JVt) \tag{3.2}$$

The mean time of formation of the first nucleus can be defined as

$$t_{ind}^{\mathrm{MN}} = \int_0^\infty t \, dP_1(t) \tag{3.3}$$

(Kashchiev et al., 1991; Toschev et al., 1972). Thus, inserting the differential dP_1 with respect to t from Eq. 3.2 into Eq. 3.3 gives the induction period for the MN mechanism as a measure of the nucleation rate J:

$$t_{ind}^{\mathrm{MN}} = 1/JV \tag{3.4}$$

The other limiting case, given by the PN approach, describes that multiple progressively growing nuclei bring the solution out of the metastable state (Kashchiev and van Rosmalen, 2003). Assuming linear 3D growth of spherical nuclei, the probability of the formation can be expressed as

$$P(t) = 1 - \exp\left(-\frac{\pi}{3} R^3 J t^4\right) \tag{3.5}$$

where R is the growth rate (Kashchiev et al., 1991). Analogously to MN, the induction period of PN can be defined by the mean time of formation, which yields

$$t_{ind}^{\mathrm{PN}} = \left(\frac{3\alpha}{\pi R^3 J}\right)^{\frac{1}{4}} \tag{3.6}$$

where α is the experimentally detectable volume fraction ($V_{\mathrm{min}}/V \approx 10^{-7}$) (Kashchiev et al., 1991).

Using the classical definition of the steady-state nucleation rate of three-dimensional nuclei J, t_{ind}^{MN} and t_{ind}^{PN} can each be expressed as a function of supersaturation Ω (Verdoes et al.,

1992). The steady-state nucleation rate of three-dimensional calcium carbonate nuclei can be represented as

$$J = A\,\Omega^{\frac{1}{2}} exp\left[-\frac{\beta\gamma^3 V_m^2 f(\theta) N_A}{\nu^2 (RT)^3 ln^2 \Omega^{\frac{1}{2}}}\right] \tag{3.7}$$

with A: kinetic pre-factor, β: shape factor (16π/3 for a spherical nucleus), V_m: molecular volume (114 cm³/mol for ikaite), $f(\theta)$: correction factor ($f(\theta)$ = 1 for homogeneous nucleation and $f(\theta)$ < 1 for heterogeneous nucleation), N_A: Avogadro number, ν: number of ions in a molecular unit (ν = 2 for ikaite), R: gas constant, T: temperature (Mullin, 2001; Söhnel and Mullin, 1988). The saturation state Ω was defined as

$$\Omega = \frac{\mathrm{IAP}}{K_{sp}} \tag{3.8}$$

where IAP stands for the ionic activity product and K_{sp} for the solubility product of the mineral phase. Using equations 3.4 and 3.7, the induction period as a function of supersaturation for the MN approach can be expressed as

$$\log t_{ind}^{\mathrm{MN}} = \frac{B}{log^2 \Omega} - C \tag{3.9}$$

with

$$C = log\,(A\Omega^{\frac{1}{2}}) \tag{3.10}$$

and

$$B = \frac{\beta\gamma^3 V_m^2 f(\theta) N_A}{\nu^2 (2.3RT)^3}. \tag{3.11}$$

The logarithmic expression (log or ln) of Eq. 3.9 is convenient, as it enables the interpretation of the dependence of t_{ind} and Ω in a plot of $\log t_{ind}^{\mathrm{MN}}$ versus $(\log \Omega)^{-2}$. Here, the parameter B can be derived by the best fit of a straight line. Knowing B, the interfacial energy γ can be calculated from equation 3.11 (Mullin, 2001; Söhnel and Mullin, 1988).

Similarly, the polynuclear approach enables the quantification of the interfacial energy. For this, a growth rate law that expresses the growth rate R as a function of Ω is included:

$$R = k_i\, f(\Omega) \tag{3.12}$$

where k_i is the growth rate constant (Gómez-Morales et al., 1996). Inserting equation 3.12 into Eq. 3.6, the rearranged combination of equations 3.6 and 3.7 yields the induction period as a function of supersaturation for the PN approach:

$$\ln\left(t_{ind}^{\mathrm{PN}}\, \Omega^{\frac{1}{8}} f(\Omega)^{\frac{3}{4}}\right) = \frac{B}{ln^2 \Omega} + \ln\left(\frac{3\alpha}{\pi {k_i}^3 A}\right)^{\frac{1}{4}} \tag{3.13}$$

where B is

$$B = \frac{\beta\gamma^3 V_m^2 f(\theta) N_A}{\nu^2 (RT)^3} \tag{3.14}$$

and can be obtained from a linear fit in a plot of $\ln\left(t_{ind}^{\mathrm{PN}}\,\Omega^{\frac{1}{8}}\,f(\Omega)^{\frac{3}{4}}\right)$ versus $(\ln\Omega)^{-2}$.

Although the PN approach involves the formation of multiple nuclei and their growth to a detectable size, it does not necessarily provide a better fit to experimental data of induction periods than the MN mechanism (Gómez-Morales et al., 1996; Sangwal, 2007; Verdoes et al., 1992). This may be associated with deviating contributions of t_n and t_g to induction periods (cf. Eq. 3.1, Sangwal, 2007). Consequently, both approaches might allow an applicable interpretation of induction periods in order to derive interfacial energies of nuclei.

In contrast, the extraction of the supersaturation independent kinetic pre-factor A using these approaches is more complex. This is reflected by scattered values of A for the nucleation of anhydrous calcium carbonate minerals in the literature (Bergwerff and van Paassen, 2021; Cedeno et al., 2023; Devos et al., 2021; Vekilov, 2010). Although equations 3.9 and 3.13 indicate that the intercept of a linear fit of both the MN and PN approach provide an estimation of A, the scattered values of A imply a more limited applicability of the extraction of A from induction periods compared to that for the interfacial energy γ.

3.2 Cryo-mixed-flow reactor experiments

Seed syntheses

Ikaite seed crystals for cryo-mixed-flow reactor (CMFR) growth experiments were synthesized following the procedure of Bischoff et al. (1993a) by mixing 100 ml each of 0.1 M $CaCl_2$ and K_2CO_3 solutions into a 0.04 M KOH solution (400 ml) at 1 °C. $CaCl_2$ and K_2CO_3 solutions were added drop by drop via two separate channels of a peristaltic pump (Ismatec IPC-N) with a flow rate of 0.8–1 ml/min. K_2HPO_4 solution was added to the mixture simultaneously, resulting in phosphate concentrations of 33–200 µM throughout the synthesis. All aqueous solutions for seed syntheses were prepared by dissolving reagent grade $CaCl_2x2H_2O$, K_2CO_3, KOH and K_2HPO_4 in deionized water (resistivity 18.2 MΩ cm). After mixing, the solutions were kept at 1 °C under stirring for 24 hours before the precipitate was filtered, washed with ethanol (T = –18 °C) and stored at –18 °C to ensure the persistence of ikaite seeds.

In addition, calcite seeds were synthesized by temperature-induced transformation of ikaite in order to yield a synthetically disintegrated ikaite as a proxy for manifold decomposed ikaite specimens (e.g. Bischoff et al., 1993b; Boch et al., 2015; Németh et al., 2022; Schultz et al., 2023; Vickers et al., 2022). For this purpose, ikaite seeds were first synthesized as described above and then exposed to temperature fluctuations (temperature maximum 10 °C for 24 hours) to induce transformation into calcite.

Experimental procedure of CMFR growth experiments

Seeded growth experiments were carried out using PFA cryo-mixed-flow reactor (total reactor volume: 120 ml, Fig. 4) similar to the experiments described in detail by Lindner and Jordan (2018) and Saldi et al. (2021). Inside the reactor, a seed crystal powder was placed to grow from solution. 1.5 g of the synthesized ikaite and calcite seeds, respectively, were used for CMFR growth experiments. The specific surface area of ikaite seed crystals was estimated from cryo SEM-images (Fig. 14, chapter 4.2.1) applying a cubic shape model. Here, an average crystal diameter of ~50 µm was approximated, which led to a specific surface area of 984 cm^2/g.

After the addition of seed crystals to the reactor, constant flow rates over a total run time between 22 and 46 hours were applied. Experiments were conducted in a cooling incubator in order to maintain a constant temperature of 1 °C. The Ca- and bicarbonate- containing growth solution was injected into the reactor via two separate channels of a peristaltic pump with constant flow rates (Table 6, chapter 4.2.1). Solutions were prepared using reagent grade compounds and high-purity deionized water (resistivity 18.2 MΩ cm). Compositions of inlet solutions are listed in Table 6. Ionic strength of solutions was adjusted to 0.1 M with NaCl solution (1 M). pH was set to ~8.5 using small amounts of 1 M NaOH solution. In the reactor, a magnetic PTFE coated stirrer allowed rapid mixing of two inlet solutions. The steady outflow of solution was ensured by an effluent channel, which was equipped with a PTFE membrane filter (pore size: 0.45 µm) to prevent a loss of crystals from the reactor.

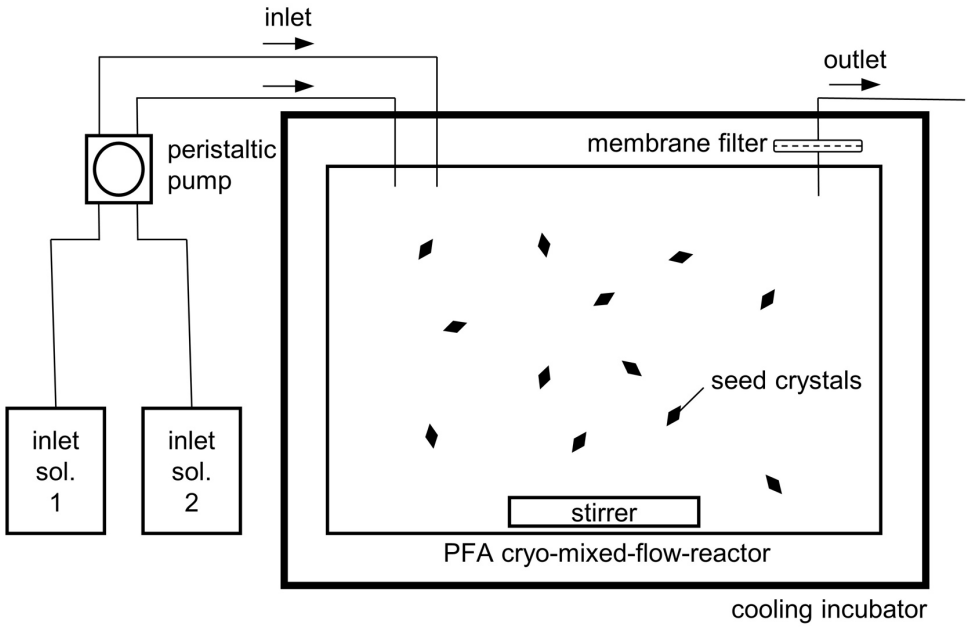

Figure 4. Experimental setup of cryo-mixed-flow reactor (CMFR) experiments.

The growth of calcium carbonate crystals from a growth solution in the CMFR led to a depletion of Ca concentrations and total alkalinity in the effluent solution relative to the inlet solution. Once these parameters indicated constant solution compositions, steady-state condition was approximated and growth rate of ikaite was calculated using the equation

$$R = \frac{\Delta\mathrm{Ca}\, F}{m\, A_S} \tag{3.15}$$

where ΔCa is the difference of the Ca concentration between inlet and outlet solution, F is the outlet flow rate, m is the mass of the crystals, and A_S is the specific surface area.

To analyse the composition of solutions, samples were taken from the effluent channel at time intervals of several hours. Immediately after sampling, the pH of solution was measured at 25 °C using a standard glass electrode calibrated with NIST certified pH 4.01, 7.01 and 10.01 buffer solutions. Total alkalinity was analysed by potentiometric end-point titrations with an uncertainty of ±2% (detection limit: 5 x 10^{-5} eq/l) using a Schott TA 10plus automatic titrator and 0.01 M or 0.05 M HCl standard solution. Furthermore, subsamples of solutions were acidified with ultrapure concentrated HNO_3 and used for Ca and P analyses. Ca concentrations were measured by flame atomic absorption spectroscopy (AAS) using a Perkin Elmer AANalyst 400 atomic absorption spectrometer with an uncertainty of ±2% and a detection limit of 1 x 10^{-6} M. For the analysis of P, inductively coupled plasma optical emission spectroscopy (ICP-OES; Horiba Ultima 2) with an uncertainty of ±1.5% and a detection limit of 1 x 10^{-6} M was used. Ca, P and alkalinity analyses of inlet and reactive solutions are listed in Table 6.

3.3 XRD and SEM analysis of precipitates

Cooled precipitates retrieved from CMBR experiments and crystal powders before and after CMFR experiments were analysed by X-ray powder diffraction (XRD, GE Seifert or Bruker D8 Advance A25, Cu$K\alpha_1$ radiation, λ = 1.5406 Å) with scattering angles of 10° ≤ 2θ ≤ 60°. In order to prevent a temperature-induced phase transition during the measurement, sample holders were precooled (–18 °C) and routine analyses were conducted within a short measurement time of 12 minutes. In addition to X-ray routine analysis, precipitates extracted from solution during the initial stage of CMBR experiments (t < 8 min) were analyzed within a reduced range of scattering angles (12° ≤ 2θ ≤ 32°) using faster scans (3 min) to identify highly instable amorphous phase(s).

Furthermore, selected samples of solids from CMBR and CMFR experiments were visualised using cryo scanning electron microscopy (cryo SEM, Zeiss EVO 15, Quanta 250 FEG FEI, Thermo Fisher Quattro S equipped with a cool stage). Secondary electron and back scattered electron signals provided the imaging mode using an accelerating voltage of ≤ 20 kV.

3.4 Modelling of solution compositions, speciations and saturation states

For both CMFR and CMBR experiments, solution compositions, aqueous speciations and saturations states of solutions with respect to solid phases of interest (Ω, Eq. 3.8) were calculated with the geochemical code PHREEQC version 3.7.0 (Parkhurst and Appelo, 2013) using the llnl database. The llnl database was modified inserting the solubility constants of ikaite (log K_{sp} = 0.15981 – 2011.1/T, Bischoff et al., 1993a), vaterite (log K_{sp} = –172.1295 – 0.077993 T + 3074.688/T + 71.595 log T, Plummer and Busenberg, 1982), amorphous calcium carbonate (ACC, log K_{sp} = –12.919 + 0.054538 T – 0.0001096 T^2, Brečević and Nielsen, 1989), and the carbonic acid dissociation constants from Millero et al. (2007).

4 Results and discussion

4.1 Nucleation of ikaite in the presence and absence of mineral surfaces

4.1.1 Results

Precipitated phases

In all CMBR experiments, at least one phase precipitated from supersaturated solution (Table 2). Ikaite, however, did not crystallize under all conditions. In absence of mineral substrates, ikaite only formed in solutions with an initial supersaturation Ω_{ikaite} of at least 15 (Table 2, exp. # 16, 19, 22, 25), whereas in solutions with lower Ω_{ikaite}, calcite and vaterite could be identified (Fig. 5). In presence of 0.5 g quartz or 0.1 g mica substrates, in contrast, ikaite precipitated over the whole range of supersaturation $1.6 \leq \Omega_{ikaite} \leq 51$ (Fig. 6). Experiments with increased amounts of substrates (5 g, 10 g) did neither cause a change in the phase inventory nor a significant reduction of t_{ind} (Fig. 7). In order to attain comparable conditions, the minimum amounts of crystals (0.5 g quartz, 0.1 g mica) have been added to the experiments by default.

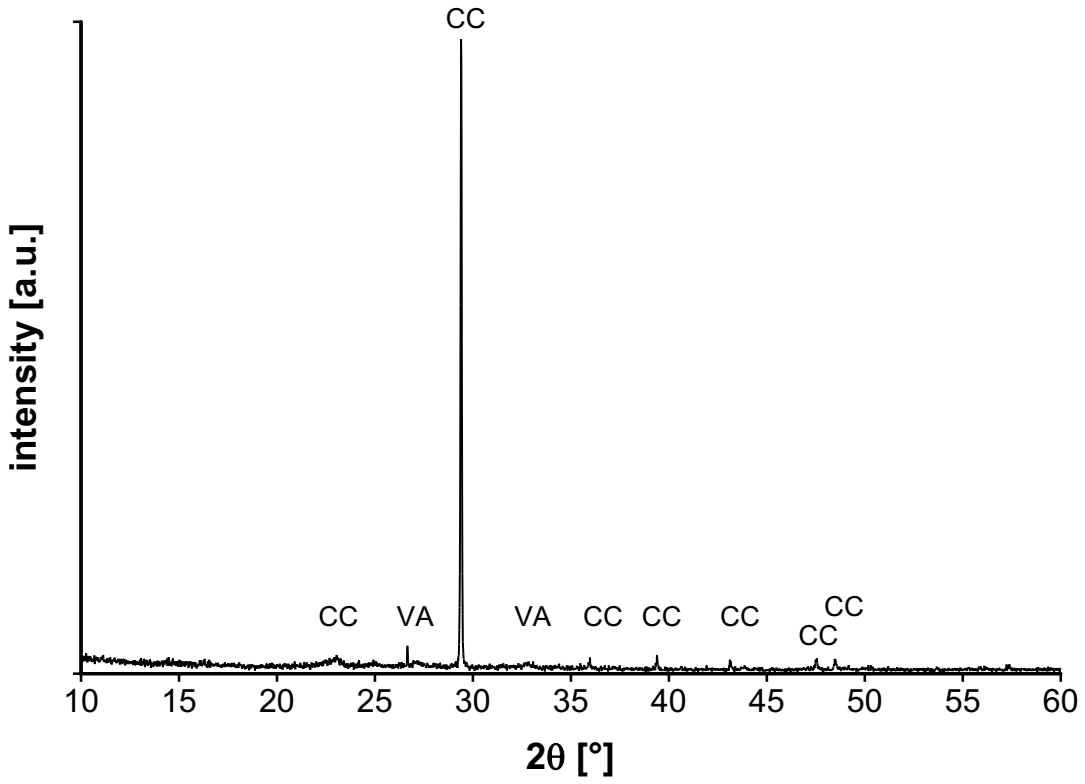

Figure 5. X-ray diffractogram (Cu$K\alpha$) of precipitates retrieved from CMBR experiments in absence of quartz or mica substrates with an initial supersaturation of Ω_{ikaite} = 11 (exp. # 13.1). Diffraction peaks correspond to calcite (CC) and vaterite (VA).

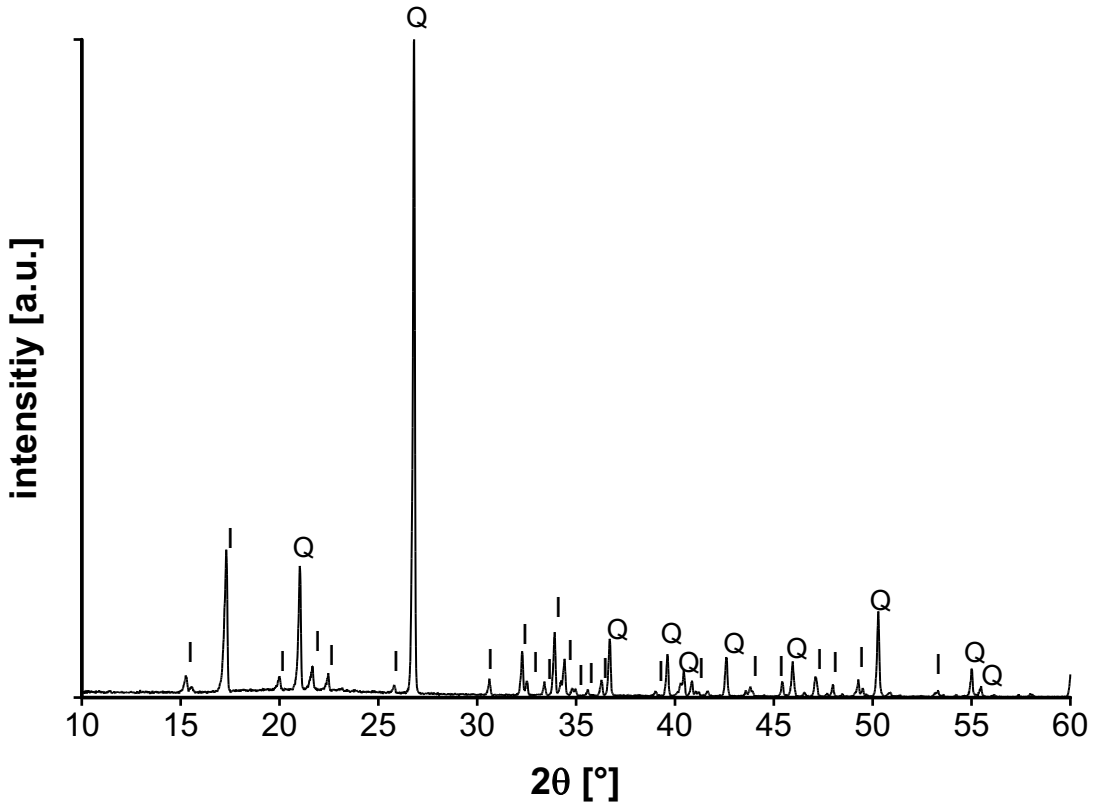

Figure 6. X-ray diffractogram (CuKα) of precipitates retrieved from CMBR experiments in presence of quartz substrates with an initial supersaturation of Ω_{ikaite} = 22 (exp. # 23.3). Diffraction peaks correspond to ikaite (I) and quartz (Q).

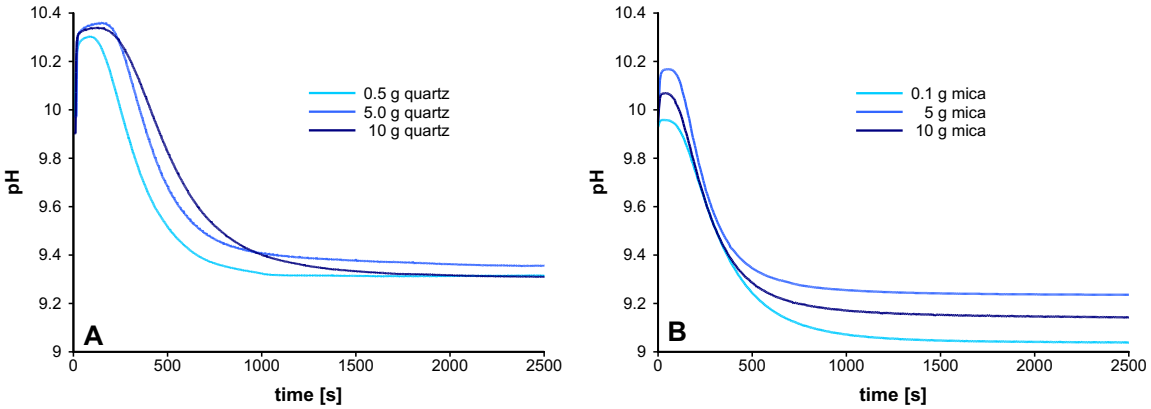

Figure 7. Desupersaturation curves from CMBR experiments with an initial supersaturation of Ω_{ikaite} = 11. **A**) In presence of different amounts of quartz. **B**) In presence of different amounts of mica.

Besides crystalline phases, an amorphous phase was found in X-ray analyses of solids from CMBR experiments with an initial supersaturation $\Omega_{ikaite} \geq 26$, if the samples were retrieved within the first 30 s of the experimental run. During repeated X-ray diffraction scans (each taken over 3 min at room temperature on a pre-cooled but warming sample holder), the

amorphous phase transformed into calcite and vaterite (Fig. 8). If the solids were retrieved from reactor later than 30 s after starting the experimental run, the amorphous phase was no longer detectable by X-ray analysis.

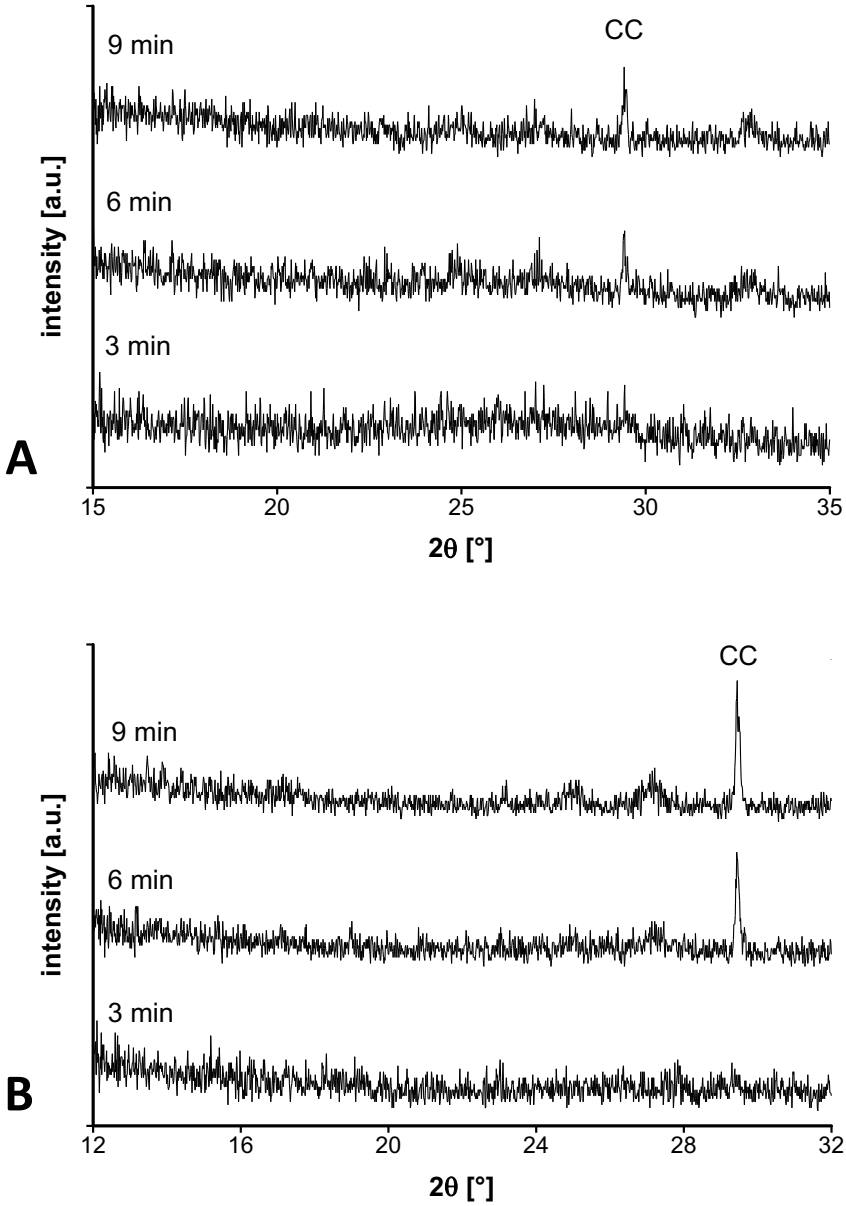

Figure 8. Series of three X-ray diffraction patterns (Cu$K\alpha_1$) of a powder which was retrieved from CMBR experiments with Ω_{ikaite}= 26 (**A**) and Ω_{ikaite}= 51 (**B**) immediately after adding the second solution to the reactor. Each scan lasted 3 min. Note that the sample temperature increased during the period of data acquisition causing a transformation of the amorphous phase. This elevated temperature, consequently, caused the formation of calcite (CC).

Cryo SEM revealed different morphologies of precipitates depending on the moment they were retrieved from CMBR (Fig. 9). Precipitates retrieved within the first 30 s after attaining a supersaturated solution consisted of granules partly forming larger anhedral units or aggregates with diameters up to 2 µm (Fig. 9A). Very few euhedral platelets coexist with the granular mass at this early stage of experiments (Fig. 9B). In samples which were retrieved at a later stage of experiments, however, these euhedral crystals became the sole phase while the granular shaped phase vanished (Fig. 9C, D).

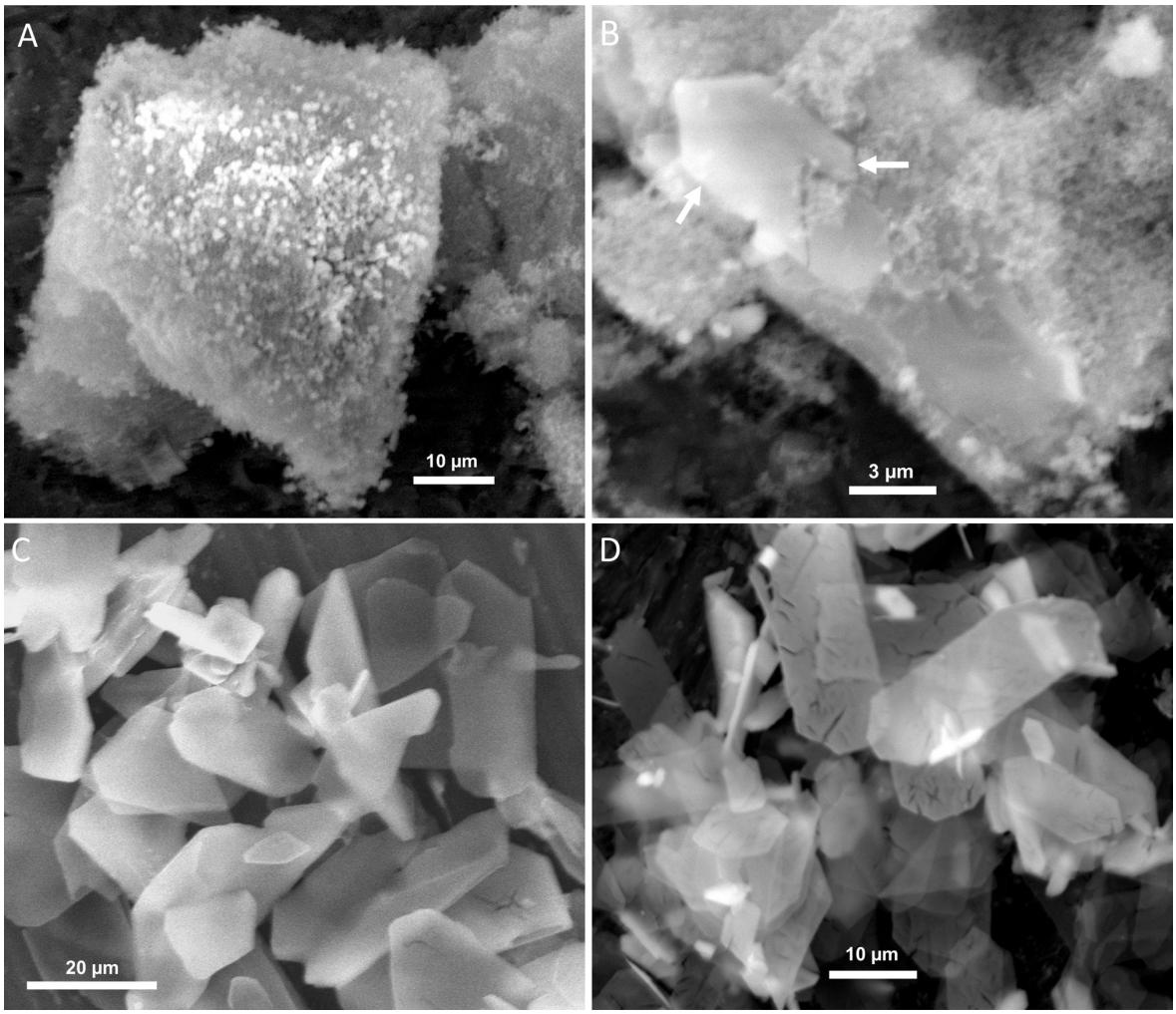

Figure 9. Cryo SEM images of precipitates retrieved from CMBR experiments (Ω_{ikaite} = 51) at different moments of desupersaturation. **A, B**) In samples retrieved within 30 s of attaining supersaturation, granular shaped fine precipitates forming larger aggregates and very few euhedral platelet-shaped crystals (white arrows in image B) were detected. **C**) Samples retrieved between 30 and 60 s of attaining supersaturation show euhedral platelet-shaped crystals exclusively. **D**) Samples retrieved after ~ 800 s of attaining supersaturation did not show any further changes in the phase inventory.

Desupersaturation of solutions and solubility of precipitated phases

The evolution of pH during precipitation from supersaturated solution led to a reproducible curve shape in pH vs. time graphs (Fig. 10). The pH values were plotted from the moment of addition of the carbonate containing solution to the Ca^{2+} solution within the reactor (0 s). Upon addition, the pH value increased for a few seconds until the two solutions were homogeneously mixed within the reactor. In the subsequent period, the curve approached a constant pH until nucleation of any carbonate containing phase consumed alkaline solutes which then resulted in a decrease of solution pH. The end of the precipitation process within the reactor is marked by the two electrodes attaining constant values. These values then reflect that the composition of solution within the reactor reached the solubility of the precipitated phase. Comparisons of solution composition are compiled in Tables 3–5. From the data, the solubility constant for ikaite (T = 0 °C) can be derived:

$$\log K_{sp\,\mathrm{ikaite}} = -7.3 \pm 0.1$$

This value agrees well with the value $\log K_{sp\,\mathrm{ikaite}} = -7.2$ reported by Bischoff et al. (1993a). The solubility constant of Bischoff et al. (1993a) is most appropriate for comparison because it was derived from experiments at temperatures down to 0.3 °C.

Desupersaturation curves originating from pseudohomogeneous precipitation matched with those recorded in presence of quartz or mica at supersaturations $\Omega_{\mathrm{ikaite}} \geq 15$ and show the decrease of pH due to fast ikaite formation (Fig. 10B). In more diluted solutions, however, the pH evolutions in substrate-free experiments (Table 2, exp. # 1, 4, 7, 10, 13) were different compared to experiments that contain quartz or mica (Table 2, exp. # 2, 3, 5, 6, 8, 9, 11, 12, 14, 15). The pH evolution in the substrate-free runs showed a significantly extended induction time. Furthermore, pH approached a constant value which was lower compared to experiments with quartz or mica substrates. Correspondingly, precipitates retrieved from substrate equipped reactors were calcite and vaterite instead of ikaite. Noteworthy, desupersaturation curves of solutions in presence of quartz compared to mica did not show a significantly different pH evolution.

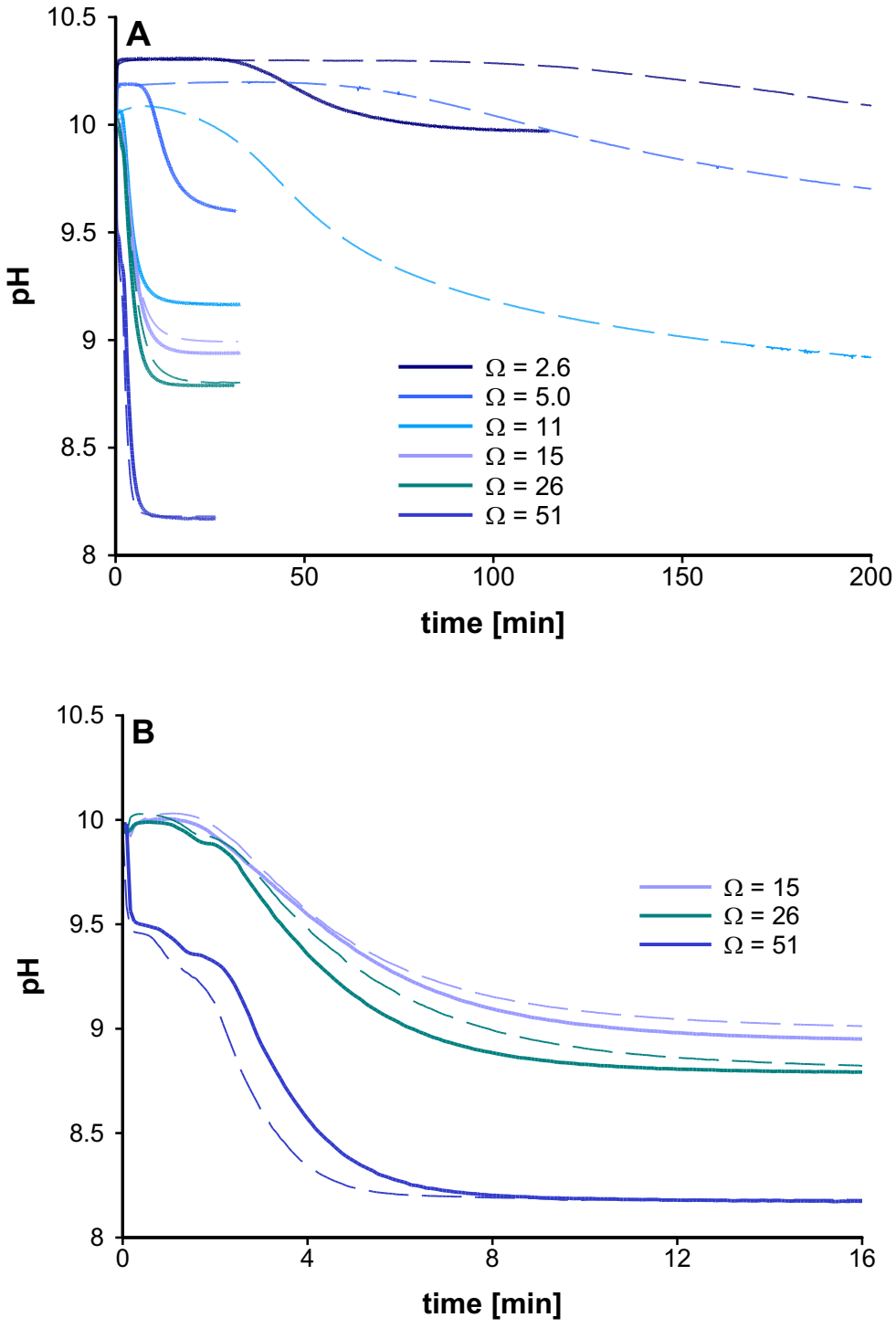

Figure 10. A) Desupersaturation curves from CMBR experiments in presence of quartz substrates (solid lines) and at pseudohomogeneous conditions (dotted lines). **B**) Zoom into desupersaturation curves of (A). The curves shown are from experiments with supersaturations with respect to ikaite Ω_{ikaite} = 15, 26, and 51.

A further detail in the desupersaturation curves needs to be pointed out: In all experiments with a supersaturation $\Omega_{ikaite} \geq 18$ (irrespectively of the presence of substrates), the decrease of supersaturation caused by nucleating/growing carbonate phases was coming to a temporary halt or slow-down resulting in a kink in the shape of the desupersaturation curves (labelled with arrows in Fig. 11). The halt or slow-down typically took place ca. 1 min after the start of desupersaturation and lasted for less than a minute until eventually desupersaturation continued. The phenomenon was clearly detectable in both the pH-value and the Ca^{2+} concentration resulting from the potential of the Ca^{2+}-ISE (Fig. 11).

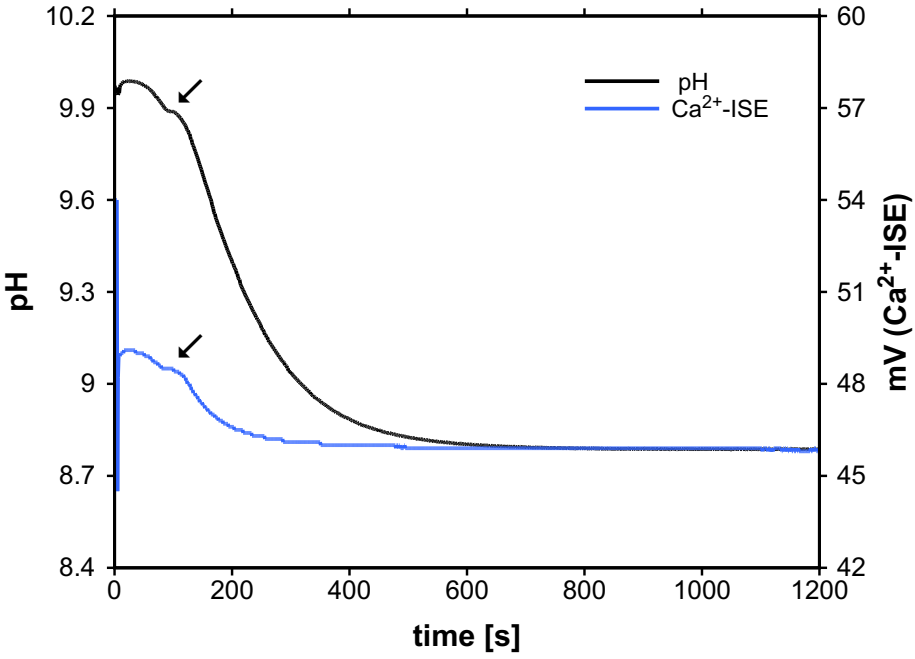

Figure 11. Desupersaturation curves (pH and Ca^{2+}-ISE-potential) from an CMBR experiment with an initial degree of supersaturation $\Omega_{ikaite} = 26$. After an initial decrease of pH and mV, the signals remained constant for a few seconds (arrows) until desupersaturation continued.

Induction periods of ikaite formation (t_{ind}) and interfacial energy γ

In our study, induction periods for ikaite formation were obtained from desupersaturation curves in experiments covering the range $1.6 \leq \Omega_{ikaite} \leq 15$. At supersaturations $\Omega_{ikaite} \geq 18$, the occurrence of an amorphous phase along with the kinky shape of the desupersaturation curves disabled determination of t_{ind} for ikaite. Table 2 shows the results of all t_{ind} values for ikaite precipitation as a function of solution conditions in absence and presence of quartz or mica.

Induction periods of ikaite formation t_{ind} were plotted versus the reciprocal square of the logarithm of the supersaturation with respect to ikaite $(\log \Omega)^{-2}$ (Fig. 12). As shown in Figure 12A, separate linear regressions within two different supersaturation ranges (above and below $\log^{-2} \Omega = 1.23$) provide good fits to our data. The interfacial energy γ between a spherical ikaite nuclei ($\beta = 16\pi/3$) and solution was calculated using the slope B from data at $\log^{-2} \Omega \leq 1.23$. In this range of supersaturations, t_{ind} was not significantly affected by the presence or absence of quartz or mica. Both types of experiments yielded slopes of

$0.68 \leq B \leq 0.73$ (Fig. 12B). A value of 15 ± 3 mJ/m² resulted for the effective interfacial energy by using all experimental data (with and without substrates).

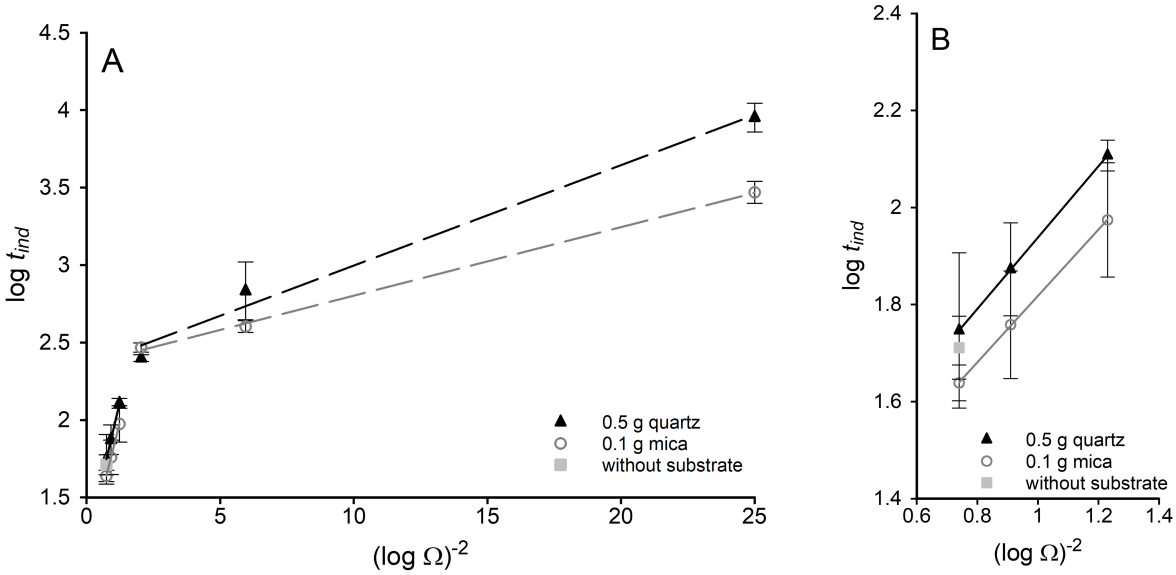

Figure 12. Plot of log t_{ind} vs. (log Ω)$^{-2}$ for ikaite formation in absence (grey squares) and presence of quartz (black triangles) and mica (open circles) substrates, respectively. **A**) Two dashed lines represent linear regressions of the data obtained in experiments with $\log^{-2} \Omega_{ikaite} > 1.23$ ($B_{mica} = 0.04$ and $B_{quartz} = 0.06$). **B**) Enlarged illustration of the data obtained at $\log^{-2} \Omega_{ikaite} \leq 1.23$. The lines represent linear regressions of the respective data points.

The regression of t_{ind} at $\log^{-2} \Omega > 1.23$ indicates a decreased interfacial energy. Application of Eq. 3.11 yielded a value of 6 ± 3 mJ/m² for the interfacial energy from the regression of the combined quartz and mica data. It needs to be noted, however, that $f(\theta) = 1$ in Eq. 3.11 is only valid for homogeneous nucleation. In the case of heterogeneous nucleation, a decreased value for $f(\theta)$ leads to an increased value for the interfacial energy. At present, however, it remains unclear by how much $f(\theta)$ is reduced.

Besides interfacial energies of ikaite, those of calcite and vaterite were calculated using induction periods from CMBR experiments which led to the formation of anhydrous calcium carbonates ($\Omega_{ikaite} \leq 11$). These calculations are both based on 15 induction periods which were determined for five different supersaturations in absence of mineral substrates (Table 2, exp. # 1, 4, 7, 10, 13) (Fig. 13). By using the same experimental t_{ind} values for both phases, inserting individual values for the molar volume of calcite and vaterite, respectively, and taking into account the respective supersaturations, Eq. 3.11 yielded a value of 58 ± 3 mJ/m² for $\gamma_{calcite}$ and 35 ± 3 mJ/m² for $\gamma_{vaterite}$.

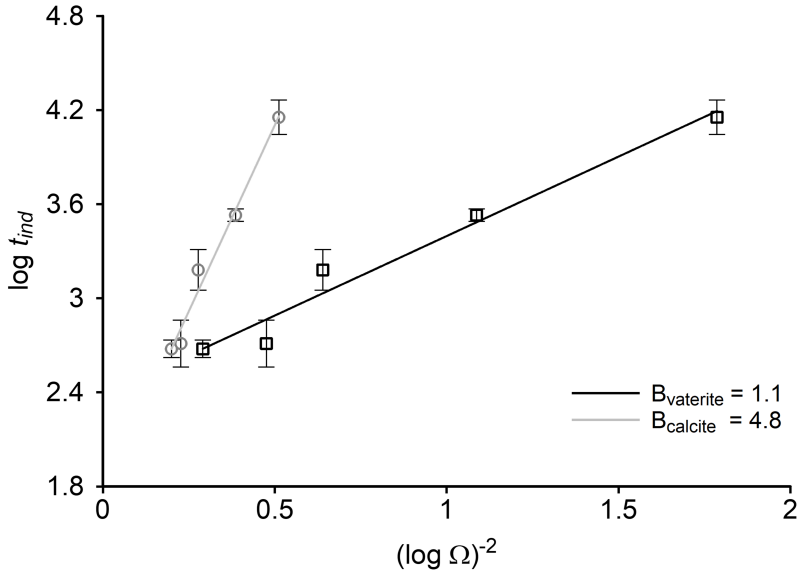

Figure 13. Plot of log t_{ind} vs. (log Ω)$^{-2}$ for calcite/vaterite formation in absence of mineral substrates.

4.1.2 Discussion

Formation conditions of ikaite

In substrate-free experiments with a supersaturation $\Omega_{ikaite} \leq 11$ (pH ≈ 10.0), no ikaite but calcite and vaterite precipitated at T = 0 °C. Ikaite precipitation was observed in substrate-free solutions with higher supersaturations instead. This finding agrees well with previously reported inhibitor-free formation conditions of ikaite in alkaline solutions (pH > 11) (Boch et al., 2015; Hu et al., 2015; Rodríguez-Ruiz et al., 2014).

Quartz or mica added to the reactor led to ikaite nucleation over a much broader supersaturation range than in substrate free experiments. Even in solutions with a supersaturation of Ω_{ikaite} = 1.6, promotion of ikaite formation by quartz or mica surpassed any possible promotion of the formation of anhydrous phases. Similarly strong effects leading to the nucleation of ikaite rather than anhydrous calcium carbonate minerals were previously attributed to calcite-inhibiting additives like Mg^{2+} and phosphate exclusively (e.g. Hu et al., 2015; Stockmann et al., 2018; Tollefsen et al., 2018). Our results, though, show that the presence of mineral surfaces in general play an important role for ikaite formation. A comprehensive understanding of the ikaite formation conditions in natural settings, therefore, requires consideration not only of the presence of calcite-inhibiting substances but also of the presence or absence of mineral surfaces capable of promoting heterogeneous nucleation of ikaite.

The occurrence of an amorphous phase at elevated Ω_{ikaite}

At elevated supersaturations ($\Omega_{ikaite} \geq 15$), ikaite formation was largely unaffected by the presence or absence of quartz or mica substrates. According to the classical nucleation theory (Kashchiev and van Rosmalen, 2003; Mullin, 2001; Sangwal, 2007), such a behaviour is not uncommon and may be explained with (pseudo-)homogeneous or volume nucleation in which the rate of nucleation within the bulk solution is so fast that substrate induced nuclei do not any longer contribute to the overall nucleation rate significantly. In this type of experiments, desupersaturation of the solution caused by ikaite nucleation and growth was characterized by a continuous decrease of pH-value and Ca^{2+}-concentration (i.e. potential of Ca^{2+}-ISE). However, the range of experimental starting conditions, which led to such a continuous decrease of pH and Ca^{2+}-concentration, was narrow. In experiments starting at supersaturations $\Omega_{ikaite} \geq 18$, desupersaturation curves revealed a kinky shape by a temporary halt or slow-down of proton release and Ca^{2+}-consumption (Fig. 10). This implies a transient stop or retardation of total calcium carbonate precipitation within the reactor and, therefore, a modified mechanism of carbonate precipitation within the reactor. In fact, the phases detected in the precipitates of these experiments depended on the time when the precipitate was retrieved from the reactor. In experiments running for > 30 s, ikaite was detected (as in the case of experiments started at $\Omega_{ikaite} < 18$). X-ray analyses of precipitates retrieved from the reactor within the first 30 s after mixing, however, did not reveal ikaite (Table 2, exp. # 19–29). At this early stage of experiments, though, the total amount of precipitate often was too low for successful X-ray analyses. Only experiments with an initial supersaturation of at least $\Omega_{ikaite} \geq 26$ provided the necessary sample mass to detect an amorphous phase at this early stage of CMBR experiments. Cryo SEM provided more detailed information about the phase inventory of precipitates from this early stage of CMBR experiments ($\Omega_{ikaite} = 51$). The SEM images revealed significant amounts of amorphous phase besides very few ikaite crystals. As all experiments in the supersaturation range $18 \leq \Omega_{ikaite} \leq 51$ show comparable kink shapes in the pH and Ca^{2+}-concentration curves, an initial presence of an amorphous phase must be inferred at least for this entire saturation range.

A similar evolution of desupersaturation curves for the precipitation of ikaite from alkaline solutions at elevated Ω_{ikaite} was reported by Zou et al. (2018). These authors state that an amorphous calcium carbonate phase was formed instantaneously while pH and potential of Ca^{2+}-ISE reached a constant value before a subsequent decrease of both pH and Ca^{2+}-concentration indicated rapid nucleation and growth of ikaite. Our findings are further corroborated by Besselink et al. (2017) who observed the formation of an amorphous calcium carbonate precursor which likely started disappearing during the crystallization of ikaite in a highly supersaturated solution at low temperatures (2–12 °C). Despite these observations at conditions different to ours, evidence for the ikaite formation mechanism in the presence of an amorphous phase valid over the entire range of conditions is missing still. At least at the conditions applied here, the coexistence of the amorphous phase and ikaite shown in cryo SEM images (Fig. 9B) implies that ikaite nucleates independently of the amorphous phase.

Interfacial energy and the effect of substrates

The effect of quartz and mica on the formation of ikaite was pronounced at supersaturations $\Omega_{ikaite} < 15$ as these minerals controlled the nucleating phase. In classical nucleation theory (CNT), this control is attributed to the interfacial energy which is reduced by foreign surfaces leading to a lower nucleation barrier. Therefore, interfacial energy is an essential quantity revealing the effect of foreign surfaces on nucleation. Our data were permissive of estimating the effective interfacial energy of ikaite from experimentally determined induction periods t_{ind} by applying CNT. In general, CNT had been used to discuss the various complex pathways of calcium carbonate nucleation (e.g. De Yoreo et al., 2013; Gómez-Morales et al., 1996; Hamm et al., 2014; Hu et al., 2012; Li et al., 2014; Lioliou et al., 2007; Söhnel and Mullin, 1978). Judging by these studies, CNT may provide a useful approach to an interpretation of nucleation kinetics, even if nucleation pathways are diverse and do not completely agree with a classical description of nucleation (van Driessche et al., 2019).

According to CNT, a linear relationship between log t_{ind} and $\log^{-2} \Omega_{ikaite}$ marks a range of experimental conditions, in which the interfacial energy of ikaite and, therefore, the nucleation mechanism is supposed to be constant. Experimental log t_{ind} vs. $\log^{-2}\Omega$ data often reveal two different linear ranges (e.g. He et al., 1994; Lancia et al., 1999; Söhnel and Mullin, 1978): at low values of $\log^{-2}\Omega$ with a high interfacial energy and vice versa. The high energy relates to homogeneous nucleation whereas the low energy points towards heterogeneous nucleation. The log t_{ind} vs. $\log^{-2} \Omega_{ikaite}$ data derived from our experiments obviously also reveal two ranges with linear relationships (Fig. 12A): *i*) $\Omega_{ikaite} \geq 8$ ($\log^{-2} \Omega_{ikaite} \leq 1.23$) and *ii*) $\Omega_{ikaite} \leq 5$ ($\log^{-2} \Omega_{ikaite} \geq 2$).

In the higher supersaturation range (*i*), an effective interfacial energy of 15 ± 3 mJ/m² was obtained by assuming homogeneously formed nuclei (i.e. correction factor $f(\theta) = 1$) with a spherical shape (i.e. shape factor $\beta = 16\pi/3$) (Mullin, 2001; Söhnel and Mullin, 1988). In the low range of supersaturation (*ii*), ikaite was only forming, if minerals were present in the reactor. A value of 6 ± 3 mJ/m² resulted for the interfacial energy in this range. For the calculation, the same shape and correction factors as above were used. This low interfacial energy supports the assumption that heterogeneous nucleation dominated range (*ii*). As mentioned above, however, a lower correction factor (e.g. Söhnel and Handlířová, 1984) may lead to a higher interfacial energy. This may limit the applicability of Eqs. 3.9–3.11 for the interpretation of our data. Also, the transition between the two linear ranges of log t_{ind} vs. $\log^{-2}\Omega$ data located between $5 \leq \Omega_{ikaite} \leq 8$ does not precisely coincide with our observation that ikaite nucleates from solutions with $\Omega_{ikaite} < 15$ solely in presence of quartz or mica. At this point, applicability of CNT interpreting our experimental data obviously reaches its limitation.

Our result of 15 ± 3 mJ/m² for γ_{ikaite} is remarkably low compared to reported interfacial energies between nuclei of anhydrous calcium carbonates and solution. Söhnel and Mullin (1978) determined a theoretical value of $\gamma_{CaCO_3} = 124$ mJ/m² and an experimental value of 83 mJ/m². Lower values of interfacial energies of calcite (e.g. $\gamma = 64$ mJ/m², Lioliou et al., 2007) and vaterite (e.g. $\gamma = 37$ mJ/m², Verdoes et al., 1992; $\gamma = 41$ mJ/m², Gómez-Morales et al., 1996)

have also been reported and were attributed to some degree of heterogeneous nucleation. The latter interfacial energies well agree with our values of $\gamma_{vaterite}$ = 35 ± 3 mJ/m² and $\gamma_{calcite}$ = 58 ± 3 mJ/m² for pseudohomogeneous nucleation. Li et al. (2014) reported interfacial energies with values between 47 and 24 mJ/m² for vaterite and calcite nuclei on quartz and mica substrates. The results of Li et al. (2014) imply that quartz and mica substrates may contribute to the formation of anhydrous $CaCO_3$ phases by decreasing the interfacial energy of nuclei.

Two points should be noted here. Firstly, our values for γ_{ikaite} (irrespectively of the presence or absence of mineral substrates) are significantly lower compared to the values of anhydrous $CaCO_3$ phases. This clearly reflects the highly hydrated character of the ikaite structure involving predominantly weak hydrogen bonds at the interface. Secondly, the value of interfacial energy within the lower supersaturation range is not reduced by much (from 15 to 6 mJ/m²). This may indicate that the contribution of the ikaite-substrate interface to the reduction of the nucleation barrier is less compared to the contribution of interfaces between anhydrous calcium carbonates and substrates. This low interfacial contribution to ikaite formation might as well be associated with its highly hydrated character and might reflect the low energy formation pathway of ikaite nucleation as suggested by Chaka (2018) via an assemblage of aqueous $CaCO_3^0 \cdot 6H_2O$ ion pair complexes. Substrates, in this case, would promote an accumulation of the hydrous pair complexes rather than a dehydration of aqueous ionic complexes – as it is the case for nucleation of anhydrous phases. The similar degree of promotion of ikaite nucleation by mica and quartz might indicate that the similar surface chemical characteristics of these two minerals affect heterogeneous nucleation much stronger than their different surface structural characteristics. This finding contrasts with the effects of quartz and mica on anhydrous $CaCO_3$ nuclei which were assumed being dependent on the degree of lattice fit (Li et al., 2014). In the range of conditions examined here, one might speculate that the velocity of structural ordering of adsorbed complexes at the interface is not the rate determining step for heterogeneous ikaite nucleation. At Ω_{ikaite} = 1.6, the similarity of the promotion by mica and quartz weakens. The experimental approach of this study, however, is inapt to test whether the dissimilarity becomes significant at Ω_{ikaite} < 1.6. At such low supersaturations, the induction periods rise to many hours or even days. Within these long periods, artefacts due to unavoidable impurities within the reactor cannot be excluded any longer.

From our results it can be suggested that the phase formation kinetics at cold temperatures is controlled by the condition whether solutes are required to dehydrate or not. Because the formation rate of the amorphous phase in our experiments is at least as fast as the ikaite formation rate, it must be hypothesized that the amorphous phase is highly hydrated as well. Such a highly hydrated phase would agree with an extensive polyamorphism of calcium carbonate which involves varying water contents (Cartwright et al., 2012). The formation rate of a lowly hydrated phase may not compete with the formation rate of ikaite at temperatures close to the freezing point of water. A lowly hydrated amorphous phase, though, might form via

a dehydration of $CaCO_3 \cdot 6H_2O$ phases (Addadi et al., 2003; Tlili et al., 2002). Subsequently, such a lowly hydrated phase may lead to anhydrous calcium carbonates (Besselink et al., 2017; Radha et al., 2010).

Table 2. Precipitates and induction periods of formation as a function of solution conditions. Activities and supersaturations (Ω) were calculated using PHREEQC (Parkhurst and Appelo, 2013) and correspond to the initial state of mixed solutions.

Experiment		**solution speciation**[a]					**saturation state**[a]					**precipitates and t_{ind}**	
exp no	substrate	pH	$a_{Ca^{2+}}$ [mM]	$a_{HCO_3^-}$ [mM]	$a_{CO_3^{2-}}$ [mM]	$a_{CaCO_3^0}$ [mM]	$\boldsymbol{\Omega_{ikaite}}$	$\boldsymbol{\log^{-2}\Omega_{ikaite}}$	Ω_{CC}[b]	Ω_{VA}[b]	Ω_{ACC}[b]	phase[b]	t_{ind} [s]
1.1	none	10.18	0.55	0.52	0.19	0.13	**1.6**	**24**	25	6	0.16	CC, VA	15470
1.2	none	"	"	"	"	"	"	"	"	"	"	CC, VA	10220
1.3	none	"	"	"	"	"	"	"	"	"	"	CC	18370
2.1	0.5 g quartz	"	"	"	"	"	"	"	"	"	"	IK	6765
2.2	0.5 g quartz	"	"	"	"	"	"	"	"	"	"	IK	9365
2.3	0.5 g quartz	"	"	"	"	"	"	"	"	"	"	IK	11365
3.1	0.1g mica	"	"	"	"	"	"	"	"	"	"	IK	3485
3.2	0.1g mica	"	"	"	"	"	"	"	"	"	"	IK	2365
3.3	0.1g mica	"	"	"	"	"	"	"	"	"	"	IK	3110
4.1	none	10.16	0.71	0.68	0.23	0.21	**2.6**	**6**	41	9	0.26	CC, VA	3585
4.2	none	"	"	"	"	"	"	"	"	"	"	CC, VA	3240
4.3	none	"	"	"	"	"	"	"	"	"	"	CC, VA	3360
5.1	0.5 g quartz	"	"	"	"	"	"	"	"	"	"	IK	1222
5.2	0.5 g quartz	"	"	"	"	"	"	"	"	"	"	IK	589
5.3	0.5 g quartz	"	"	"	"	"	"	"	"	"	"	IK	440
6.1	0.1 g mica	"	"	"	"	"	"	"	"	"	"	IK	420
6.2	0.1 g mica	"	"	"	"	"	"	"	"	"	"	IK	433
6.3	0.1 g mica	"	"	"	"	"	"	"	"	"	"	IK	355
7.1	none	10.12	1.02	1.01	0.32	0.42	**5**	**2**	79	18	0.51	CC, VA	1630
7.2	none	"	"	"	"	"	"	"	"	"	"	CC, VA	1020
7.3	none	"	"	"	"	"	"	"	"	"	"	CC, VA	2100
8.1	0.5 g quartz	"	"	"	"	"	"	"	"	"	"	IK	269
8.2	0.5 g quartz	"	"	"	"	"	"	"	"	"	"	IK	238
8.3	0.5 g quartz	"	"	"	"	"	"	"	"	"	"	IK	246
9.1	0.1 g mica	"	"	"	"	"	"	"	"	"	"	IK	269
9.2	0.1 g mica	"	"	"	"	"	"	"	"	"	"	IK	294
9.3	0.1 g mica	"	"	"	"	"	"	"	"	"	"	IK	319
10.1	none	10.09	1.30	1.34	0.39	0.65	**8**	**1.23**	126	28	0.81	CC, VA	363
10.2	none	"	"	"	"	"	"	"	"	"	"	CC, VA	455
10.3	none	"	"	"	"	"	"	"	"	"	"	CC, VA	825

Table 2 (continued)

Experiment		solution speciation[a]					saturation state[a]					precipitates and t_{ind}	
exp no	substrate	pH	$a_{Ca^{2+}}$ [mM]	$a_{HCO_3^-}$ [mM]	$a_{CO_3^{2-}}$ [mM]	$a_{CaCO_3^0}$ [mM]	Ω_{ikaite}	$\log^{-2}\Omega_{ikaite}$	Ω_{CC}[b]	Ω_{VA}[b]	Ω_{ACC}[b]	phase[b]	t_{ind} [s]
11.1	0.5 g quartz	"	"	"	"	"	"	"	"	"	"	IK	138
11.2	0.5 g quartz	"	"	"	"	"	"	"	"	"	"	IK	131
11.3	0.5 g quartz	"	"	"	"	"	"	"	"	"	"	IK	116
12.1	0.1 g mica	"	"	"	"	"	"	"	"	"	"	IK	138
12.2	0.1 g mica	"	"	"	"	"	"	"	"	"	"	IK	81
12.3	0.1 g mica	"	"	"	"	"	"	"	"	"	"	IK	75
13.1	none	10.07	1.57	1.66	0.45	0.92	**11**	**0.92**	174	40	1.1	CC, VA	429
13.2	none	"	"	"	"	"	"	"	"	"	"	CC, VA	440
13.3	none	"	"	"	"	"	"	"	"	"	"	CC, VA	570
14.1	0.5 g quartz	"	"	"	"	"	"	"	"	"	"	IK	92
14.2	0.5 g quartz	"	"	"	"	"	"	"	"	"	"	IK	55
14.3	0.5 g quartz	"	"	"	"	"	"	"	"	"	"	IK	82
14.4	5 g quartz	"	"	"	"	"	"	"	"	"	"	IK	130
14.5	10 g quartz	"	"	"	"	"	"	"	"	"	"	IK	114
15.1	0.1 g mica	"	"	"	"	"	"	"	"	"	"	IK	46
15.2	0.1 g mica	"	"	"	"	"	"	"	"	"	"	IK	82
15.3	0.1 g mica	"	"	"	"	"	"	"	"	"	"	IK	50
15.4	5 g mica	"	"	"	"	"	"	"	"	"	"	IK	51
15.5	10 g mica	"	"	"	"	"	"	"	"	"	"	IK	45
16.1	none	10.04	1.83	1.97	0.51	1.2	**15**	**0.72**	229	51	1.5	IK	43
16.2	none	"	"	"	"	"	"	"	"	"	"	IK	51
16.3	none	"	"	"	"	"	"	"	"	"	"	IK	62
17.1	0.5 g quartz	"	"	"	"	"	"	"	"	"	"	IK	94
17.2	0.5 g quartz	"	"	"	"	"	"	"	"	"	"	IK	43
17.3	0.5 g quartz	"	"	"	"	"	"	"	"	"	"	IK	43
18.1	0.1 g mica	"	"	"	"	"	"	"	"	"	"	IK	39
18.2	0.1 g mica	"	"	"	"	"	"	"	"	"	"	IK	48
18.3	0.1 g mica	"	"	"	"	"	"	"	"	"	"	IK	44
19.1	none	10.02	2.07	2.29	0.56	1.5	**18**	**0.63**	288	65	1.9	IK	N/A
19.2	none	"	"	"	"	"	"	"	"	"	"	IK	N/A
19.3	none	"	"	"	"	"	"	"	"	"	"	IK	N/A
20.1	0.5 g quartz	"	"	"	"	"	"	"	"	"	"	IK	N/A
20.2	0.5 g quartz	"	"	"	"	"	"	"	"	"	"	IK	N/A
20.3	0.5 g quartz	"	"	"	"	"	"	"	"	"	"	IK	N/A
21.1	0.1 g mica	"	"	"	"	"	"	"	"	"	"	IK	N/A
21.2	0.1 g mica	"	"	"	"	"	"	"	"	"	"	IK	N/A
21.3	0.1 g mica	"	"	"	"	"	"	"	"	"	"	IK	N/A

Table 2 (continued)

Experiment		solution speciation[a]					saturation state[a]					precipitates and t_{ind}	
exp no	substrate	pH	$a_{Ca^{2+}}$ [mM]	$a_{HCO_3^-}$ [mM]	$a_{CO_3^{2-}}$ [mM]	$a_{CaCO_3^0}$ [mM]	Ω_{ikaite}	$\log^{-2}\Omega_{ikaite}$	Ω_{CC}[b]	Ω_{VA}[b]	Ω_{ACC}[b]	phase[b]	t_{ind} [s]
22.1	none	10.00	2.31	2.60	0.61	1.81	**22**	**0.55**	347	78	2.2	IK	N/A
22.2	none	"	"	"	"	"	"	"	"	"	"	IK	N/A
22.3	none	"	"	"	"	"	"	"	"	"	"	IK	N/A
23.1	0.5 g quartz	"	"	"	"	"	"	"	"	"	"	IK	N/A
23.2	0.5 g quartz	"	"	"	"	"	"	"	"	"	"	IK	N/A
23.3	0.5 g quartz	"	"	"	"	"	"	"	"	"	"	IK	N/A
24.1	0.1 g mica	"	"	"	"	"	"	"	"	"	"	IK	N/A
24.2	0.1 g mica	"	"	"	"	"	"	"	"	"	"	IK	N/A
24.3	0.1 g mica	"	"	"	"	"	"	"	"	"	"	IK	N/A
25.1	none	9.98	2.53	2.91	0.66	2.13	**26**	**0.50**	407	91	2.6	IK	N/A
25.2	none	"	"	"	"	"	"	"	"	"	"	IK	N/A
25.3	none	"	"	"	"	"	"	"	"	"	"	IK	N/A
26.1	0.5 g quartz	"	"	"	"	"	"	"	"	"	"	IK	N/A
26.2	0.5 g quartz	"	"	"	"	"	"	"	"	"	"	IK	N/A
26.3	0.5 g quartz	"	"	"	"	"	"	"	"	"	"	IK	N/A
27.1	0.1 g mica	"	"	"	"	"	"	"	"	"	"	IK	N/A
27.2	0.1 g mica	"	"	"	"	"	"	"	"	"	"	IK	N/A
27.3	0.1 g mica	"	"	"	"	"	"	"	"	"	"	IK	N/A
28.1	none	9.90	3.77	4.70	0.87	4.20	**51**	**0.34**	794	182	5	IK	N/A
28.2	none	"	"	"	"	"	"	"	"	"	"	IK	N/A
28.3	none	"	"	"	"	"	"	"	"	"	"	IK	N/A
29.1	0.5 g quartz	"	"	"	"	"	"	"	"	"	"	IK	N/A
29.2	0.5 g quartz	"	"	"	"	"	"	"	"	"	"	IK	N/A
29.3	0.5 g quartz	"	"	"	"	"	"	"	"	"	"	IK	N/A

[a] solution speciation and saturation were calculated using PHREEQC (Parkhurst and Appelo, 2013).

[b] CC: calcite, VA: vaterite, IK: ikaite, ACC: amorphous calcium carbonate.

Table 3. Analyses of solutions of CMBR experiments in presence of **0.5 g quartz**. Reported values of alkalinity and Ca^{2+} concentration were determined by titration. Solution speciations and solubility products were calculated from these analyses using PHREEQC (Parkhurst and Appelo, 2013).

experiment			**analyses of solution**			**solution speciation**[a]				**solubility product**
exp no	substrate	elapsed time [s]	pH	alkalinity [meq/L]	$c_{Ca^{2+}}$ [mM]	$a_{Ca^{2+}}$ [mM]	$a_{HCO_3^-}$ [mM]	$a_{CO_3^{2-}}$ [mM]	$a_{CaCO_3^0}$ [mM]	log K_{sp} (IK)[b]
2.1	**0.5 g quartz**	60000	9.96	1.88	1.42	0.54	0.58	0.13	0.09	–7.18
2.2	"	72500	9.99	2.03	1.52	0.57	0.60	0.14	0.10	–7.12
2.3	"	26350	10.05	1.37	0.97	0.37	0.39	0.10	0.05	–7.43
5.1	"	3500	9.95	2.14	1.30	0.49	0.67	0.14	0.09	–7.17
5.2	"	3500	10.00	2.01	1.02	0.38	0.61	0.14	0.07	–7.27
5.3	"	7000	9.97	1.94	1.48	0.56	0.59	0.13	0.09	–7.15
8.2	"	2000	9.57	2.06	1.66	0.64	0.93	0.08	0.07	–7.30
8.3	"	2000	9.60	2.15	1.55	0.59	0.95	0.09	0.07	–7.29
11.1	"	2000	9.40	1.98	2.16	0.83	0.97	0.06	0.06	–7.33
11.2	"	2000	9.34	2.04	2.24	0.87	1.04	0.05	0.06	–7.34
11.3	"	2000	9.33	1.90	2.35	0.91	0.97	0.05	0.06	–7.36
14.1	"	3000	9.10	2.27	2.95	1.14	1.26	0.04	0.05	–7.38
14.2	"	3000	9.13	2.67	2.43	0.93	1.49	0.05	0.06	–7.37
17.1	"	2000	9.11	2.85	2.78	1.06	1.58	0.05	0.07	–7.30
17.2	"	2000	8.92	3.67	3.04	1.16	2.15	0.04	0.06	–7.32
17.3	"	2000	8.94	2.80	3.04	1.17	1.63	0.03	0.05	–7.42
20.1	"	2000	8.98	3.85	3.51	1.32	2.20	0.05	0.08	–7.19
20.2	"	2000	8.97	3.69	3.70	1.40	2.10	0.05	0.08	–7.20
20.3	"	2000	9.00	3.91	3.39	1.28	2.22	0.05	0.09	–7.18
23.1	"	2000	8.81	4.33	4.03	1.51	2.56	0.04	0.08	–7.24
23.2	"	2000	8.84	4.33	3.97	1.49	2.54	0.04	0.08	–7.21
26.1	"	2000	8.79	4.59	4.35	1.63	2.71	0.04	0.08	–7.20
26.2	"	2000	8.79	4.50	4.46	1.67	2.65	0.04	0.08	–7.20
26.3	"	2000	8.81	4.61	4.37	1.63	2.70	0.04	0.09	–7.18

[a]solution speciations were calculated from analyses of solutions using PHREEQC (Parkhurst and Appelo, 2013) together with a modified llnl database.

[b]IK: ikaite

Table 4. Analyses of solutions of CMBR experiments in presence of **0.1 g mica**. Reported values of alkalinity and Ca^{2+} concentration were determined by titration. Solution speciations and solubility products were calculated from these analyses using PHREEQC (Parkhurst and Appelo, 2013).

experiment			**analyses of solution**			**solution speciation**[a]				**solubility product**
exp no	substrate	elapsed time [s]	pH	alkalinity [meq/L]	$c_{Ca^{2+}}$ [mM]	$a_{Ca^{2+}}$ [mM]	$a_{HCO_3^-}$ [mM]	$a_{CO_3^{2-}}$ [mM]	$a_{CaCO_3^0}$ [mM]	log K_{sp} (IK)[b]
3.1	**0.1 g mica**	60000	9.95	n.d.[c]	1.13	0.43	0.49	0.10	0.06	–7.36
3.3	"	18000	10.10	1.71	1.42	0.54	0.44	0.13	0.09	–7.17
6.1	"	5400	9.72	1.49	1.47	0.57	0.59	0.07	0.05	–7.39
6.2	"	5400	9.83	1.73	1.24	0.47	0.63	0.10	0.06	–7.33
6.3	"	5800	9.78	1.86	1.46	0.56	0.70	0.10	0.07	–7.26
9.1	"	5400	9.46	1.75	1.83	0.71	0.84	0.06	0.05	–7.40
9.2	"	5400	9.46	2.08	1.86	0.72	1.00	0.07	0.06	–7.32
12.1	"	3000	9.28	2.06	2.26	0.87	1.08	0.05	0.05	–7.38
12.2	"	3400	9.37	2.40	2.37	0.91	1.20	0.07	0.08	–7.23
12.3	"	4100	9.31	2.41	2.40	0.92	1.24	0.06	0.07	–7.27
15.1	"	3000	9.04	2.83	2.26	0.87	1.63	0.04	0.05	–7.44
15.2	"	4600	9.07	2.88	2.74	1.05	1.63	0.05	0.06	–7.33
15.3	"	4400	9.07	2.86	2.82	1.08	1.61	0.04	0.06	–7.32
18.1	"	3000	8.91	3.04	3.31	1.27	1.78	0.03	0.06	–7.37
18.2	"	3000	9.00	3.03	3.21	1.22	1.73	0.04	0.06	–7.31
18.3	"	3300	9.07	3.03	3.27	1.24	1.69	0.05	0.07	–7.24
21.1	"	3000	8.75	3.54	3.53	1.34	2.14	0.03	0.05	–7.43
21.2	"	3000	8.81	3.60	3.63	1.38	2.14	0.03	0.06	–7.36
21.3	"	3000	8.81	3.35	3.74	1.42	1.99	0.03	0.06	–7.37
24.1	"	3000	8.68	4.18	4.26	1.61	2.53	0.03	0.06	–7.35
24.2	"	3000	8.68	3.75	3.99	1.51	2.28	0.03	0.05	–7.42
24.3	"	3300	8.80	3.85	4.43	1.67	2.27	0.03	0.07	–7.26
27.1	"	3000	8.57	4.56	4.62	1.73	2.79	0.02	0.05	–7.38
27.2	"	3000	8.60	3.91	4.56	1.72	2.38	0.02	0.05	–7.42
27.3	"	3300	8.62	4.33	4.66	1.75	2.63	0.03	0.06	–7.35

[a]solution speciations were calculated from analyses of solutions using PHREEQC (Parkhurst and Appelo, 2013) together with a modified llnl database.

[b]IK: ikaite

[c]n.d.: not determined. When alkalinity was not determined, it was approximated by stoichiometrically decreasing the initial alkalinity of a solution by twice of the Ca^{2+} decrease.

Table 5. Analyses of solutions of CMBR experiments in **absence of substrates**. Reported values of alkalinity and Ca^{2+} concentration were determined by titration. Solution speciation, solubility products and saturations were calculated from these analyses using PHREEQC (Parkhurst and Appelo, 2013). The dashed line subdivides experiments leading to the formation of ikaite and those showing the appearance of calcite/vaterite.

experiment			**analyses of solution**			**solution speciation**[a]				**solubility product**	**saturation**[a]	
exp no	sub-strate	elapsed time [s]	pH (end)	alkalinity [meq/L]	$c_{Ca^{2+}}$ [mM]	$a_{Ca^{2+}}$ [mM]	$a_{HCO_3^-}$ [mM]	$a_{CO_3^{2-}}$ [mM]	$a_{CaCO_3^0}$ [mM]	log K_{sp} (IK)[b]	Ω calcite	Ω vaterite
4.1	**none**	80000	9.52	n.d.[c]	1.26	0.49	0.74	0.06	0.04	n.d.	7.0	1.6
4.2	"	25000	9.17	n.d.[c]	1.40	0.55	1.04	0.04	0.03	n.d.	4.9	1.1
7.2	"	80000	9.13	n.d.[c]	1.79	0.92	1.15	0.04	0.05	n.d.	6.6	1.5
10.1	"	80000	9.15	n.d.[c]	2.15	0.85	0.47	0.02	0.02	n.d.	3.3	0.7
13.1	"	65000	8.76	n.d.[c]	2.65	1.04	0.82	0.01	0.01	n.d.	2.8	0.6
13.2	"	80000	8.86	n.d.[c]	2.74	1.06	1.81	0.03	0.04	n.d.	8.0	1.8
16.1	"	2750	8.97	2.83	3.03	1.16	1.64	0.04	0.05	−7.39	10.3	2.3
16.2	"	3900	8.99	2.87	2.84	1.09	1.66	0.04	0.05	−7.39	10.2	2.3
16.3	"	4600	8.98	2.89	3.18	1.22	1.66	0.04	0.06	−7.35	11.2	2.5
19.1	"	4000	8.85	n.d.[c]	3.24	1.24	1.80	0.03	0.05	−7.44	9.1	2.1
19.2	"	2050	8.83	n.d.[c]	3.39	1.29	1.98	0.03	0.05	−7.40	10.0	2.3
19.3	"	4800	8.91	n.d.[c]	3.49	1.32	2.05	0.04	0.07	−7.29	12.8	2.9
22.1	"	5900	8.79	3.98	3.87	1.46	2.37	0.03	0.06	−7.31	12.3	2.8
22.2	"	2500	8.77	4.06	3.73	1.41	2.43	0.03	0.06	−7.33	11.7	2.6
22.3	"	2100	8.81	4.16	3.83	1.44	2.47	0.04	0.07	−7.28	13.3	3.0
25.1	"	8000	8.81	n.d.[c]	3.88	1.47	1.95	0.03	0.06	−7.37	10.7	2.4
25.2	"	2800	8.84	n.d.[c]	4.28	1.60	2.40	0.04	0.08	−7.21	15.4	3.5
25.3	"	5200	8.69	n.d.[c]	4.43	1.66	2.65	0.03	0.07	−7.30	12.5	2.8

[a]solution speciations and saturations were calculated from analyses of solution using PHREEQC (Parkhurst and Appelo, 2013) together with a modified llnl database.

[b]IK: ikaite

[c]n.d.: not determined. When alkalinity was not determined, it was approximated by stoichiometrically decreasing the initial alkalinity of a solution.

4.2 Growth of ikaite in the presence of phosphate

4.2.1 Results

Analysis of solids

Cryo-SEM images of the synthesized ikaite seeds before growth experiments revealed a homogeneous euhedral morphology (Fig. 14a). In contrast, the seeds, which have undergone an additional subsequent temperature-induced transformation into calcite, comprise spherical and partially coalescing anhedral aggregates (Fig. 14b). After the growth experiments, these calcite aggregates remained unaltered and coexisted with euhedral ikaite crystals, which newly formed during the experiment (Fig. 14c). X-ray powder diffraction analyses of the powders retrieved from these growth experiments confirm the coexistence of calcite with a significant amount of ikaite (Fig. 15). For ikaite-seeded experiments, X-ray diffractograms of crystals retrieved from cryo-mixed-flow reactor revealed ikaite (Fig. 16). The minor traces of calcite which were detected by X-ray phase analysis of ikaite seeds ($2\theta \approx 29.45°$) had no impact on the growth rates in ikaite-seeded experiments (Ika_1–Ika_4) as they mostly reflect the artefactual transformation of ikaite in air during the time of X-ray analysis rather than the calcite formation during the experiments. Although all reactor solutions were supersaturated vs. hydroxyapatite, no sign of this phase was found by XRD.

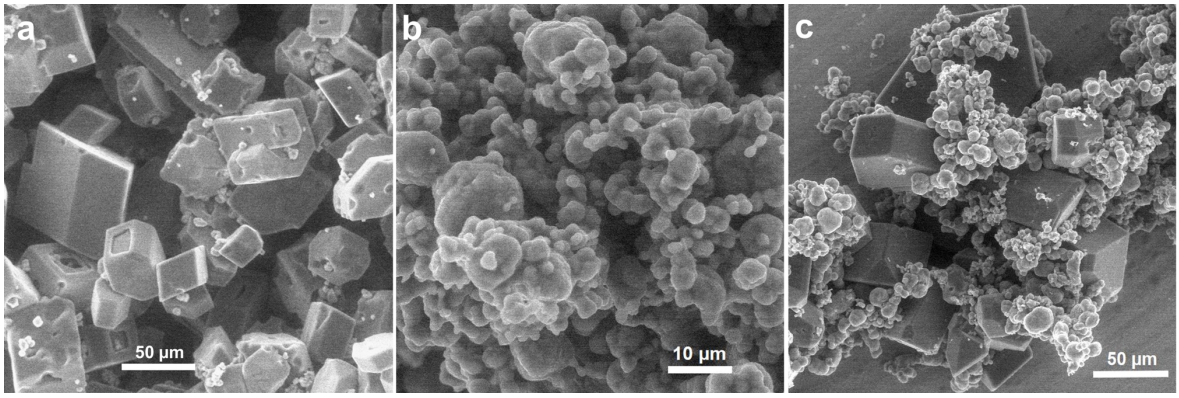

Figure 14. Cryo SEM images of synthesized seeds and crystals retrieved from CMFR experiment. **a**) Euhedral ikaite seed crystals before growth experiment. **b**) Anhedral calcite seed crystals before growth experiment. **c**) Newly formed euhedral ikaite crystals coexisting with anhedral crystals after growth experiment (Ika_15).

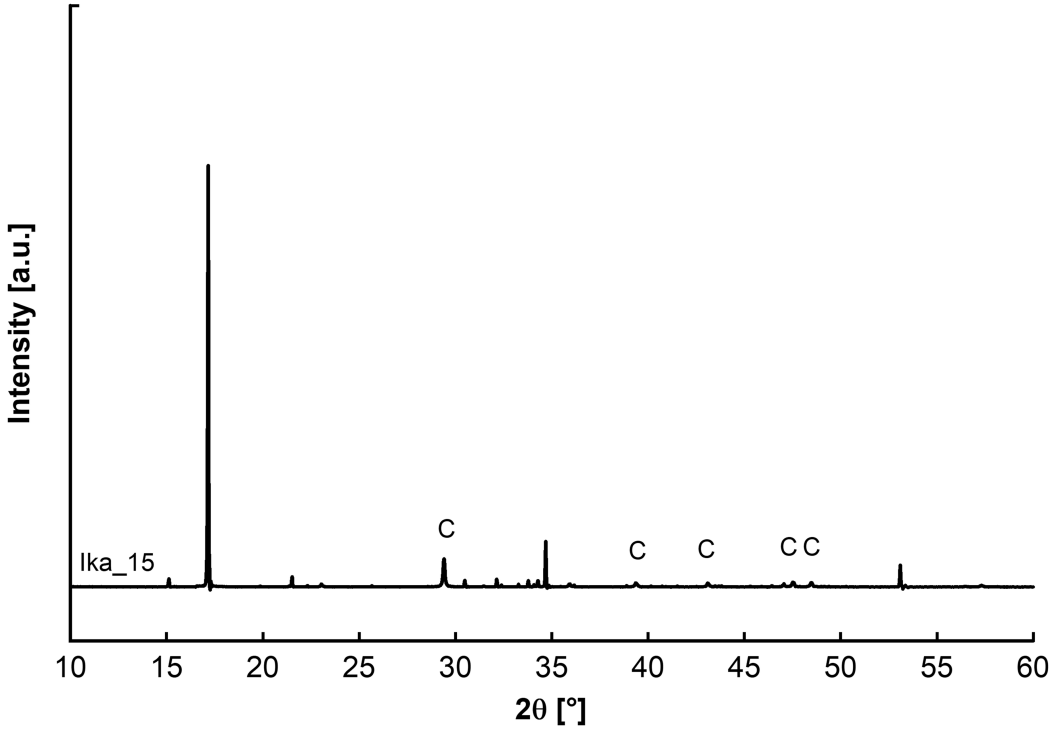

Figure 15. X-ray powder diffraction pattern (CuKα_1) of crystals retrieved from calcite-seeded growth experiment Ika_15. Diffraction peaks correspond to calcite (C) and newly formed ikaite.

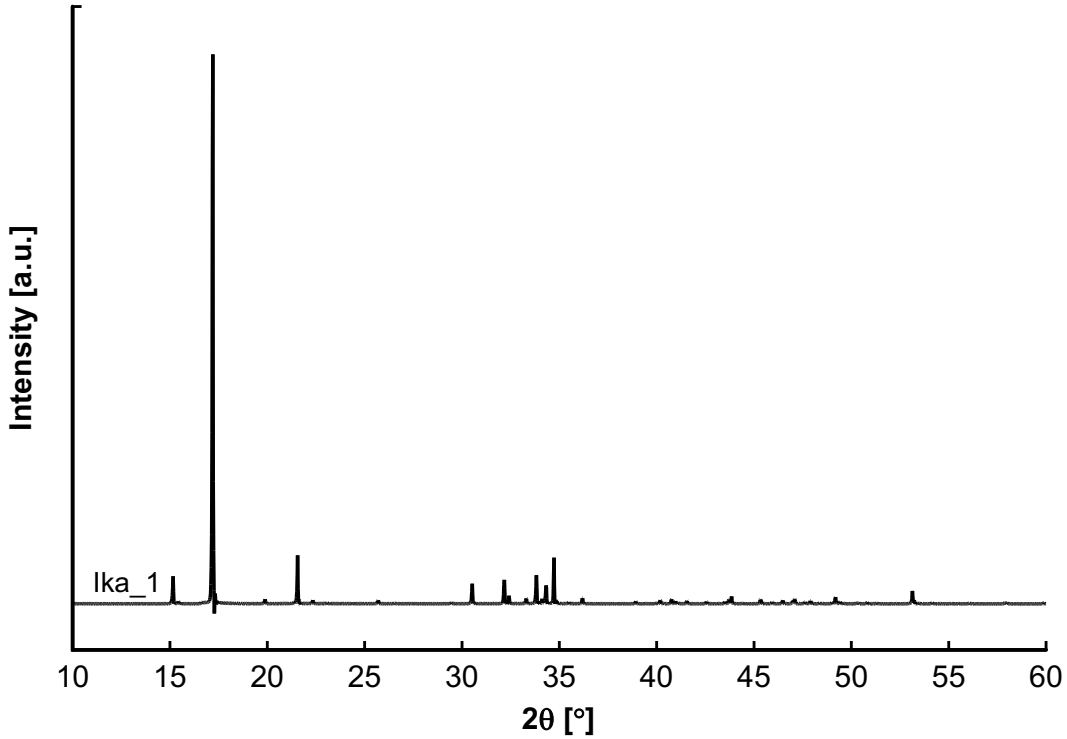

Figure 16. X-ray powder diffraction pattern (CuKα_1) of crystals retrieved from ikaite-seeded growth experiment Ika_1. Diffraction peaks correspond to ikaite.

Chemical analysis of solutions

Analyses of the inlet and outlet solutions of CMFR experiments were performed for each run and are summarized in Table 6, which reports the compositions of the effluent solutions of the reactor at steady state conditions. In all runs, the samples of the effluent revealed decreased Ca concentrations and total alkalinity relative to the corresponding inlet solutions (ΔCa and Δtotal alkalinity) indicating substantial growth within the reactor. P concentrations, in contrast, remained constant in all tested growth experiments.

Table 6. Compositions of cryo-mixed-flow reactor inlet solutions and effluent solutions at steady state conditions for the growth experiments conducted in this study.

Sample	Seed crystals	Flowrate [ml/min]	pH (25 °C)	Total alkalinity [meq/l]	Ca [mM]	P [mM]	Δ total alkalinity [meq/l]	ΔCa [mM]	ΔP [mM]	Est. A_S [cm²]	Ω_{ikaite}
Ika_1_inlet			8.64	50.58	1.518	0.190					3.8
Ika_1_1	ikaite	0.71	8.45	49.73	0.819	0.189	−0.85	−0.698	−0.001	984	1.4
Ika_1_2	"	0.71	8.48	49.68	0.817	0.195	−0.90	−0.701	0.005	984	1.5
Ika_1_3	"	0.71	8.47	49.63	0.823	0.199	−0.95	−0.695	0.009	984	1.5
Ika_2_inlet			8.49	49.76	1.303	n.d.					2.5
Ika_2_1	ikaite	0.61	8.53	n.d.[a]	0.656	n.d.	n.d.	−0.647	n.d.	984	1.3
Ika_2_2	"	0.61	8.54	48.98	0.653	n.d.	−0.78	−0.651	n.d.	984	1.3
Ika_2_3	"	0.61	8.54	49.09	0.643	n.d.	−0.67	−0.661	n.d.	984	1.3
Ika_3_inlet			8.41	46.91	4.189	n.d.					6.9
Ika_3_1	ikaite	0.82	8.25	46.27	2.252	n.d.	−0.64	−1.937	n.d.	984	2.6
Ika_3_2	"	0.82	8.26	46.31	2.224	n.d.	−0.60	−1.965	n.d.	984	2.6
Ika_4_inlet			8.25	61.71	7.329	n.d.					11
Ika_4_1	ikaite	0.77	8.28	n.d.[a]	3.456	n.d.	n.d.	−3.947	n.d.	984	4.8
Ika_4_2	"	0.76	8.29	55.02	3.376	n.d.	−6.69	−3.953	n.d.	984	4.9
Ika_8_inlet			8.75	50.25	2.710	0.186					8.1
Ika_8_1	calcite	0.60	8.42	46.23	1.040	0.188	−4.02	−1.670	0.002	n.d.	1.7
Ika_8_2	"	0.60	8.44	46.38	1.020	0.190	−3.87	−1.690	0.004	n.d.	1.7
Ika_13_inlet			8.45	15.19	3.874	0.193					2.7
Ika_13_1	calcite	0.58	8.34	14.18	3.366	0.202	−1.01	−0.508	0.009	n.d.	1.7
Ika_13_2	"	0.58	8.35	14.10	3.335	0.198	−1.09	−0.539	0.005	n.d.	1.7
Ika_15_inlet			8.60	24.50	4.954	0.191					7.1
Ika_15_1	calcite	0.58	8.30	n.d.[a]	3.715	n.d.	n.d.	−1.239	n.d.	n.d.	2.8
Ika_15_2	"	0.58	8.34	22.40	3.666	0.197	−2.10	−1.289	0.006	n.d.	2.9

[a] n.d. = not determined. When alkalinity was not determined, it was approximated for the calculation of Ω_{ikaite} by stoichiometrically decreasing the initial alkalinity of the solution by twice of the corresponding Ca^{2+} decrease.

Growth kinetics of ikaite

Although ikaite growth was evident from XRD and solution analyses for both ikaite- and calcite-seeded experiments, surface normalized growth rates could only be derived from ikaite-seeded experiments (Ika_1–Ika_4). In calcite-seeded experiments (Ika_8, Ika_13, Ika_15), the unknown length of the ikaite nucleation period negated any surface area normalization of the detected consumption of material by the growing ikaite within the reactor. This applies all the more as some volume nucleation was observed additionally to surface nucleation at the reactor walls and calcite seeds.

Ikaite-seeded experiments (Ika_1–Ika_4) provided surface normalized growth rates unequivocally, although trace amounts of freshly formed ikaite crystals were also observed in the experiments. Both growth of initial ikaite seed crystals and nucleation and growth of new ikaite crystals led to an increase of the ikaite surface area within the reactor during the experimental runs. While the increase of surface area resulting from nucleation of new ikaite crystals was negligible, the increase of surface area resulting from the growth of ikaite seeds was apparent and, therefore, considered in the rate calculations. The increase of ikaite surface area was calculated from the measured ΔCa values and the corresponding ikaite mass increase, assuming that the specific surface area (A_S) of the solid remained constant. Mean growth rates at steady state conditions (Ika_1–Ika_4) were plotted as a function of the fluid saturation ratio with respect to ikaite (Ω_{ikaite}) (Fig. 17).

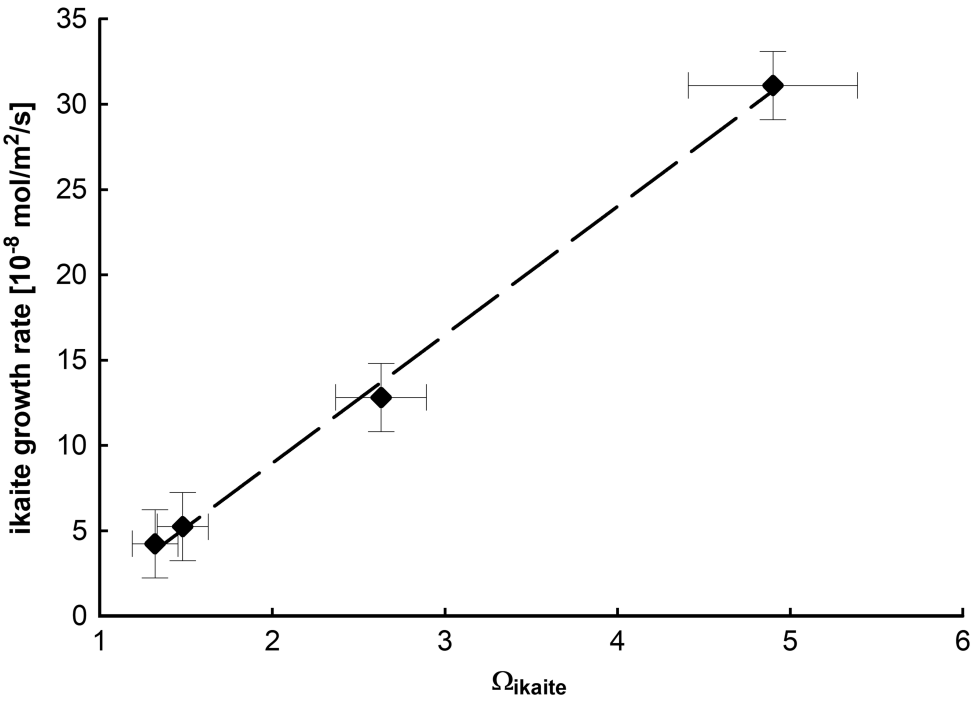

Figure 17. CMFR growth rates of ikaite as a function of saturation ratio. The dashed line represents the linear regression of the growth rates.

To calculate the rate constant k and the reaction order n of ikaite growth, the empirical equation

$$R = k(\Omega - 1)^n, \tag{4.1}$$

which has been commonly used for the growth of calcium carbonate minerals (e.g. Busenberg and Plummer, 1986; Dromgoole and Walter, 1990; Gutjahr et al., 1996; Morse et al., 2007; Nancollas and Reddy, 1971), was used to generate a fit of the measured growth rates (Fig. 18). The best fit of the experimental data yielded a reaction order n = 0.8 ± 0.3 and a rate constant k = 0.10 ± 0.03 µmol/m²/s.

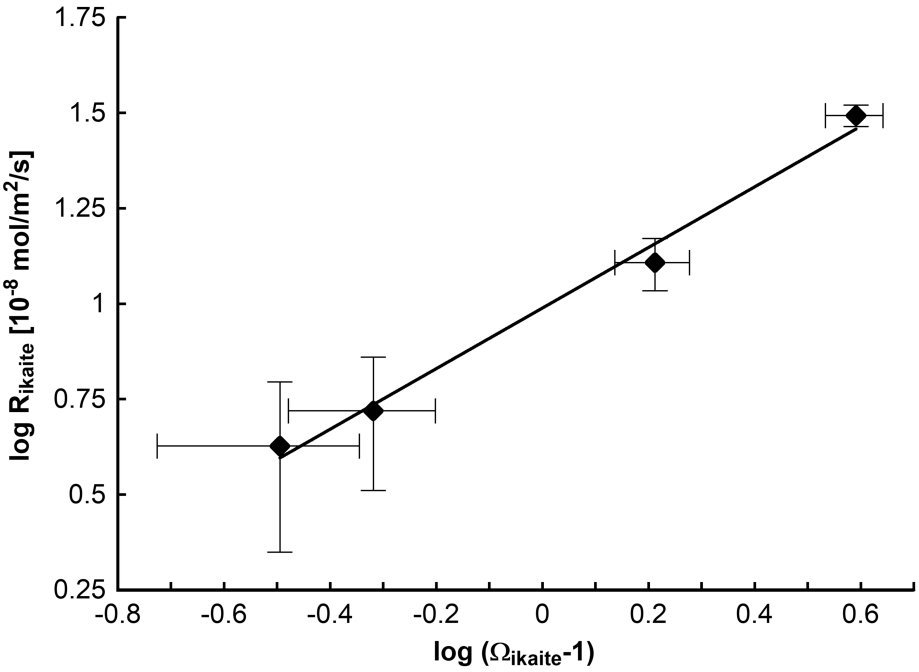

Figure 18. Logarithmic plot of ikaite growth rates as a function of degree of supersaturation with respect to ikaite. The linear regression drawn on the plot provides a reaction order n = 0.8 ± 0.3 and a rate constant k = 0.10 ± 0.03 µmol/m²/s for equation 4.1.

4.2.2 Discussion

Growth of ikaite

In calcite-seeded growth experiments (Ika_8, Ika_13 and Ika_15), newly formed ikaite led to a decrease of Ca concentrations and total alkalinity relative to inlet solutions. As indicated by cryo SEM images (Fig. 14), calcite seeds did not reveal any significant growth during CMFR experiments. Because the calcite seeds were synthesized from ikaite via a temperature-induced transformation, no other chemical component than the phosphate added to the CMFR inlet solution is the likely cause of the observed absence of noticeable calcite growth.

The reduction of calcite growth to an imperceptible amount is an explicit indicator for the phosphate solution concentration being high enough to potentially influence ikaite growth as well. Ikaite growth, however, was not noticeably influenced by the added phosphate, which supports the results of Bischoff et al. (1993a), who revealed no detectable inhibition of ikaite crystallization by phosphate, while the precipitation of calcite, aragonite and vaterite was suppressed. Although the growing ikaite crystals led to a detectable Ca withdrawal in our calcite-seeded experiments, the impossibility of normalizing this withdrawal to the temporal development of the ikaite surface area disabled the calculation of ikaite growth rates. Thus, surface area normalized growth rates could be derived from ikaite-seeded experiments exclusively (Ika_1–Ika_4).

A plot of ikaite growth rates as a function of the corresponding saturation sate of the aqueous solutions with respect to this phase (Ω_{ikaite}) revealed a linear dependence of rates on supersaturation (Fig. 17). Our growth rate constant (k = 0.10 ± 0.03 µmol/m²/s) is higher than the rate constant of approx. 0.03 µmol/m²/s determined by Papadimitriou et al. (2014) which was derived from precipitation in seawater and seawater-derived brines at salinities S = 66 ‰ (T = –3.6 °C) and S = 102 ‰ (T = –5.9 °C). The increased value in our study relative to the one published by Papadimitriou et al. (2014) might be explained by different solution conditions. Although Papadimitriou et al. (2014) did not detect a significant difference of rate constants within their salinity and temperature interval, our rate constant obtained from solutions with tremendously lower salinity and slightly higher temperature (ionic strength of 0.1 M corresponding to $S \approx 6$ ‰, T = +1.0 °C) might point towards either a weak direct correlation of the rate constant with temperature or an inverse correlation of the constant with salinity or both. Whether the aqueous phosphate in our experiments compared those of Papadimitriou et al. (2014) influences ikaite growth, cannot be assessed as the phosphate concentrations of the poorly defined solutions used by Papadimitriou et al. (2014) are unknown.

The reaction order of n = 0.8 ± 0.3, which was derived from the empirical equation $R = k(\Omega - 1)^n$, points towards first order reaction kinetics. This is in good agreement with the reaction order of n = 1.23 ± 0.42 obtained by Papadimitriou et al. (2014) and in contrast to growth kinetics of calcite in sea water at 25 °C. For the latter, the empirical rate equation frequently indicated second to third order reaction kinetics (e.g. Burton and Walter, 1990; Lopez et al., 2009; Mucci, 1986; Zhong and Mucci, 1993). Furthermore, the presence of phosphate in artificial sea water led to a slight increase of the reaction order of calcite relative to that determined for phosphate-free solution (Mucci, 1986). Such an increase of the reaction order can be ruled out for ikaite as phosphate does not retard ikaite growth in similar way to calcite growth (Bischoff et al., 1993a; Hu et al., 2015). For ikaite, the obtained first order reaction kinetics for growth in phosphate-containing solutions implies a transport or adsorption process as the rate controlling mechanism (e.g. Nielsen 1983). Although this macroscopic approach does not provide direct evidence for the growth rate controlling reactions, as microscopic surface processes may lead to deviations from the predictions of rate laws (Teng et al., 2000), a transport or adsorption-controlled growth mechanism is consistent with the way an extremely hydrated phase such as ikaite could grow. The classical model of

calcite growth via attachment, dehydration and incorporation of growth units (e.g. Gratz et al., 1993; Morse et al., 2007) may not apply to ikaite as a complete dehydration of attaching species is not required. Ikaite growth might simply comprise an incorporation of a $CaCO_3^0$ ion pair together with six water molecules. Density functional theory (DFT) calculations of Chaka (2018) confirmed this low energy pathway of crystallization via the assemblage of aqueous $CaCO_3^0 \cdot 6H_2O$ ion pair complexes. This low energy pathway was further corroborated by low interfacial energies of ikaite nuclei (chapter 4.1).

The insignificance of phosphate uptake by ikaite during growth

In the CMFR growth experiments (saturation state $1.5 \leq \Omega_{ikaite} \leq 2.9$), measured phosphate concentrations revealed no evidence of phosphate incorporation into ikaite crystals. During ikaite seed synthesis, which was conducted at much higher supersaturation, a phosphate uptake cannot be ruled out per se as phosphate partitioning between precipitate and solution might be increasing at an increasing distance from equilibrium. Furthermore, a significant withdrawal of aqueous phosphate concomitant to the onset of ikaite precipitation was observed in a laboratory study by Hu et al. (2014). However, any significant phosphate uptake of ikaite during our seed synthesis is questionable. Disintegration of ikaite causes the release of its weakly bonded water (e.g. Németh et al., 2022; Vickers et al., 2022). If phosphate had been taken up during ikaite seed synthesis, the subsequent transformation of the filtered ikaite seeds into calcite would have been taken place in a phosphate containing solution. Within such a phosphate containing solution, however, the formation of calcite is impeded, as even minor amounts of phosphate (1 µM) are known to interfere with the nucleation of calcite (Lin and Singer, 2006). This inhibition of calcite nucleation and promotion of ikaite appearance (or persistence) was found to apply at temperatures up to 25 °C (Clarkson et al., 1992). As the transformation of our filtered ikaite seeds into calcite took place without any problems, it can be assumed that the phosphate uptake from solution during seed synthesis due to coprecipitation with ikaite is likely very limited. Furthermore, it is noteworthy that the $[Ca^{2+}]$:$[CO_3^{2-}]$ ratio varied in our growth experiments (Ika_1: $[Ca^{2+}]$:$[CO_3^{2-}] \approx 0.6$, Ika_13: $[Ca^{2+}]$:$[CO_3^{2-}] \approx 12$). Thus, the results also show that a decreased $[CO_3^{2-}]$ concentration does not promote substitution of carbonate by phosphate ions during ikaite growth. Substitution of these anions might be expected if carbonate and phosphate ions were competing for incorporation.

The lack of phosphate coprecipitation with ikaite contrasts with calcite. While laboratory studies showed that calcite was capable of incorporating detectable amounts of phosphate from solution during growth (Hartley et al., 1997; House and Donaldson, 1986; Ishikawa and Ichikuni, 1981), phosphate coprecipitation is not observed during ikaite growth in our study. The distinct growth mechanisms of the different calcium carbonate phases might explain this discrepancy. The incorporation of adsorbed phosphate into calcite most likely occurs at active growth surface sites (House and Donaldson, 1986), which is in agreement with the classical model of calcite growth. Incorporation of phosphate ions into growing ikaite by substitution of

carbonate ions, in contrast, might be less compatible with a growth mechanism via an assembling of hydrous $CaCO_3^0$ ion pair complexes.

In summary, there was no sign of phosphate uptake by ikaite from all the experiments performed in this study. This finding supports the results of Hu and Wang (2020), who did not obtain a detectable coprecipitation of phosphate with ikaite in samples grown in sea ice. Based on the experimental data, therefore, it needs to be taken into account that phosphate coprecipitation with ikaite in sea ice may not necessarily contribute significantly to seasonal phosphate accumulations in Antarctic landfast and pack ice (e.g. Cozzi, 2008; Fripiat et al., 2017; Jones et al., 2023b; Meiners et al., 2011). Even though ikaite formation in sea ice may occur with high temporal dynamics (Papadimitriou et al., 2014; Rysgaard et al., 2014) and, thus, nucleation and growth conditions of ikaite in sea ice might not exactly match the conditions of this study in all respects, the absence of any signs of phosphate uptake by ikaite rather supports the importance of previously proposed biotic pathways like phosphate remineralization in biofilm microenvironments and phosphate accumulation due to sea ice algae (Fripiat et al., 2017; van der Linden et al., 2020).

4.3 The ephemeral occurrence of ikaite in aqueous solutions from 0–20 °C

4.3.1 Results

Desupersaturation curves and phase analyses of experiments at T = 10 °C

In-situ pH-monitoring of solutions in CMBR experiments revealed multi-step desupersaturation curves due to the precipitation of different $CaCO_3$ phases, which led to a decrease of supersaturation over time at different and varying rates (Fig. 19). Upon addition of carbonate solution to the Ca^{2+} solution within the reactor (t = 0 s), an instantaneous precipitation led to a sharp decrease in pH (Fig. 19). After this initial sharp decrease, pH reduction slowed down. X-ray diffraction (XRD) analyses of precipitates retrieved from the reactor in experiments with run time r_1 (point A in Fig. 19) showed the sole presence of an amorphous phase (Fig. 20). No information about the water content and structural peculiarities of this phase is available so far. Consequently, the degree of similarity of this phase to commonly reported ACC (Brečević and Nielsen, 1989; Lázár et al., 2023; Levi-Kalisman et al., 2002; Radha et al., 2010) remains unclear. Hereinafter, therefore, we will call this amorphous phase ACC*. If extrapolated from point A, the pH-curve would asymptotically approach a constant pH-value (dotted line in Fig. 19). This pH-value may indicate a solution which is saturated with respect to ACC*. The course of the pH-curve, however, did not follow this extrapolation.

At point B an inflection occurred and pH-decrease speeded up again due to an increased consumption of alkalinity by the mineralization of a new phase. When the solution concentration fell below the inflection at point C (= ACC* saturation), dissolution of ACC* started compensating the precipitation of the new phase. XRD analyses of precipitates sampled between point C and D (run time r_2) showed the sole presence of ikaite (Fig. 20). It needs to be stressed, however, that X-ray scattering of an amorphous phase in between the ikaite reflections cannot be excluded. The persistence of ACC* between point C and D, therefore, is very likely. This is especially valid, because maximum relative compensation of ikaite growth by ACC* dissolution was not attained before the next infection at point D.

With increasing ikaite precipitation rate, pH-values decreased increasingly fast reaching maximum at the inflection point E. Starting from point E, the pH-curve approached a constant pH-value which indicated a solution saturated with respect to ikaite (pH ≈ 8.46). The onset of precipitation of a new phase in amounts large enough to be detectable by the pH-electrode, however, resulted in an inflection (point F) at which the pH curve abandoned the asymptotic approach towards ikaite saturation. Again, the pH-values started to decrease with increasing speed. Cryo SEM was performed at a sample retrieved shortly after inflection point F (run time r_3; Fig. 21). The images revealed the existence of minor amounts of spherical vaterite aggregates. The vaterite crystals were found to possess no strict spatial relation to the euhedral ikaite crystals indicating an independent nucleation (Fig. 21B).

Later between point F and G, XRD analyses of precipitates sampled at run time r_4 yielded ikaite in an amount almost equal to the anhydrous phases vaterite and calcite. As soon as the solution composition falls below ikaite saturation, dissolution of ikaite will compensate for the withdrawal of alkalinity by the growing anhydrous phases. At the inflection point G, the maximum rate of the withdrawal of alkalinity by vaterite/calcite precipitation has been reached. In the absence of a distinct marker identifying the point of complete ikaite dissolution in the pH-curves, we define this inflection point G as a proxy for the endpoint of ikaite existence, although ikaite might have been existing beyond this point.

Far beyond point G, the pH-curve finally approached a value which corresponded to a solution which is in saturation with calcite (pH ≈ 7.62). Preexisting vaterite, which needed to dissolve in favor of calcite growth, influenced the shape of the pH-curve to some degree. The vaterite-calcite transformation, however, needs to be part of separate investigations (e.g. Ogino et al., 1987).

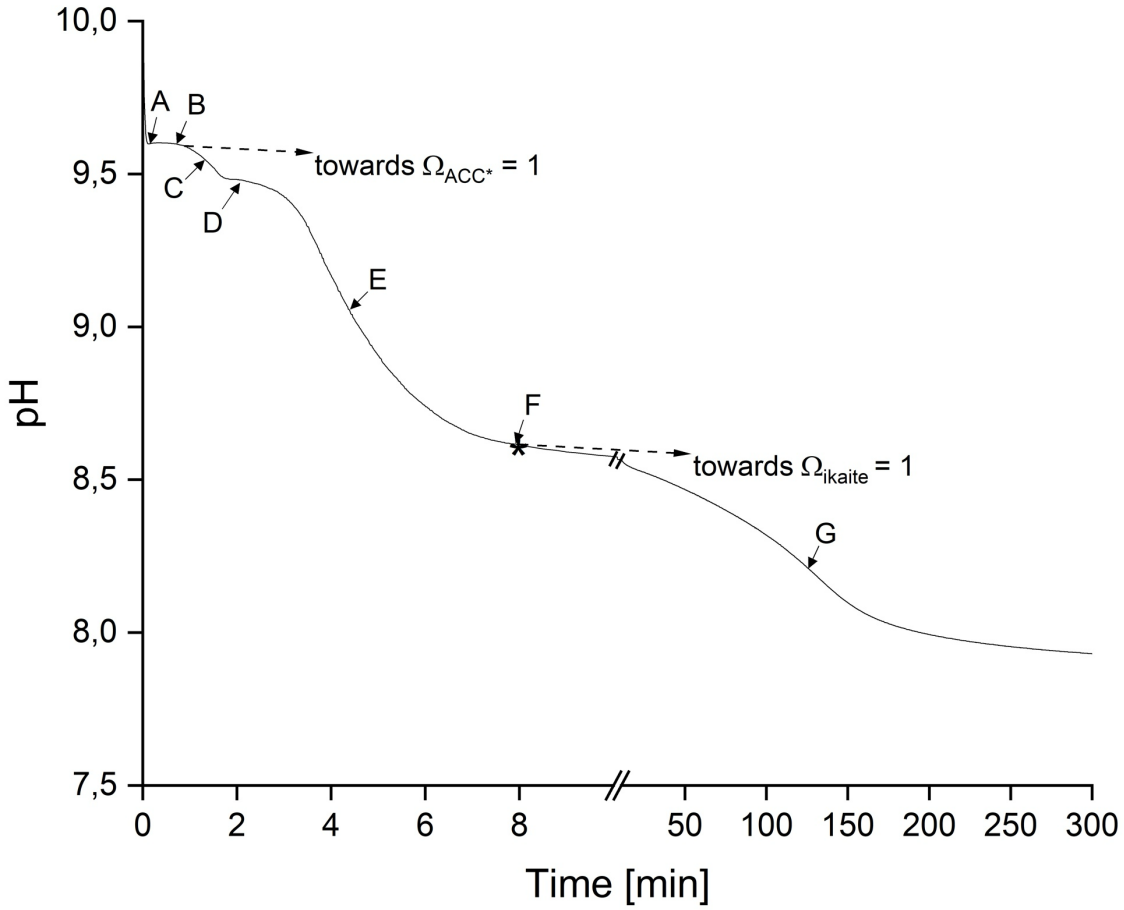

Figure 19. Multistep desupersaturation curve obtained in the CMBR experiment at T = 10 °C. The precipitation of different $CaCO_3$-phases at different and varying rates led to multiple inflection points (A–G). Asterisk (*) marks the position of the sample taken at r_3 which is shown in cryo SEM images (see Fig. 21).

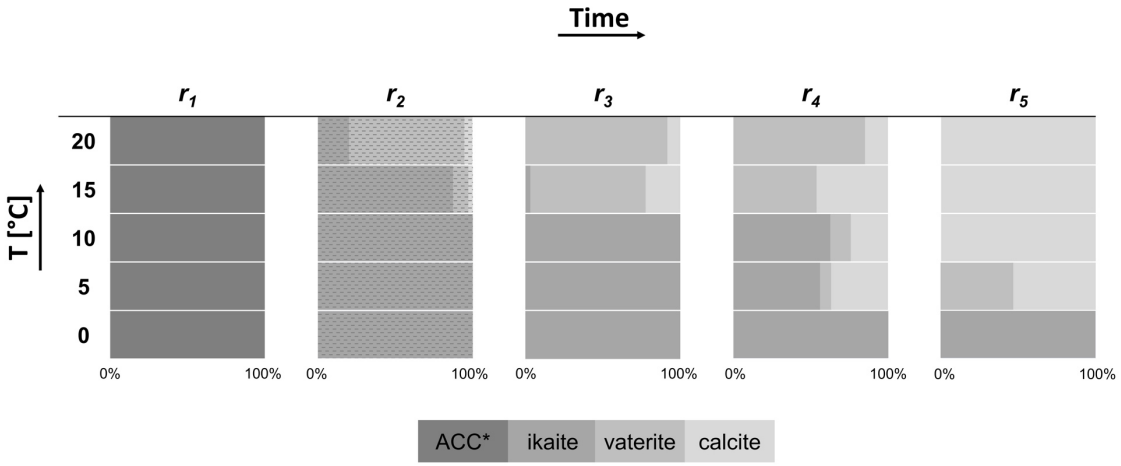

Figure 20. Phase inventory of precipitates retrieved from CMBR experiments at different run times (r_1–r_5) and temperatures (0–20 °C). Estimations of relative amounts of phases were derived from Rietveld refinements of XRD analyses. Dotted areas mark the potential persistence of ACC* alongside crystalline $CaCO_3$ phases. Note: existence of vaterite and calcite in amounts below XRD detection limit is possible also in cases showing 100 % other phases.

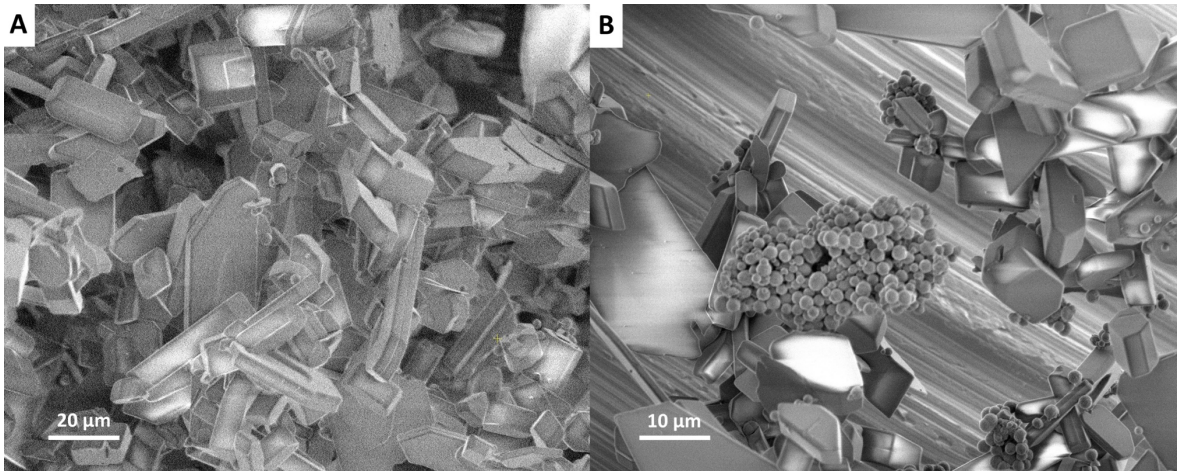

Figure 21. Cryo SEM images of precipitates retrieved from reactive solution after 8 minutes at 10 °C. (**A**) Besides a dominating quantity of euhedral ikaite crystals, rare amounts of spherical vaterite aggregates occurred. The vaterite concentration remained below detection limit of XRD analyses (Fig. 22). (**B**) The occasionally occurring spherical vaterite aggregates nucleated independently of ikaite.

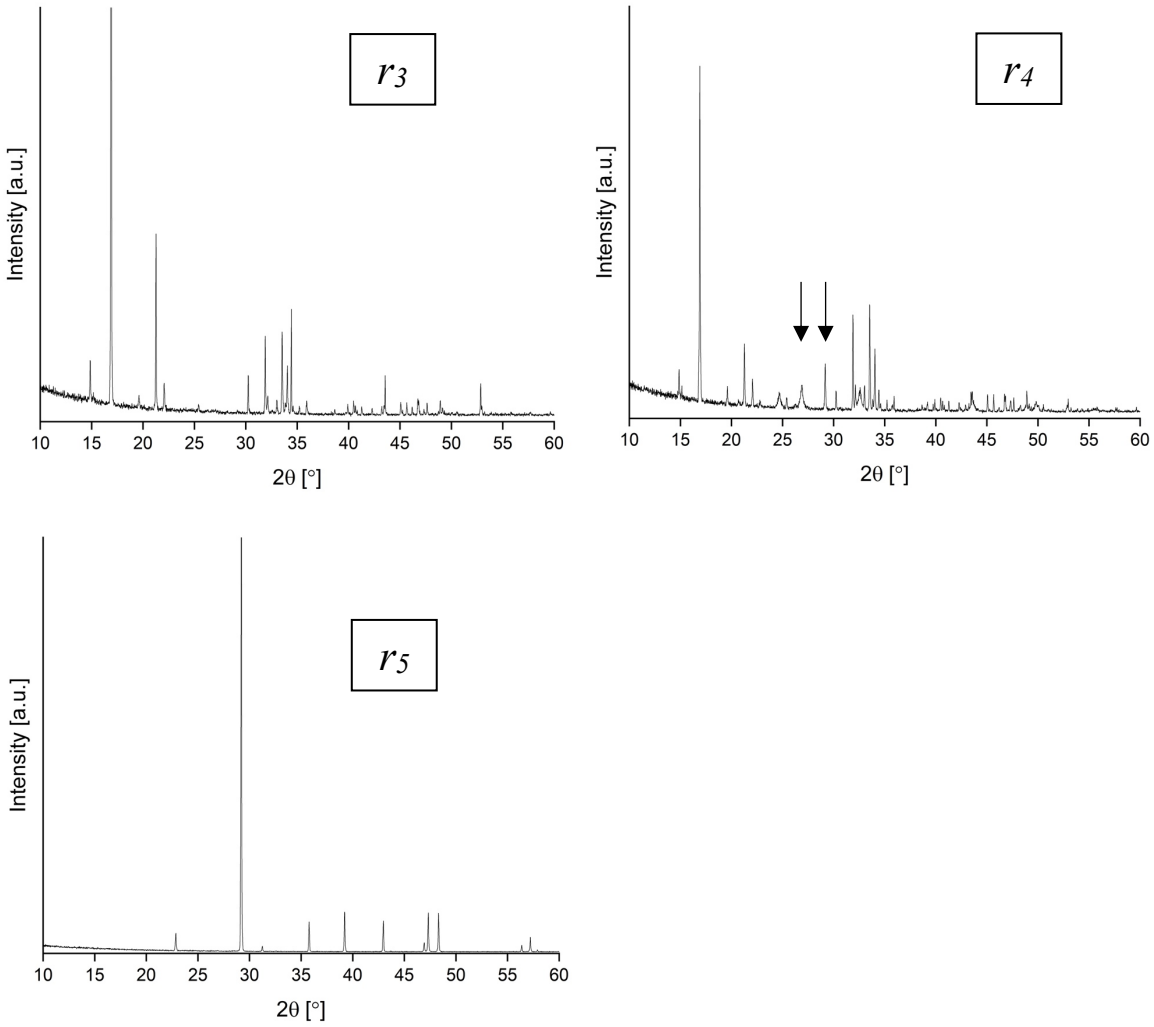

Figure 22. X-ray powder diffraction pattern (CuKα$_1$) of crystals retrieved from CMBR experiments at run times r_3, r_4, r_5 at 10 °C. Diffraction peaks correspond to ikaite at $\boldsymbol{r_3}$. The minor amount of vaterite observed in cryo SEM imaging is below the detection limit. At $\boldsymbol{r_4}$, the relative amounts of vaterite and calcite increased above the detection limit. After 24 hours ($\boldsymbol{r_5}$), XRD analysis revealed the disappearance of vaterite and ikaite, as all diffraction peaks belong to calcite.

Desupersaturation curves and phase analyses of experiments at T < 10 °C

The main difference between desupersaturation curves taken at T = 10 °C (as shown above) and at T = 5 and 0 °C is that point F (the onset of detectable precipitation of anhydrous calcium carbonate phases) was shifted to significantly later times at colder temperatures (Figs. 23, 24). Consequently, phase analyses of samples from run time r_4 (40 minutes after start of the experiment; Fig. 20) revealed more (5 °C) or solely (0 °C) ikaite. Likewise at run time r_4, analyses of the solutions from experiments at T = 5 and 0 °C revealed compositions which were closer to ikaite saturation than the solution retrieved from the experiment at T = 10 °C (Table 7).

At T = 5 °C, the inflection point G (marking the maximum removal of alkalinity and denoting the endpoint of ikaite occurrence by definition) was delayed by about 4 hours vs. T = 10 °C. At T = 0 °C, ikaite persisted for more than 24 hours and XRD analyses solely revealed ikaite (samples from run time r_5; Fig. 20). Decreasing pH-values caused by the onset of carbonate-consumption by vaterite and/or calcite growth (point F) were not noticed before 26 hours after start of the experiment at T = 0 °C (Fig. 23). Inflection G took place at approx. 28 hours. This finding at T = 0 °C marked the upper limit of persistence of ikaite, which precipitated from a solution at Ω_{ikaite} = 18 and remained in a saturated solution (Ω_{ikaite} = 1).

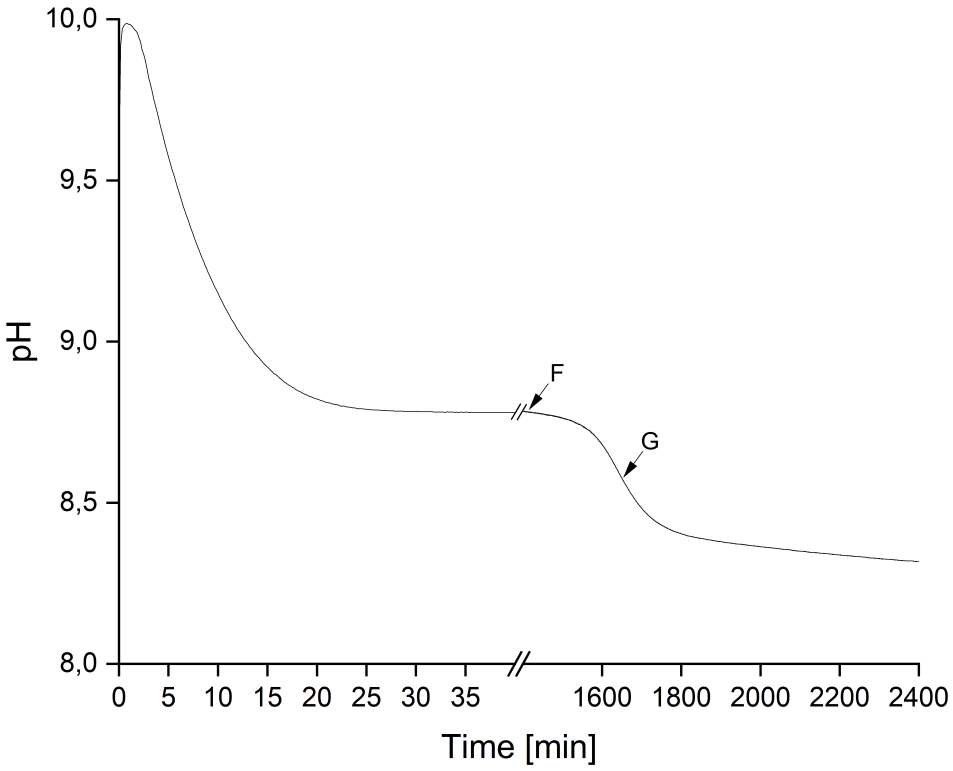

Figure 23. Desupersaturation curve at T = 0 °C. The formation of vaterite and calcite at the expense of ikaite led to the disappearance of ikaite after 1660 minutes.

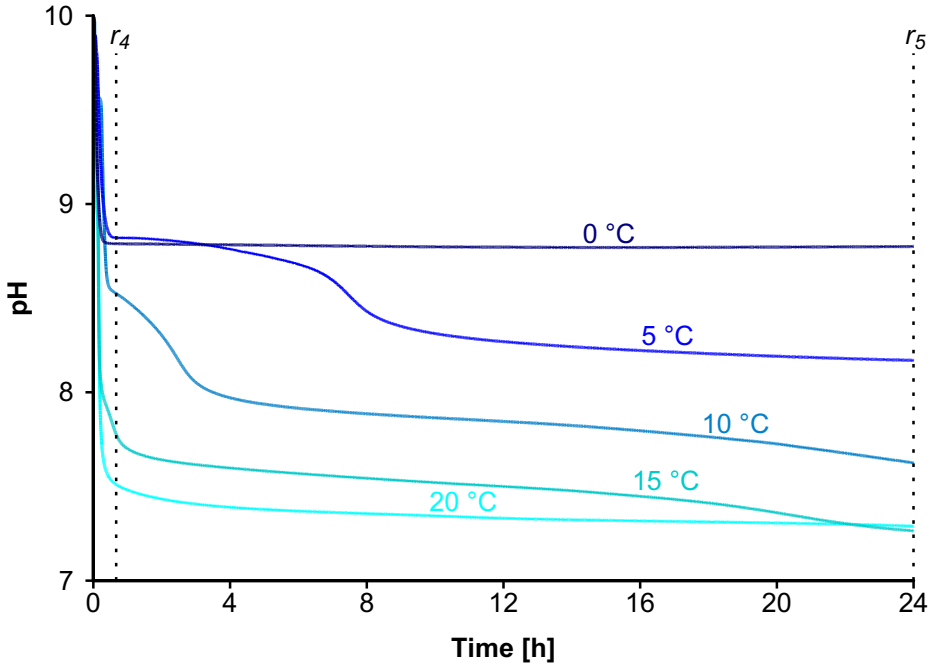

Figure 24. Desupersaturation curves during experimental run times of 24 hours.

Table 7. Composition of solution analyzed ex-situ upon the end of cryo-mixed-batch reactor experiments.

Experiment			Analyses of solution			Saturation state		
Sample	Temperature [°C]	Sampling (elapsed time)	pH	Tot. Alk. [meq/l]	Ca [mM]	Ω_{ikaite}	$\Omega_{vaterite}$	$\Omega_{calcite}$
H0_18_40_1	0	r_4 (40 min)	8.82	3.75	3.69	0.8	2.7	12
H5_18_40_1	5	r_4 (40 min)	8.74	4.71	4.41	0.9	3.3	15
H10_18_40_1	10	r_4 (40 min)	8.46	5.82	5.10	0.7	2.6	11
H15_18_40_2	15	r_4 (40 min)	7.74	7.02	5.83	0.2	0.7	3.0
H20_18_40_2	20	r_4 (40 min)	7.50	8.54	6.56	0.1	0.5	2.3
H0_18_24_1	0	r_5 (24 h)	8.77	3.68	3.65	0.7	2.4	11
H5_18_24_1	5	r_5 (24 h)	8.17	3.98	3.79	0.2	0.7	3.2
H10_18_24_1	10	r_5 (24 h)	7.62	4.70	4.40	0.1	0.3	1.2
H15_18_24_1	15	r_5 (24 h)	7.26	5.53	5.21	0.0	0.2	0.7
H20_18_24_1	20	r_5 (24 h)	7.29	6.91	5.59	0.1	0.2	1.0

Desupersaturation curves and phase analyses of experiments at T > 10 °C

Experimental series were performed at 15 and 20 °C. Because all experiments were started at supersaturation Ω_{ikaite} = 18, the solutions of the experimental runs at increased temperature were increasingly supersaturated with respect to vaterite and calcite (Table 1, chapter 3.1.1). These higher $\Omega_{vaterite}$ and $\Omega_{calcite}$ values led to significantly reduced induction periods for vaterite and calcite (induction period = time required for the formation of a detectable number of nuclei), whereas the induction period of ikaite was only affected by the increased temperature but not by an increased supersaturation (because Ω_{ikaite} = 18 had been held constant at all experimental temperatures). Consequently, point F of the desupersaturation curves (the onset of detectable precipitation of anhydrous calcium carbonate phases) shifted to earlier moments and interfered with the points marking the onset of detectable precipitation of ikaite and the maximum precipitation rate of ikaite (cf. points D and E in Fig. 19). As a result, periods of major nucleation of ikaite and the anhydrous phases overlapped. Thus, the number of inflections of the desupersaturation curve at T = 20 °C (Fig. 25) was reduced if compared with the curves at T = 10 °C (Fig. 19). This finding is confirmed by XRD analyses of samples from run time r_2 (approx. 4 minutes after starting the experiment, Fig. 20), which revealed vaterite being the main phase along with minor amounts of ikaite and calcite.

The coexistence of vaterite, ikaite and calcite in the early stage of experiments was further confirmed by cryo SEM imaging of samples at T = 20 °C retrieved from the reactor after run time r_2 (Fig. 26). Besides minor amounts of ikaite crystals, which were partially decomposed, the SEM images revealed a dominant presence of spherical vaterite and few calcite crystals. Noteworthy, SEM images clearly showed that there is no spatial relation between ikaite crystals and the anhydrous phases. The nucleation of both ikaite and anhydrous phases, thus, were parallel and independent processes.

At T = 20 °C, however, the coexistence of the three $CaCO_3$ minerals did last few minutes only. XRD analyses at the next sampling point r_3 (i.e. after 8 minutes of experimental run time) showed that ikaite vanished and vaterite as well as calcite were the only phases remaining.

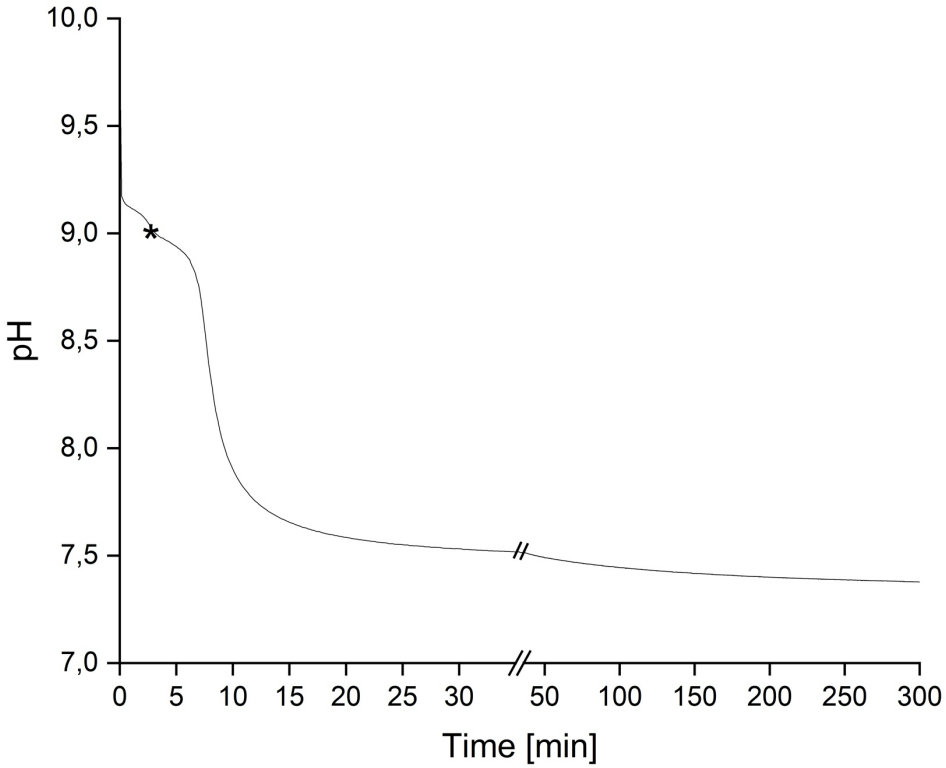

Figure 25. Desupersaturation curve at T = 20 °C. In contrast to desupersaturation curves obtained at T ≤ 10 °C, pH did not approach a constant value corresponding to the solution composition which is saturated with respect to ikaite but decreased further due to the early onset of the nucleation of vaterite and calcite. Asterisk (*) marks the position of the sample taken at r_2 which is shown in cryo SEM images (see Fig. 26).

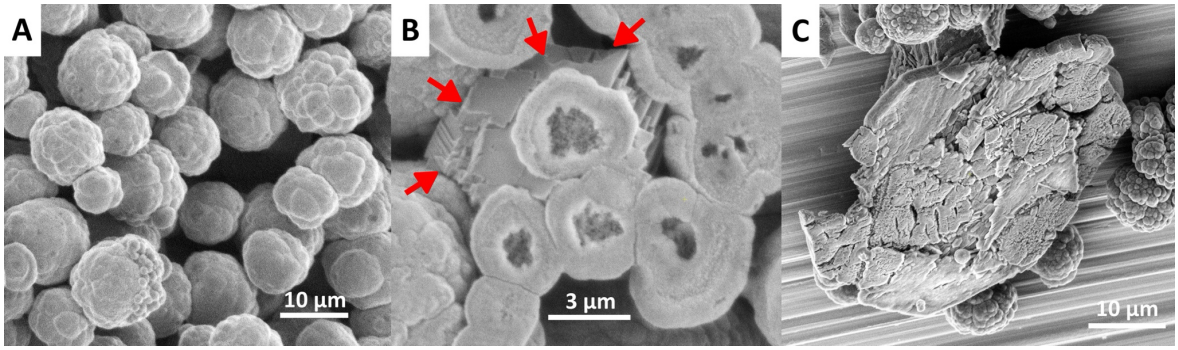

Figure 26. Cryo SEM images of precipitates retrieved from solution after 2–3 minutes (r_2) at T = 20 °C. Spherical vaterite aggregates (**A**) dominated the phase inventory. As marked in (**B**), few rhombohedral calcite crystals were found next to spherical vaterite (see arrows). In very rare cases, partially disintegrated crystals of ikaite were present (**C**).

Estimation of the nucleation rate of ikaite at T = 0 °C

At T = 0 °C, ikaite nucleation rates $J_{\mathrm{ikaite}}^{\mathrm{exp}}$ can be roughly estimated by a comparison of the amount of material consumed by crystallization between Ω_{ikaite} = 18 and 1 (measured by ex-situ analyses, Table 2), by the time required for this consumption (indicated by the desupersaturation curves from in-stu pH monitoring, Fig. 23), and by the ikaite crystal sizes (detected in cryo SEM images sampled at near-equilibrium solution conditions of ikaite; run time r_4; Figs. 21A and 27).

From the two different solution compositions, it follows that up to ~135 mg of ikaite precipitated within the reactor volume. Applying a cubic shape model to single ikaite crystals (diameters 5–50 µm, Figs. 21A, 27), the mass of a single crystal and, ultimately, the range of the total number of ikaite nuclei formed in the experiments can be estimated. Assuming the period of nucleation lies between 1 and 10 minutes (Fig. 23) and assuming steady nucleation dynamics exists within the interval of supersaturation, a range of nucleation rates can be calculated. In this way, the experimental data at 0 °C yielded a maximum and minimum ikaite nucleation rate of $J_{\mathrm{ikaite}}^{\mathrm{exp-max}}$ = 10^5 cm^{-3} s^{-1} and $J_{\mathrm{ikaite}}^{\mathrm{exp-min}}$ = 10^0 cm^{-3} s^{-1}, respectively.

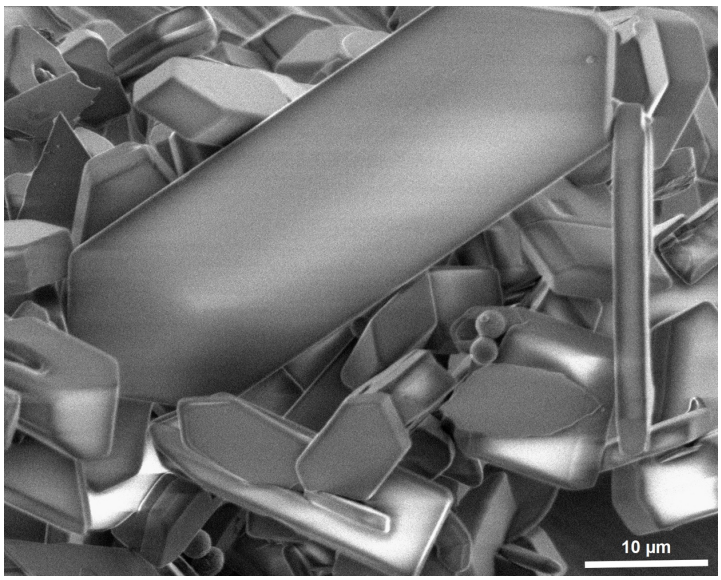

Figure 27. Cryo SEM image of precipitates retrieved from reactive solution after 8 minutes at 10 °C. Besides a dominating quantity of euhedral ikaite crystals, rare amounts of spherical vaterite aggregates occurred.

4.3.2 Discussion

The transient occurrence of ikaite

The appearance of ikaite in our experiments at temperatures up to 20 °C well exceeded its reported temperature range of formation in nature ($T \leq 9$ °C; Bischoff et al., 1993b; Huggett et al., 2005; Kennedy, 2022; Stockmann et al., 2022). The amount of ikaite occurring in our experiments was temperature-dependent and its persistence was limited at all tested temperatures. While at $T = 0$ °C, ikaite endured for up to 28 hours, it disappeared within less than 4 minutes at $T = 20$ °C under the tested conditions with an initial supersaturation $\Omega_{ikaite} = 18$. Thus, ikaite endurance strongly decreased with temperature. The main reason for the limited ikaite persistence was the precipitation of anhydrous $CaCO_3$ minerals. The growth of the anhydrous phases led to a withdrawal of calcium and carbonate from the solution and, therefore, led to a solution composition which became undersaturated with respect to ikaite. Important to note, the precipitation of the anhydrous phases largely took place independent of the existing ikaite crystals.

The extent of competitional precipitation of anhydrous phases increased in experiments at increased temperature because the constant initial supersaturation Ω_{ikaite} led to an increasing $\Omega_{calcite}$ with increasing temperature. A constant initial concentration or a constant initial supersaturation $\Omega_{calcite}$ was no option for the experimental parameterization, because then Ω_{ikaite} would have decreased with increasing temperature and would have fallen below saturation above a certain temperature. In the experiments at high temperatures, therefore, the increased initial concentration favored the occurrence of anhydrous phases along with instantaneous ACC* formation. This favored precipitation of the anhydrous phases together with the ACC* formation led to an increasingly rapid drop of the solution concentration below ikaite saturation with increasing temperature.

At present, role and nature of ACC* are insufficiently understood. Although some knowledge exists on the relations between ACC and anhydrous $CaCO_3$ phases, the known formation pathways of the anhydrous phases, which involve the transient appearance of an amorphous phase, are complex and manifold (Cartwright et al., 2012; Gebauer and Cölfen, 2011; Henzler et al., 2018; Hu et al., 2012). These formation pathways, however, may not be applicable to ikaite. Due to the highly hydrated nature of ikaite, its nucleation mechanism significantly contrasts the mechanism of anhydrous phases (chapter 4.1 and 4.2; Buchardt et al., 2001; Chaka, 2018; Stockmann et al., 2018). Therefore, little is known about the effect of ACC* on ikaite formation, although its presence was reproducibly observed prior or in parallel to the appearance of ikaite (chapter 4.1; Besselink et al., 2017; Lázár et al., 2023; Tollefsen et al., 2020; Zou et al., 2018). Nevertheless, the independent nucleation of ikaite during and after the formation of ACC* (see chapter 4.1) suggests that an effect of ACC* on the formation of ikaite beyond the reduction of solution supersaturation is unlikely.

Within the range of studied conditions, in summary, the persistence of ikaite depends on the nucleation rate of anhydrous phases. An increase of ikaite persistence, therefore, requires a major external intervention such as the addition of nucleation inhibitors for vaterite and calcite. As the effectiveness of additives in inhibiting growth of anhydrous $CaCO_3$ phases often depends on supersaturation (House, 1987; Mills et al., 2022), complete inhibition becomes increasingly difficult at increasing temperature. Incomplete inhibition of anhydrous $CaCO_3$ phases will inevitably lead to ikaite dissolution.

Within the tested temperature range, the disappearance of ikaite in favor of vaterite and calcite took place without any significant spatial relation between ikaite and the product phases, irrespective of the lifetime of ikaite. The ikaite-calcite/vaterite transformation, therefore, most likely proceeded via a coupled dissolution-precipitation mechanism, as it was proposed in previous studies on the stability and transformation of ikaite (Besselink et al., 2017; Purgstaller et al., 2017; Sánchez-Pastor et al., 2016; Tollefsen et al., 2020).

The formation of ikaite in the light of classical nucleation theory CNT

Our experiments revealed a coexistence of ikaite and anhydrous $CaCO_3$ minerals due to independent nucleation events and, therefore, reflect a parallel multi-phase formation rather than a succession of nucleation events proceeding along the degree of metastability of $CaCO_3$ phases. Thus, Ostwald's rule of stages (Ostwald, 1897) provides an inappropriate description of the occurrence of ikaite, as this rule proposes a sequential nucleation of phases in descending order of metastability. The observed mineralization with ikaite as the dominant phase during early crystallization at $T \leq 10$ °C rather suggests a sequential disappearance of metastable phases after parallel nucleation. Such a behavior might be consistent with predictions provided by CNT (Cardew, 2023). In the light of CNT, dominant or concomitant formation of metastable phases relative to stable ones is feasible but implies distinct thermodynamic and kinetic prerequisites for achieving a sufficiently high nucleation rate (Cardew, 2023; Navrotsky, 2004).

Using CNT (Mullin, 2001; Söhnel and Mullin, 1988; Verdoes et al., 1992), the independent nucleation rate J_i of a phase i can be calculated by equation 3.7. In order to apply Eq. 3.7 to our experiments, the corresponding key parameters, namely the kinetic pre-factors A and the interfacial energies γ of $CaCO_3$ minerals are required. Interfacial energies of ikaite nuclei have been determined experimentally in one study (chapter 4.1) only and revealed a low value of γ_{ikaite} = 15 mJ/m² relative to γ_{vaterite} = 35 mJ/m² and γ_{calcite} = 58 mJ/m² using a mononuclear approach of CNT. While a mononuclear relation of induction periods t_{ind} (i.e. time required to form detectable nuclei) and nucleation rate J by CNT provided an adequate interpretation of interfacial energies from experimental data (chapter 4.1), a polynuclear approach (Eq. 3.6) is required for a satisfactory extraction of the kinetic pre-factor (Kashchiev and van Rosmalen, 2003; Verdoes et al., 1992). The growth of nuclei to a detectable volume was estimated by applying the empirical equation 4.1 (chapter 4.2; Berninger et al., 2016; Gautier et al., 2015; Lindner and Jordan, 2018; Morse, 1983; Mucci and Morse, 1983; Shiraki and Brantley, 1995) with $k_{\text{ikaite}} \approx 1.1 \times 10^{-11}$ m s^{-1} and $n_{\text{ikaite}} \approx 1$ (see chapter 4.2). The rearranged combination of

Eqs. 3.6, 3.7 and 4.1 allows the calculation of the kinetic pre-factor $A_{\text{ikaite}}^{\text{CNT}}$ = 2 x 10^9 cm^{-3} s^{-1} (Fig. 28). Applying the parameters A and γ, the nucleation rate of ikaite ($J_{\text{ikaite}}^{\text{CNT-mod}}$) was calculated and plotted as a function of the solution supersaturation Ω versus ikaite (Fig. 29).

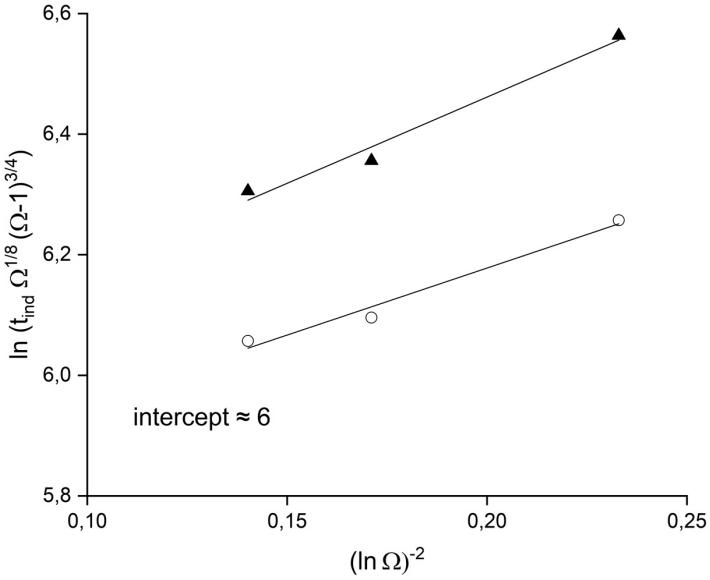

Figure 28. Extraction of the supersaturation independent kinetic pre-factor A using the PN approach. Applying induction times and corresponding initial supersaturation ratios Ω_{ikaite} obtained in chapter 4.1, the intercept is approximately 6. Inserting the values of α and k_i led to $A_{\text{ikaite}}^{\text{CNT}} \approx 2 \times 10^{-9}\ cm^{-3}s^{-1}$(see chapter 3.1.2).

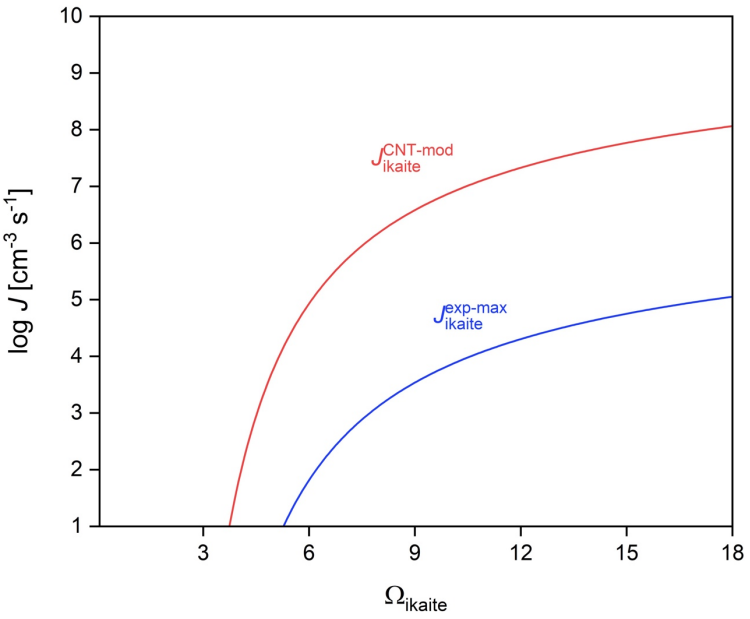

Figure 29. Plots of nucleation rates J_{ikaite} as a function of solution supersaturation with respect to ikaite. The red curve ($J_{\text{ikaite}}^{\text{CNT-mod}}$) shows the nucleation rate of ikaite applying the kinetic pre-factor $A_{\text{ikaite}}^{\text{CNT}}$ = 2 x 10^9 cm^{-3} s^{-1}, which was derived from a polynuclear approach at T = 0 °C. The blue curve shows the experimentally derived maximum nucleation rate $J_{\text{ikaite}}^{\text{exp-max}}$ using $A_{\text{ikaite}}^{\text{exp}}$ = 2 x 10^6 cm^{-3} s^{-1}.

It needs to be kept in mind, though, that the data in chapter 4.1 were exclusively obtained in the absence of any detectable previous or parallel precipitation of ACC*. This, however, is no reason for excluding the data from an application in CNT, as ikaite and ACC* were suggested to form in parallel and independent of another (see chapter 4.1). Likewise, the experiments conducted here provided no sign of an interference between the instantaneous precipitation of ACC* and ikaite nucleation, other than the sharp drop of the initial solution concentration mainly induced by the extensive ACC* formation.

Even if an instantaneous precipitation of ACC* were reducing the supersaturation ratio with respect to ikaite to some degree, the magnitude of ikaite nucleation rates $J_{\mathrm{ikaite}}^{\mathrm{CNT-mod}}$ predicted by CNT covers a sufficiently broad range of supersaturation (Fig. 29). This CNT derived nucleation rate (Fig. 28) is at least 3 orders of magnitude higher than the maximum experimentally derived rate $J_{\mathrm{ikaite}}^{\mathrm{exp-max}}$ = 10^5 cm^{-3} s^{-1}. This significant difference likely results from an overestimation of the kinetic pre-factor $A_{\mathrm{ikaite}}^{\mathrm{CNT}}$ by CNT. The interpretation of the kinetic pre-factor, however, is complex as it involves multiple parameters controlling the attachment of monomers to the nucleus (i.e. attachment-detachment frequency, viscosity, diffusivity, Zeldovich factor, concentration of nucleation sites; see e.g. Cedeno et al., 2023). Nevertheless, an overestimated kinetic pre-factor A leading to a tremendously enhanced $J_{\mathrm{ikaite}}^{\mathrm{CNT-mod}}$ agrees with previous findings on the applicability of CNT-based nucleation rates and confirms indications of limitations of the predictive nature of CNT (Devos et al., 2021; Vekilov, 2010).

In the present study, though, the CNT-based nucleation rates can be compared by nucleation rates derived from experimental data (cf. section 4.3.1: *Estimation of the nucleation rate of ikaite at T = 0 °C*). For this, an experimental kinetic pre-factor $A_{\mathrm{ikaite}}^{\mathrm{exp}}$= 2 x 10^6 cm^{-3} s^{-1} has been calculated by assigning the maximum experimental nucleation rate $J_{\mathrm{ikaite}}^{\mathrm{exp-max}}$ = 10^5 cm^{-3} s^{-1} to the saturation state Ω_{ikaite} = 18. Using this experimental kinetic pre-factor in Eq. 3.7, the maximum experimental nucleation rate can be calculated as a function of saturation state (Fig. 29). The comparison of the CNT-based nucleation rates with the experimental data depicts the above-mentioned discrepancy between the two data sets of approximately 3 orders of magnitude.

Relation between the nucleation rates of ikaite and anhydrous polymorphs

In the CNT model, supersaturation provides the driving force of nucleation and acts as a quantity which is not independent of polymorphs (Cardew, 2023). As the solubility product of ikaite exceeds that of calcite and vaterite at and above the freezing point of water (chapter 4.1; Bischoff et al., 1993a; Clarkson et al., 1992), a solution supersaturated with respect to metastable ikaite is always sufficiently concentrated for all other calcium carbonate minerals to potentially nucleate. In order to quantify the proportion of nuclei of the metastable phase, the so-called proportional nucleation rate χ_{N} can be defined as

$$\chi_{\mathrm{N}}(\Omega) = \frac{J_{\mathrm{m}}}{J_{\mathrm{s}} + J_{\mathrm{m}}} \qquad (4.2)$$

where J_m is the nucleation rate of the metastable phase and J_s that of the stable phases (Cardew, 2023). Here, J_m corresponds to the nucleation rate of ikaite and J_s to the sum of vaterite and calcite rates (Fig. 30). For an unequivocally dominant occurrence of ikaite, a proportional nucleation rate χ_N of at least 0.99 is required (Cardew, 2023).

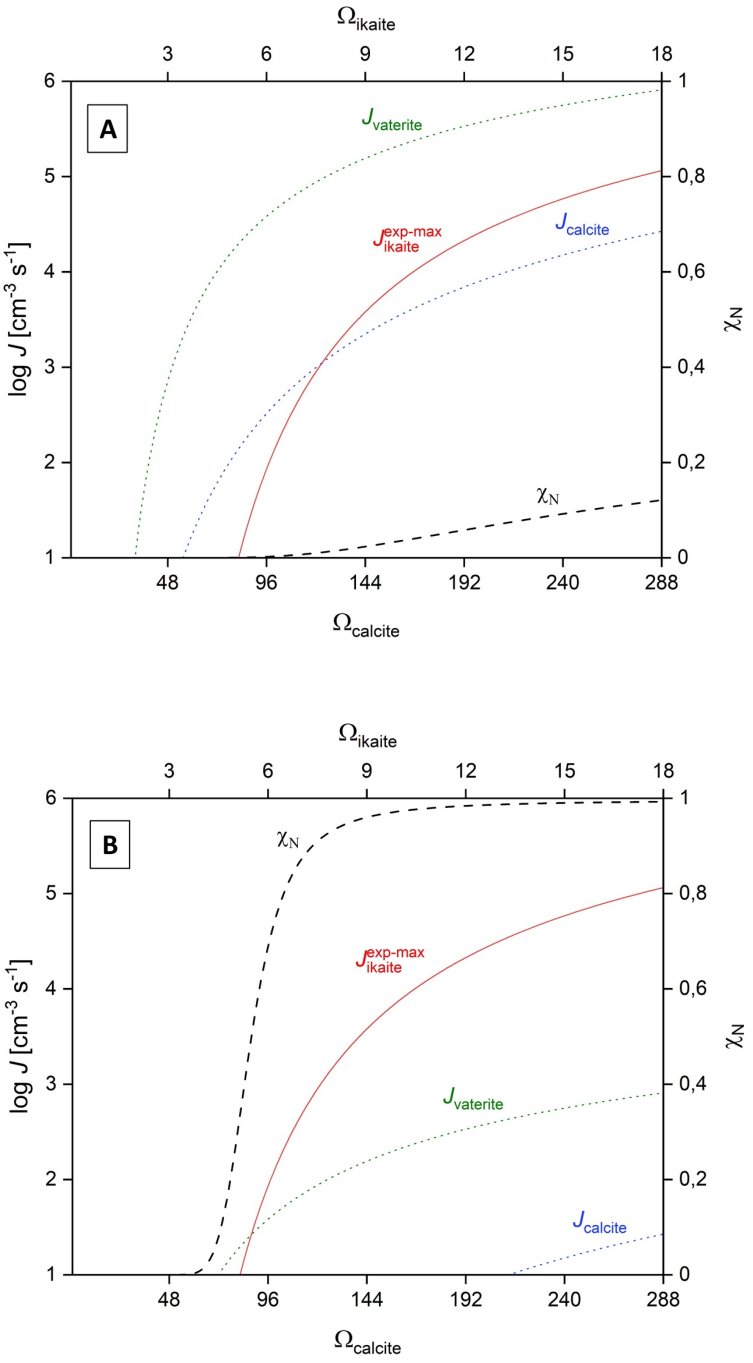

Figure 30. Plots of nucleation rates J as a function of solution composition expressed in terms of supersaturation with respect to ikaite and calcite. (**A**) The rates were calculated by applying experimental data from CMBR experiments at T = 0 °C (see chapter 4.1) with equal kinetic pre-factors $A^{exp}_{ikaite} = A_{vaterite} = A_{calcite} = 2 \times 10^6$ cm^{-3} s^{-1}. (**B**) $A_{vaterite}$ and $A_{calcite}$ were decreased by 3 orders of magnitude relative to (A) in order to attain a proportional nucleation rate χ_N = 0.99 which corresponds to an unequivocally dominant occurrence of ikaite nuclei.

The primary problem in calculating the nucleation rates of the anhydrous polymorphs J_{vaterite} and J_{calcite} lies in the determination of the kinetic pre-factors A_{calcite} and A_{vaterite}. Parameters for vaterite and calcite derived from CNT in literature are not applicable to our model as these vary widely and show a strong dependence on the method of determination (e.g. $10^4 \leq A \leq 10^{30}$ cm^{-3} s^{-1}; Bergwerff and van Paassen, 2021). Thus, in a first attempt, the evolution of nucleation rates for vaterite and calcite at $\Omega_{\text{ikaite}} \leq 18$ (= $\Omega_{\text{calcite}} \leq 288$) was calculated using equal kinetic pre-factors for all phases $A_i = A_{\text{ikaite}}^{\text{exp}} = 2 \times 10^6$ cm^{-3} s^{-1} (Fig. 30A). This scenario gave a nucleation rate of ikaite which, however, remained lower than that of vaterite over the entire range of relevant supersaturation ratios. Consequently, the proportional nucleation rate χ_N obtained by using equal kinetic pre-factors (Fig. 30A) described an equivalent ikaite nucleation rather than a dominant ikaite formation as it was observed in the experiments.

A sufficiently dominant ikaite formation, in contrast, can be achieved by using kinetic pre-factors A_{calcite} and A_{vaterite} which are 3 orders of magnitude lower than $A_{\text{ikaite}}^{\text{exp}}$. These values were plotted in the second scenario of the evolution of nucleation rates (Fig. 30B). This parameterization results in an extensive ikaite nucleation, as it was observed in our precipitation experiments at T = 0 °C.

The kinetic advantage of ikaite nucleation, induced by the higher kinetic parameter A, might reflect the different formation mechanism of ikaite compared to the more stable anhydrous $CaCO_3$ polymorphs. The ikaite nucleation mechanism most likely involves a dominant role of aqueous $CaCO_3^0 \cdot 6H_2O$ complexes (chapter 4.1; Buchardt et al., 2001; Chaka, 2018; Stockmann et al., 2018) and, therefore, provides a low energy pathway of crystallization without dehydration (chapter 4.1; Chaka, 2018). Analogously, it was proposed that an aggregation of oriented multi-ion-complexes can enhance the rate of cluster formation relative to condensation via the addition of monomers (De Yoreo et al., 2015; De Yoreo, 2022).

Although these reasonable kinetic assumptions easily allow a CNT-based modelling of a realistic relation between the nucleation rates of ikaite and the anhydrous phases (Fig. 30B), it needs to be noted that this does not validate the capability of CNT for providing a correct explanation of the dominant nucleation of ikaite over less soluble $CaCO_3$ minerals, unless sufficiently accurate and internally consistent kinetic pre-factors A_i become available.

Implications for the natural occurrence of ikaite

Ikaite nucleation was evident at temperatures of up to T = 20 °C. In none of our experiments, however, continuous ikaite growth was established as nucleation of anhydrous phases caused the solution concentrations to fall below ikaite saturation. At all conditions of our study, therefore, ikaite persistence was limited to less than 48 h. This finding clearly shows that prolonged endurance of ikaite within aqueous solutions requires an effective inactivation of anhydrous phases. A relevant possibility of such an inactivation is the presence of selective nucleation inhibitors. As chemical compositions of natural settings are complex, inhibitors are often present. Additionally to inhibitors, the preservation of mineral surfaces by biofilms might

stabilize ikaite. Furthermore, rapid overgrowth of the anhydrous phases by ikaite could contribute to prevent solution compositions from falling below ikaite saturation. Due to the retrograde solubility of the anhydrous phases, however, passivation of anhydrous phases by overgrowing ikaite becomes less likely with increasing temperature. Also the activity of inhibitors decreases with increasing supersaturation and, therefore, with increasing temperature.

The emphasis of ikaite endurance to near freezing temperatures as observed in our experiments agrees with natural settings where extensive growth of ikaite is well documented at $T \leq 9$ °C. Nevertheless, this narrow range of temperature for ikaite formation was frequently questioned, as the precipitation of ikaite in laboratory studies succeeded at $T > 9$ °C (Purgstaller et al., 2017; Stockmann et al., 2018; Tollefsen et al., 2020). Furthermore, an incoherence of the spatial or timely appearance of certain glendonite sites and low temperature conditions gave rise to suggestions that the occurrence of ikaite in nature is not necessarily limited to near-freezing environments (Popov et al., 2019; Rogov et al., 2021; Rogov et al., 2023). In this context, our results confirm that formation of ikaite at $T > 9$ °C is possible in general, irrespective of the presence of inhibitors of anhydrous $CaCO_3$ minerals. The extent of persistence of ikaite particularly at increased temperatures, however, depends on whether the system meets specific prerequisites. Besides the separation of ikaite from the aqueous medium, the presence of an adequate quantity of substances inhibiting nucleation of the more stable calcium carbonate phase seems to be essential. Such prerequisites might be critical for the potential origin of ikaite in environments with temperatures exceeding near-freezing values. Optimum persistence of such ikaite aggregates might result if the inhibitors for the anhydrous phases were coprecipitating with ikaite. Such inhibitors may efficiently slow down the replacement rate and, therefore, could support accurate pseudomorphosis.

Further implications follow for sea water alkalinity and CO_2 removal. In our experiments, dissolution of ikaite was driven by the formation of anhydrous phases within the bulk solution which led to an undersaturation of the solution with respect to ikaite. Vaterite or calcite growth concomitant to ikaite dissolution precludes an increase of solution alkalinity. An inhibition of vaterite/calcite formation, therefore, is mandatory to allow for an enhancement of solution alkalinity due to ikaite dissolution. Such an increase of alkalinity was suggested to affect the inorganic carbon dynamics in sea water during sea ice melting (Jones et al., 2023b) and might even provide a pathway for an increased atmospheric CO_2 removal (Renforth et al., 2022).

5 Conclusions

Fundamental formation kinetics of ikaite

The investigations of the crystallization of ikaite reported in this doctoral thesis provide new insights into the fundamental kinetics of the formation of ikaite.

Using induction periods from ikaite-forming CMBR experiments, the study of heterogeneous nucleation revealed that the presence of mineral substrates at $\Omega_{ikaite} \leq 5$ led to a different nucleation behaviour than pseudohomogeneous conditions. Within this low supersaturation regime ($\Omega_{ikaite} \leq 5$), a pronounced promotion by foreign mineral substrates indicated a high degree of heterogeneous nucleation. The impact of heterogenous nucleation diminishes in favour of homogeneous nucleation at enhanced degrees of supersaturation ($\Omega_{ikaite} \geq 8$). This finding revealed that mineral surfaces are an important nucleation parameter.

Furthermore, induction periods measured in both supersaturation regimes enabled the determination of the interfacial energy of ikaite nucleation. The interpretation of induction periods by classical nucleation theory (CNT) yielded an effective interfacial energy of 15 ± 3 mJ/m^2, which might be reduced to a value of 6 ± 3 mJ/m^2, depending on the degree of heterogeneous nucleation. These interfacial energies are significantly lower than reported values for anhydrous calcium carbonate minerals. Therefore, the interpretation of interfacial energies by CNT is in agreement with the structural implication that the formation of highly hydrated ikaite nuclei from aqueous solution relates to a low interfacial energy. Moreover, the low interfacial energy most likely leads to a substantially decreased nucleation barrier relative to anhydrous $CaCO_3$ minerals, suggesting the formation of ikaite via a low energy formation pathway. Such a low energy formation pathway may support a formation mechanism involving an ordering of aqueous ion pair complexes without extensive dehydration, that has previously been indicated through Density Functional Theory (DFT) calculations by Chaka (2018).

Further hints at this specific low energy formation pathway of ikaite, which differs significantly from the formation mechanism of anhydrous $CaCO_3$ minerals, might be given by the extent of decrease in interfacial energy due to heterogeneous nucleation. In contrast to the tremendous reductions of interfacial energies for vaterite and calcite by heterogeneous nucleation reported in literature, the interfacial energies of ikaite determined here indicated a weak decrease at conditions of heterogeneous nucleation. Apart from that, the low value of γ_{ikaite} does not allow a similar reduction by heterogeneous conditions as in the case of vaterite and calcite. Again, this finding might be associated with the formation mechanism without extensive dehydration of ikaite, as foreign active surfaces may not be as effective for attachment of aqueous ion pairs as for dehydration of aqueous ion pair complexes by ligand exchange.

Likewise, the growth kinetics of ikaite supports the low energy formation pathway. In contrast to the second to third order reaction kinetics of calcite growth in sea water, a first order rate law was derived for ikaite applying empirical rate equation to the measured growth rates. This first order reaction kinetics of ikaite implies a transport- or adsorption-controlled growth mechanism and, therefore, contrasts ligand exchange as the rate-limiting step of calcite growth

kinetics. Instead, the transport- or adsorption-controlled growth of ikaite can likely be associated with an attachment of hydrated $CaCO_3^0$ ion pairs without extensive dehydration.

A formation mechanism of ikaite via the attachment of hydrous ion pair complexes has important implications for the controls of ikaite precipitation in the multi-phase precipitating systems of calcium carbonate minerals. In the multi-phase precipitating system observed here, the nucleation of ikaite occurred alongside to less soluble anhydrous $CaCO_3$ minerals instead of sequential nucleation events of metastable calcium carbonate phases. This finding implied a limited applicability of Ostwald's rule of stages. CNT calculations could be used to model the observed multi-phase nucleation of calcium carbonate minerals. From the perspective of the resulting models, the concomitant nucleation might be associated with different formation mechanisms of ikaite and vaterite/calcite leading to significantly different kinetic pre-factors. Thus, the specific formation mechanism of ikaite may affect the kinetics of the concomitant nucleation of calcium carbonate phases altogether.

In addition to the above conclusions, the findings on the formation kinetics rise new questions about the identity of amorphous calcium carbonate (ACC*) and its role in subsequent crystallization. From CMBR experiments and SEM images, ACC* was indicated as a transient phase that altered formation conditions but precipitated independent of ikaite nucleation. However, a more detailed description of the impact of ACC* on calcium carbonate crystallization remains challenging as both the identity and role of ACC* have not been clearly specified yet (e.g. Lázár et al., 2023; Zou et al., 2018). Therefore, a profound understanding of the identity, appearance and decomposition of the amorphous phase prior and in parallel to ikaite nucleation would be a desirable supplement to the findings on the crystallization process of ikaite presented here. Particularly knowledge of the degree of hydration of the amorphous phase may have important implications for the crystallization of calcium carbonate minerals.

Formation conditions of ikaite

Apart from the insights into the fundamental formation kinetics, the studies reported here contribute to a better understanding of conditions that can promote the crystallization of ikaite. The presence of quartz and mica substrates led to nucleation of ikaite within a significantly broader supersaturation range compared to pseudohomogeneous formation conditions. Both tested mineral surfaces were similarly effective in promoting the nucleation of ikaite at supersaturations (Ω_{ikaite}) between 1.6 and 15. Within this range, the promotion of ikaite exceeded the promotion of the precipitation of anhydrous calcium carbonate minerals. Therefore, it must be assumed that the ubiquitous appearance of mineral surfaces may have a significant impact on the nucleation of ikaite in manifold environments of Earth, similar to the presence of common inhibitors of the formation of anhydrous $CaCO_3$ minerals such as Mg or phosphate ions.

It remains ambiguous, however, whether the presence of foreign mineral substrates supports the persistence in a similar efficiency as inhibitory additives, which are known to suppress a concomitant formation of competing anhydrous $CaCO_3$ minerals. Particularly

because quartz and mica surfaces are capable of being effective for the formation of both ikaite and anhydrous $CaCO_3$ minerals (vaterite and calcite; Li et al., 2014), the persistence of ikaite in presence of foreign substrates remains complex.

With respect to the role of inhibiting additives for ikaite persistence, at least in near-freezing temperature environments, sufficient persistence of ikaite for extensive growth can be provided by the presence of phosphate. Previous studies of the promotion of ikaite formation due to suppression of competing precipitation by phosphate implied that the inhibition results from different interactions of ikaite and anhydrous $CaCO_3$ minerals with phosphate, respectively (e.g. Bischoff et al., 1993a; Clarkson et al., 1992). This difference is further corroborated by the lack of phosphate uptake by ikaite during growth periods reported here ($1.5 \leq \Omega_{ikaite} \leq 2.9$), which contrasts the uptake of phosphate from solution by calcite (e.g. Hartley et al. 1997). In addition, there was no sign that the growth of ikaite is retarded significantly by the presence of phosphate. Most likely, the substitution of carbonate groups by phosphate is largely incompatible with the growth mechanism of ikaite. Ultimately, a sufficient amount of phosphate thus remains in the growth solution to support the persistence of ikaite.

Furthermore, the observations of ikaite ephemerality in CMBR experiments indicated that an inhibition of the formation of anhydrous $CaCO_3$ minerals might be an important prerequisite for extensive ikaite formation in aqueous environments of Earth. The transient occurrence of ikaite in solutions up to 20 °C suggests that an inhibition of the competing precipitation of vaterite and calcite is critical for prolonged growth conditions of ikaite. Obviously, such an inhibition, as exerted for example by substances like Mg or phosphate, applies to distinct sea water environments where extensive growth of ikaite is well documented at $T \leq 9$ °C (e.g. Buchardt et al., 1997; Papadimitriou et al., 2013; Stockmann et al., 2018; Tollefsen et al., 2018). For solution temperatures that exceed this narrow temperature range, in contrast, the increasing ephemerality of ikaite reported here implies that an effective inhibition of competing precipitation becomes more complex to achieve.

This finding has important implications for the use of ikaite pseudomorphs (glendonites) as temperature indicators. The applicability of glendonites as proxies representing near freezing temperatures has been questioned because precipitation of ikaite in previous laboratory studies (e.g. Purgstaller et al., 2017; Tollefsen et al., 2020) has been observed at temperatures exceeding near-freezing values analogous to this work. From the perspective of ikaite nucleation, the use of ikaite as indicators of near freezing environments, therefore, cannot be supported. However, the limited persistence of ikaite and complex inhibition of anhydrous $CaCO_3$ minerals with increasing temperature reported here provide a substantial limitation of ikaite growth with temperature. Thus, the applicability of glendonites as a powerful low temperature indicator in most cases is clearly supported by the findings of this work.

Implications for aqueous environments

In addition to the impact on formation conditions, the findings reported here contribute to a better understanding of the effects of ikaite precipitation on aqueous environments.

In this context, the lack of phosphate uptake observed in growth experiments has important implications for ikaite growth environments. Temporal polar nutrient dynamics, for instance, were associated with a potential uptake and rejection of phosphate by seasonal formation and dissolution of ikaite in sea ice (Hu et al., 2014; Jones et al., 2023b). The observed lack of phosphate depletion during growth in CMFR experiments, however, indicates that the growth of ikaite may not contribute significantly to seasonal phosphate dynamics in surface oceanic water. Instead, other abiotic or biotic processes, which can be triggered due to the seasonal formation and melting of sea ice (e.g. Fripiat et al., 2017; van der Linden et al., 2020), are more likely to contribute to the polar nutrient cycling.

Furthermore, the observed limited persistence of ikaite in multi-phase precipitating systems has implications for the evolution of alkalinity in sea water. Because ikaite is significantly more soluble than the anhydrous $CaCO_3$ polymorphs, ikaite usually dissolves in surface oceanic water and, therefore, is capable of contributing to alkalinity enhancement (e.g. Renforth et al., 2022). However, the observations from multi-phase precipitating systems reported here show that the contribution to alkalinity enhancement by dissolution of ikaite might be reduced significantly due to concomitant formation of less soluble anhydrous $CaCO_3$ minerals. Thus, in order to enhance the alkalinity of solution, inactivation of competing precipitation could be essential, as this may increase the degree of ikaite dissolution.

References

Addadi, L., Raz, S., Weiner, S., 2003. Taking Advantage of Disorder: Amorphous Calcium Carbonate and Its Roles in Biomineralization. Adv. Mater. 15 (12), 959–970.

Bastianini, L., Rogerson, M., Brasier, A., Prior, T.J., Hardman, K., Dempsey, E., Bird, A., Mayes, W.M., 2024. Ikaite formation in streams affected by steel waste leachate: First report and potential impact on contaminant dynamics. Chemical Geology 644, 121842.

Bergwerff, L., van Paassen, L.A., 2021. Review and Recalculation of Growth and Nucleation Kinetics for Calcite, Vaterite and Amorphous Calcium Carbonate. Crystals 11 (11), 1318.

Berninger, U.-N., Jordan, G., Lindner, M., Reul, A., Schott, J., Oelkers, E.H., 2016. On the effect of aqueous Ca on magnesite growth – Insight into trace element inhibition of carbonate mineral precipitation. Geochimica et Cosmochimica Acta 178, 195–209.

Besselink, R., Rodriguez-Blanco, J.D., Stawski, T.M., Benning, L.G., Tobler, D.J., 2017. How Short-Lived Ikaite Affects Calcite Crystallization. Crystal Growth & Design 17 (12), 6224–6230.

Bischoff, J.L., Fitzpatrick, J.A., Rosenbauer, R.J., 1993a. The Solubility and Stabilization of Ikaite ($CaCO3 \cdot 6H2O$) from 0° to 25°C: Environmental and Paleoclimatic Implications for Thinolite Tufa. The Journal of Geology 101 (1), 21–33.

Bischoff, J.L., Rosenbauer, R.J., Fitzpatrick, J.A., Stafford Jr., T.W., 1993b. Ikaite precipitation by mixing of shoreline springs and lake water, Mono Lake, California, USA. Geochimica et Cosmochimica 57 (16), 3855–3865.

Boch, R., Dietzel, M., Reichl, P., Leis, A., Baldermann, A., Mittermayr, F., Pölt, P., 2015. Rapid ikaite ($CaCO3 \cdot 6H2O$) crystallization in a man-made river bed: Hydrogeochemical monitoring of a rarely documented mineral formation. Applied Geochemistry 63, 366–379.

Brečević, L., Kralj, D., 2007. On Calcium Carbonates: from Fundamental Research to Application. Croatica Chemica Acta 80 (3-4), 467–484.

Brečević, L., Nielsen, A.E., 1989. Solubility of amorphous calcium carbonate. Journal of Crystal Growth 98 (3), 504–510.

Buchardt, B., Israelson, C., Seaman, P., Stockmann, G., 2001. Ikaite tufa towers in Ikka Fjord, southwest Greenland: their formation by mixing of seawater and alkaline spring water. Journal of Sedimentary Research 71 (1), 176–189.

Buchardt, B., Seaman, P., Stockmann, G., Vous, M., Wilken, U., Düwel, L., Kristiansen, A., Jenner, C., Whiticar, M.J., Kristensen, R.M., Petersen, G.H., Thorbjørn, L., 1997. Submarine columns of ikaite tufa. Nature 390 (6656), 129–130.

Burton, E.A., Walter, L.M., 1990. The role of pH in phosphate inhibition of calcite and aragonite precipitation rates in seawater. Geochimica et Cosmochimica Acta 54 (3), 797–808.

Busenberg, E., Plummer, L.N., 1986. A comparative study of the dissolution and crystal growth kinetics of calcite and aragonite. Studies in diagenesis, 1578, 139–168.

Caldeira, K., Wickett, M.E., 2003. Anthropogenic carbon and ocean pH. Nature 425, 365.

Cardew, P.T., 2023. Ostwald Rule of Stages—Myth or Reality? Crystal Growth & Design 23 (6), 3958–3969.

Cartwright, J.H.E., Checa, A.G., Gale, J.D., Gebauer, D., Sainz-Díaz, C.I., 2012. Calcium carbonate polyamorphism and its role in biomineralization: how many amorphous calcium carbonates are there? Angewandte Chemie (International ed. in English) 51 (48), 11960–11970.

Cedeno, R., Grossier, R., Candoni, N., Levernier, N., Flood, A.E., Veesler, S., 2023. CNT effective interfacial energy and pre-exponential kinetic factor from measured NaCl crystal nucleation time distributions in contracting microdroplets. The Journal of Chemical Physics 158 (19).

Chaka, A.M., 2018. Ab Initio Thermodynamics of Hydrated Calcium Carbonates and Calcium Analogues of Magnesium Carbonates: Implications for Carbonate Crystallization Pathways. ACS Earth Space Chem. 2 (3), 210–224.

Clarkson, J.R., Price, T.J., Adams, C.J., 1992. Role of Metastable Phases in the Spontaneous Precipitation of Calcium Carbonate. Journal of the Chemical Society, Faraday Transactions 88 (2), 243–249.

Council, T.C., Bennett, P.C., 1993. Geochemistry of ikaite formation at Mono Lake, California: Implications for the origin of tufa mounds. Geology 21 (11), 971–974.

Cozzi, S., 2008. High-resolution trends of nutrients, DOM and nitrogen uptake in the annual sea ice at Terra Nova Bay, Ross Sea. Antarctic Science 20 (5), 441–454.

Dalas, E., 1992. The overgrowth of calcium carbonate hexahydrate and calcium phosphate on new functionalized polymers. Journal of Materials Science Letters 11 (21), 1408–1410.

De Yoreo, J.J., 2022. Casting a bright light on Ostwald's rule of stages. Proceedings of the National Academy of Sciences of the United States of America 119 (7).

De Yoreo, J.J., Gilbert, P.U.P.A., Sommerdijk, N.A.J.M., Penn, R.L., Whitelam, S., Joester, D., Zhang, H., Rimer, J.D., Navrotsky, A., Banfield, J.F., Wallace, A.F., Michel, F.M., Meldrum, F.C., Cölfen, H., Dove, P.M., 2015. Crystallization by particle attachment in synthetic, biogenic, and geologic environments. Science (New York, N.Y.) 349 (6247), aaa6760.

De Yoreo, J.J., Waychunas, G.A., Jun, Y.-S., Fernandez-Martinez, A., 2013. In situ Investigations of Carbonate Nucleation on Mineral and Organic Surfaces. Reviews in Mineralogy and Geochemistry 77 (1), 229–257.

Delille, B., Vancoppenolle, M., Geilfus, N.-X., Tilbrook, B., Lannuzel, D., Schoemann, V., Becquevort, S., Carnat, G., Delille, D., Lancelot, C., Chou, L., Dieckmann, G.S., Tison, J.-L., 2014. Southern Ocean CO 2 sink: The contribution of the sea ice. Journal of Geophysical Research: Oceans 119 (9), 6340–6355.

Demichelis, R., Raiteri, P., Gale, J.D., 2014. Structure of hydrated calcium carbonates: A first-principles study. Journal of Crystal Growth 401, 33–37.

Devos, C., van Gerven, T., Kuhn, S., 2021. A Review of Experimental Methods for Nucleation Rate Determination in Large-Volume Batch and Microfluidic Crystallization. Crystal Growth & Design 21 (4), 2541–2565.

Dickens, B., Brown, E.W., 1970. The Crystal Structure of Calcium Carbonate Hexahydrate at about -120°. Inorganic Chemistry 9 (3), 480–486.

Dieckmann, G.S., Nehrke, G., Papadimitriou, S., Göttlicher, J., Steininger, R., Kennedy, H., Wolf-Gladrow, D., Thomas, D.N., 2008. Calcium carbonate as ikaite crystals in Antarctic sea ice. Geophysical Research Letters 35 (8).

Dieckmann, G.S., Nehrke, G., Uhlig, C., Göttlicher, J., Gerland, S., Granskog, M.A., Thomas, D.N., 2010. Brief Communication: Ikaite (CaCO 3 ·6H 2 O) discovered in Arctic sea ice. The Cryosphere 4 (2), 227–230.

Doney, S.C., Fabry, V.J., Feely, R.A., Kleypas, J.A., 2009. Ocean acidification: the other CO2 problem. Annual review of marine science 1, 169–192.

Dromgoole, E.L., Walter, L.M., 1990. Inhibition of calcite growth rates by Mn2+ in CaCl2 solutions at 10, 25, and 50 C. Geochimica et Cosmochimica Acta 54 (11), 2991–3000.

Fischer, M., Thomas, D.N., Krell, A., Nehrke, G., Göttlicher, J., Norman, L., Meiners, K.M., Riaux-Gobin, C., Dieckmann, G.S., 2013. Quantification of ikaite in Antarctic sea ice. Antarctic Science 25 (3), 421–432.

Fransson, A., Chierici, M., Yager, P.L., Smith, W.O., 2011. Antarctic sea ice carbon dioxide system and controls. Journal of Geophysical Research 116 (C12).

Fripiat, F., Meiners, K.M., Vancoppenolle, M., Papadimitriou, S., Thomas, D.N., Ackley, S.F., Arrigo, K.R., Carnat, G., Cozzi, S., Delille, B., Dieckmann, G.S., Dunbar, R.B., Fransson, A., Kattner, G., Kennedy, H., Lannuzel, D., Munro, D.R., Nomura, D., Rintala, J.-M., Schoemann, V., Stefels, J., Steiner, N., Tison, J.-L., 2017. Macro-nutrient concentrations in Antarctic pack ice: Overall patterns and overlooked processes. Elementa: Science of the Anthropocene 5.

Garvie, L.A.J., 2022. Seasonal formation of ikaite in slime flux jelly on an infected tree (Populus fremontii) wound from the Sonoran Desert. The Science of Nature 109 (5), 48.

Gautier, Q., Berninger, U.-N., Schott, J., Jordan, G., 2015. Influence of organic ligands on magnesite growth: A hydrothermal atomic force microscopy study. Geochimica et Cosmochimica Acta 155, 68–85.

Gebauer, D., Cölfen, H., 2011. Prenucleation clusters and non-classical nucleation. Nano Today 6 (6), 564–584.

Geilfus, N.-X., Carnat, G., Dieckmann, G.S., Halden, N., Nehrke, G., Papakyriakou, T., Tison, J.-L., Delille, B., 2013. First estimates of the contribution of CaCO 3 precipitation to the release of CO 2 to the atmosphere during young sea ice growth. Journal of Geophysical Research: Oceans 118 (1), 244–255.

Geilfus, N.-X., Galley, R.J., Else, B.G.T., Campbell, K., Papakyriakou, T., Crabeck, O., Lemes, M., Delille, B., Rysgaard, S., 2016. Estimates of ikaite export from sea ice to the underlying seawater in a sea ice–seawater mesocosm. The Cryosphere 10 (5), 2173–2189.

Gómez-Morales, J., Torrent-Burgués, J., Rodríguez-Clemente, R., 1996. Nucleation of calcium carbonate at different initial pH conditions. Journal of Crystal Growth 169 (2), 331–338.

Gratz, A.J., Hillner, P.E., Hansma, P.K., 1993. Step dynamics and spiral growth on calcite. Geochimica et Cosmochimica Acta 57 (2), 491–495.

Guinotte, J.M., Fabry, V.J., 2008. Ocean acidification and its potential effects on marine ecosystems. Annals of the New York Academy of Sciences 1134, 320–342.

Gutjahr, A., Dabringhaus, H., Lacmann, R., 1996. Studies of the growth and dissolution kinetics of the CaCO3 polymorphs calcite and aragonite I. Growth and dissolution rates in water. Journal of Crystal Growth 158 (3), 296–309.

Hamm, L.M., Giuffre, A.J., Han, N., Tao, J., Wang, D., Yoreo, J.J. de, Dove, P.M., 2014. Reconciling disparate views of template-directed nucleation through measurement of calcite nucleation kinetics and binding energies. Proceedings of the National Academy of Sciences of the United States of America 111 (4), 1304–1309.

Hartley, A.M., House, W.A., Callow, M.E., Leadbeater, B., 1997. Coprecipitation of phosphate with calcite in the presence of photosynthesizing green algae. Water Research 31 (9), 2261–2268.

He, S., Oddo, J.E., Tomson, M.B., 1994. The Nucleation Kinetics of Calcium Sulfate Dihydrate in NaCl Solutions up to 6 m and 90 °C. Journal of Colloid and Interface Science 162 (2), 297–303.

Henzler, K., Fetisov, E.O., Galib, M., Baer, M.D., Legg, B.A., Borca, C., Xto, J.M., Pin, S., Fulton, J.L., Schenter, G.K., Govind, N., Siepmann, J.I., Mundy, C.J., Huthwelker, T., De Yoreo, J.J., 2018. Supersaturated calcium carbonate solutions are classical. Science advances 4 (1), eaao6283.

Hesse, K.F., Küppers, H., Suess, E., 1983. Refinement of the structure of Ikaite, CaCO3· 6H2O. Zeitschrift für Kristallographie-Crystalline Materials 163 (3-4), 227–231.

House, W.A., 1987. Inhibition of Calcite Crystal Growth by Inorganic Phosphate. Journal of Colloid and Interface Science 119 (2), 505–511.

House, W.A., Donaldson, L., 1986. Adsorption and Coprecipitation of Phosphate on Calcite. Journal of Colloid and Interface Science 112 (2), 309–324.

Hu, Q., Nielsen, M.H., Freeman, C.L., Hamm, L.M., Tao, J., Lee, J.R.I., Han, T.Y.J., Becker, U., Harding, J.H., Dove, P.M., Yoreo, J.J. de, 2012. The thermodynamics of calcite nucleation at organic interfaces: Classical vs. non-classical pathways. Faraday Discuss. 159, 509.

Hu, Y.-B., Dieckmann, G.S., Wolf-Gladrow, D.A., Nehrke, G., 2014. Laboratory study on coprecipitation of phosphate with ikaite in sea ice. Journal of Geophysical Research: Oceans 119 (10), 7007–7015.

Hu, Y.-B., Wang, F., 2020. Effect of ikaite precipitation on phosphate removal in sea ice. Polar Research 39 (0).

Hu, Y.-B., Wolthers, M., Wolf-Gladrow, D.A., Nehrke, G., 2015. Effect of pH and Phosphate on Calcium Carbonate Polymorphs Precipitated at near-Freezing Temperature. Crystal Growth & Design 15 (4), 1596–1601.

Huggett, J.M., Schultz, B.P., Shearman, D.J., Smith, A.J., 2005. The petrology of ikaite pseudomorphs and their diagenesis. Proceedings of the Geologists' Association 116 (3-4), 207–220.

Hume, J., Topley, B., 1926. CCCXC - The Density of Calcium Carbonate Hxahydrate. Journal of the Chemical Society (resumed) 129, 2932–2934.

Ishikawa, M., Ichikuni, M., 1981. Coprecipitation of phosphate with calcite. Geochemical Journal 15 (5), 283–288.

Ito, T., 1996. Ikaite from cold spring water at Shiowakka, Hokkaido, Japan. J. Mm. Petr. Econ. Geol. 91, 209–219.

Jimoh, O.A., Ariffin, K.S., Hussin, H.B., Temitope, A.E., 2018. Synthesis of precipitated calcium carbonate: a review. Carbonates Evaporites 33 (2), 331–346.

Johnston, J., Merwin, H.E., Williams, E.D., 1916. The Several Forms of Calcium Carbonate. American Journal of Science (246), 473–512.

Jones, E.M., Chierici, M., Fransson, A., Assmann, K.M., Renner, A.H., Hodal Lødemel, H., 2023a. Inorganic carbon and nutrient dynamics in the marginal ice zone of the Barents Sea: Seasonality and implications for ocean acidification. Progress in Oceanography 219, 103131.

Jones, E.M., Henley, S.F., van Leeuwe, M.A., Stefels, J., Meredith, M.P., Fenton, M., Venables, H.J., 2023b. Carbon and nutrient cycling in Antarctic landfast sea ice from winter to summer. Limnology & Oceanography 68 (1), 208–231.

Kamal, M.S., Hussein, I., Mahmoud, M., Sultan, A.S., Saad, M.A., 2018. Oilfield scale formation and chemical removal: A review. Journal of Petroleum Science and Engineering 171, 127–139.

Karabelas, A.J., 2002. Scale formation in tubular heat exchangers - research priorities. International Journal of Thermal Sciences 41 (7), 682–692.

Kashchiev, D., 2000. Nucleation: Basic Theory with Applications. Butterworth-Heinemann, Oxford, 551 pp.

Kashchiev, D., van Rosmalen, G.M., 2003. Review: Nucleation in solutions revisited. Cryst. Res. Technol. 38 (7-8), 555–574.

Kashchiev, D., Verdoes, D., van Rosmalen, G.M., 1991. Induction time and metastability limit in new phase formation. Journal of Crystal Growth 110 (3), 373–380.

Kavitha, A.L., Vasudevan, T., Prabu, H.G., 2011. Evaluation of synthesized antiscalants for cooling water system application. Desalination 268 (1-3), 38–45.

Kennedy, G.L., 2022. Glendonites: Enigmatic Mineral Pseudomorphs and Their Ephemeral Precursor. Rocks & Minerals 97 (6), 496–509.

Krauss, F., Schriever, W., 1930. Die Hydrate des Calciumcarbonats. Zeitschrift für anorganische und allgemeine Chemie 188 (1), 259–273.

Lancia, A., Musmarra, D., Prisciandaro, M., 1999. Measuring induction period for calcium sulfate dihydrate precipitation. AIChE Journal 45 (2), 390–397.

Lázár, A., Molnár, Z., Demény, A., Kótai, L., Trif, L., Béres, K.A., Bódis, E., Bortel, G., Aradi, L.E., Karlik, M., Szabó, M.Z., Pekker, Á., Németh, G., Kamarás, K., Garvie, L.A.J., Németh, P., 2023. Insights into the amorphous calcium carbonate (ACC) → ikaite → calcite transformations. CrystEngComm 25 (5), 738–750.

Levi-Kalisman, Y., Raz, S., Weiner, S., Addadi, L., Sagi, I., 2002. Structural Differences Between Biogenic Amorphous Calcium Carbonate Phases Using X-ray Absorption Spectroscopy. Advanced Functional Materials 12 (1), 43.

Li, Q., Fernandez-Martinez, A., Lee, B., Waychunas, G.A., Jun, Y.-S., 2014. Interfacial energies for heterogeneous nucleation of calcium carbonate on mica and quartz. Environmental science & technology 48 (10), 5745–5753.

Lin, Y.-P., Singer, P.C., 2006. Inhibition of calcite precipitation by orthophosphate: Speciation and thermodynamic considerations. Geochimica et Cosmochimica Acta 70 (10), 2530–2539.

Lindner, M., Jordan, G., 2018. On the growth of witherite and its replacement by the Mg-bearing double carbonate norsethite: Implications for the dolomite problem. American Mineralogist 103 (2), 252–259.

Lioliou, M.G., Paraskeva, C.A., Koutsoukos, P.G., Payatakes, A.C., 2007. Heterogeneous nucleation and growth of calcium carbonate on calcite and quartz. Journal of Colloid and Interface Science 308 (2), 421–428.

Lopez, O., Zuddas, P., Faivre, D., 2009. The influence of temperature and seawater composition on calcite crystal growth mechanisms and kinetics: Implications for Mg incorporation in calcite lattice. Geochimica et Cosmochimica Acta 73 (2), 337–347.

MacAdam, J., Parsons, S.A., 2004. Calcium carbonate scale formation and control. Reviews in Environmental Science and Bio/Technology 3, 159–169.

MacKenzie, J.E., 1923. CCLXXIV-Calcium Carbonate Hexahydrate // CCLXXIV.—Calcium carbonate hexahydrate. Journal of the Chemical Society, Transactions 123 (0), 2409–2417.

Malkaj, P., Chrissanthopoulos, A., Dalas, E., 2002. The overgrowth of calcium carbonate hexahydrate on new functionalized polymers. Journal of Crystal Growth 242 (1-2), 233–238.

Marland, G., 1975. The stability of of CaCO3·6H2O (ikaite). Geochimica et Cosmochimica Acta 39 (1), 83–91.

Meiners, K.M., Norman, L., Granskog, M.A., Krell, A., Heil, P., Thomas, D.N., 2011. Physico-ecobiogeochemistry of East Antarctic pack ice during the winter-spring transition. Deep Sea Research Part II: Topical Studies in Oceanography 58 (9-10), 1172–1181.

Millero, F., Huang, F., Graham, T., Pierrot, D., 2007. The dissociation of carbonic acid in NaCl solutions as a function of concentration and temperature. Geochimica et Cosmochimica Acta 71 (1), 46–55.

Millero, F.J., 2013. Chemical Oceanography, 4th ed. CRC Press, Boca Raton.

Mills, J.V., Barnhart, H.A., DePaolo, D.J., Lammers, L.N., 2022. New insights into Mn2+ and Mg2+ inhibition of calcite growth. Geochimica et Cosmochimica Acta 334, 338–367.

Morales, C., Rogov, M., Wierzbowski, H., Ershova, V., Suan, G., Adatte, T., Föllmi, K.B., Tegelaar, E., Reichart, G.-J., Lange, G.J. de, Middelburg, J.J., van de Schootbrugge, B., 2017. Glendonites track methane seepage in Mesozoic polar seas. Geology 45 (6), 503–506.

Morse, J.W., 1983. The kinetics of calcium carbonate dissolution and precipitation. Rev. Mineral 11, 227–264.

Morse, J.W., Arvidson, R.S., Lüttge, A., 2007. Calcium carbonate formation and dissolution. Chemical reviews 107 (2), 342–381.

Mucci, A., 1986. Growth kinetics and composition of magnesian calcite overgrowths precipitated from seawater: Quantitative influence of orthophosphate ions. Geochimica et Cosmochimica Acta 50 (10), 2255–2265.

Mucci, A., Morse, J.W., 1983. The incorporation of Mg2+ and Sr2+ into calcite overgrowths: influences of growth rate and solution composition. Geochimica et Cosmochimica Acta 47 (2), 217–233.

Mullin, J.W., 2001. Crystallization, 4th ed. Butterworth-Heinemann, Oxford, 612 pp.

Nancollas, G.H., Reddy, M.M., 1971. The crystallization of calcium carbonate. II. Calcite growth mechanism. Journal of Colloid and Interface Science 37 (4), 824–830.

Navrotsky, A., 2004. Energetic clues to pathways to biomineralization: Precursors, clusters, and nanoparticles. Proceedings of the National Academy of Sciences of the United States of America 101 (33), 12096–12101.

Németh, P., Töchterle, P., Dublyansky, Y., Stalder, R., Molnár, Z., Klébert, S., Spötl, C., 2022. Tracing structural relicts of the ikaite-to-calcite transformation in cryogenic cave glendonite. American Mineralogist 107 (10), 1960–1967.

Nielsen, A.E., 1983. Precipitates: formations, coprecipitation, and aging. Treatise on Analytical Chemistry (eds. Kolthoff, IM and Elving, PJ), 269–347.

Oehlerich, M., Mayr, C., Griesshaber, E., Lücke, A., Oeckler, O.M., Ohlendorf, C., Schmahl, W.W., Zolitschka, B., 2013. Ikaite precipitation in a lacustrine environment – implications for palaeoclimatic studies using carbonates from Laguna Potrok Aike (Patagonia, Argentina). Quaternary Science Reviews 71, 46–53.

Ogino, T., Suzuki, T., Kiyoshi, S., 1987. The formation and transformation mechanism of calcium carbonate in water. Geochimica et Cosmochimica Acta 51 (10), 2757–2767.

Omelon, C.R., Pollard, W.H., Marion, G.M., 2001. Seasonal formation of ikaite (CaCO3· 6H2O) in saline spring discharge at Expedition Fiord, Canadian High Arctic: Assessing conditional constraints for natural crystal growth. Geochimica et Cosmochimica 65 (9), 1429–1437.

Ostwald, W., 1897. Studien über die Bildung und Umwandlung fester Körper. Zeitschrift für physikalische Chemie 22 (1), 289–330.

Papadimitriou, S., Kennedy, H., Kennedy, P., Thomas, D.N., 2013. Ikaite solubility in seawater-derived brines at 1atm and sub-zero temperatures to 265K. Geochimica et Cosmochimica Acta 109, 241–253.

Papadimitriou, S., Kennedy, H., Kennedy, P., Thomas, D.N., 2014. Kinetics of ikaite precipitation and dissolution in seawater-derived brines at sub-zero temperatures to 265 K. Geochimica et Cosmochimica Acta 140, 199–211.

Parkhurst, D.L., Appelo, C.A.J., 2013. Description of Input for PHREEQC Version 3—A Computer Program for Speciation, Batch-Reaction, One-Dimensional Transport, and Inverse Geochemical Calculations. U.S. Geological Survey, Denver, Colorado, 519 pp.

Pauly, H., 1963. “IKAITE”, A NEW MINERAL FROM GREENLAND. Arctic 16 (4), 263–264.

Peckmann, J., 2017. Unleashing the potential of glendonite: A mineral archive for biogeochemical processes and paleoenvironmental conditions. Geology 45 (6), 575–576.

Pelouze, M.J., 1865. Sur une combinaison nouvelle d’eau et de carbonate de chaux. Comptes rendus hebdomadaires des séances de l’Académie des sciences 60, 429–431.

Plummer, L.N., Busenberg, E., 1982. The solubilities of calcite, aragonite and vaterite in CO2-H20 solutions between 0 and 90 °C, and an evaluation of the aqueous model for the system CaCO3-CO2-H20. Geochimica et Cosmochimica Acta 6 (46), 1011–1040.

Popov, L.E., Álvaro, J.J., Holmer, L.E., Bauert, H., Ghobadi Pour, M., Dronov, A.V., Lehnert, O., Hints, O., Männik, P., Zhang, Z., Zhang, Z., 2019. Glendonite occurrences in the Tremadocian of Baltica: first Early Palaeozoic evidence of massive ikaite precipitation at temperate latitudes. Scientific reports 9 (1), 1–10.

Purgstaller, B., Dietzel, M., Baldermann, A., Mavromatis, V., 2017. Control of temperature and aqueous Mg 2+ /Ca 2+ ratio on the (trans-)formation of ikaite. Geochimica et Cosmochimica Acta 217, 128–143.

Qu, Y., Teichert, B.M.A., Birgel, D., Goedert, J.L., Peckmann, J., 2017. The prominent role of bacterial sulfate reduction in the formation of glendonite: a case study from Paleogene marine strata of western Washington State. Facies 63 (2).

Radha, A.V., Forbes, T.Z., Killian, C.E., Gilbert, P.U.P.A., Navrotsky, A., 2010. Transformation and crystallization energetics of synthetic and biogenic amorphous calcium carbonate. Proceedings of the National Academy of Sciences of the United States of America 107 (38), 16438–16443.

Renforth, P., Baltruschat, S., Peterson, K., Mihailova, B.D., Hartmann, J., 2022. Using ikaite and other hydrated carbonate minerals to increase ocean alkalinity for carbon dioxide removal and environmental remediation. Joule 6 (12), 2674–2679.

Ridgwell, A., Zeebe, R.E., 2005. The role of the global carbonate cycle in the regulation and evolution of the Earth system. Earth and Planetary Science Letters 234 (3-4), 299–315.

Rodríguez-Ruiz, I., Veesler, S., Gómez-Morales, J., Delgado-López, J.M., Grauby, O., Hammadi, Z., Candoni, N., García-Ruiz, J.M., 2014. Transient Calcium Carbonate Hexahydrate (Ikaite) Nucleated and Stabilized in Confined Nano- and Picovolumes. Crystal Growth & Design 14 (2), 792–802.

Rogov, M., Ershova, V., Gaina, C., Vereshchagin, O., Vasileva, K., Mikhailova, K., Krylov, A., 2023. Glendonites throughout the Phanerozoic. Earth-Science Reviews 241, 104430.

Rogov, M., Ershova, V., Vereshchagin, O., Vasileva, K., Mikhailova, K., Krylov, A., 2021. Database of global glendonite and ikaite records throughout the Phanerozoic. Earth Syst. Sci. Data 13 (2), 343–356.

Rysgaard, S., Glud, R.N., Lennert, K., Cooper, M., Halden, N., Leakey, R.J.G., Hawthorne, F.C., Barber, D., 2012. Ikaite crystals in melting sea ice – implications for pCO_2 and pH levels in Arctic surface waters. The Cryosphere 6 (4), 901–908.

Rysgaard, S., Glud, R.N., Sejr, M.K., Bendtsen, J., Christensen, P.B., 2007. Inorganic carbon transport during sea ice growth and decay: A carbon pump in polar seas. Journal of Geophysical Research: Oceans 112 (C3).

Rysgaard, S., Søgaard, D.H., Cooper, M., Pu&cacute, ko, M., Lennert, K., Papakyriakou, T.N., Wang, F., Geilfus, N.X., Glud, R.N., Ehn, J., McGinnis, D.F., Attard, K., Sievers, J., Deming, J.W., Barber, D., 2013. Ikaite crystal distribution in winter sea ice and implications for CO_2 system dynamics. The Cryosphere 7 (2), 707–718.

Rysgaard, S., Wang, F., Galley, R.J., Grimm, R., Notz, D., Lemes, M., Geilfus, N.-X., Chaulk, A., Hare, A.A., Crabeck, O., Else, B.G.T., Campbell, K., Sørensen, L.L., Sievers, J., Papakyriakou, T., 2014. Temporal dynamics of ikaite in experimental sea ice. The Cryosphere 8 (4), 1469–1478.

Saldi, G.D., Causserand, C., Schott, J., Jordan, G., 2021. Dolomite dissolution mechanisms at acidic pH: New insights from high resolution pH-stat and mixed-flow reactor experiments associated to AFM and TEM observations. Chemical Geology 584, 120521.

Sánchez-Pastor, N., Oehlerich, M., Astilleros, J.M., Kaliwoda, M., Mayr, C.C., Fernández-Díaz, L., Schmahl, W.W., 2016. Crystallization of ikaite and its pseudomorphic transformation into calcite: Raman spectroscopy evidence. Geochimica et Cosmochimica Acta 175, 271–281.

Sangwal, K., 2007. Additives and crystallization processes: From fundamentals to applications. Wiley, Chichester, xvi, 451.

Schubert, C.J., Nürnberg, D., Scheele, N., Pauer, F., Kriews, M., 1997. 13C isotope depletion in ikaite crystals: evidence for methane release from the Siberian shelves? Geo-Marine Letters 17 (2), 169–174.

Schultz, B.P., Huggett, J., Ullmann, C.V., Kassens, H., Kölling, M., 2023. Links between Ikaite Morphology, Recrystallised Ikaite Petrography and Glendonite Pseudomorphs Determined from Polar and Deep-Sea Ikaite. Minerals 13 (7), 841.

Selleck, B.W., Carr, P.F., Jones, B.G., 2007. A Review and Synthesis of Glendonites (Pseudomorphs after Ikaite) with New Data: Assessing Applicability as Recorders of Ancient Coldwater Conditions. Journal of Sedimentary Research 77 (11), 980–991.

Shearman, D.J., Smith, A.J., 1985. Ikaite, the parent mineral of jarrowite-type pseudomorphs. Proceedings of the Geologists' Association 96 (4), 305–314.

Shiraki, R., Brantley, S.L., 1995. Kinetics of near-equilibrium calcite precipitation at 100 °C: An evaluation of elementary reaction-based and affinity-based rate laws. Geochimica et Cosmochimica Acta 59 (8), 1457–1471.

Söhnel, O., Handlířová, M., 1984. Precipitation of Strontium Sulphate. Crystal Research and Technology 19 (4), 477–490.

Söhnel, O., Mullin, J.W., 1978. A method for the determination of precipitation induction periods. Journal of Crystal Growth 44 (4), 377–382.

Söhnel, O., Mullin, J.W., 1988. Interpretation of crystallization induction periods. Journal of Colloid and Interface Science 123 (1), 43–50.

Stockmann, G., Tollefsen, E., Skelton, A., Brüchert, V., Balic-Zunic, T., Langhof, J., Skogby, H., Karlsson, A., 2018. Control of a calcite inhibitor (phosphate) and temperature on ikaite precipitation in Ikka Fjord, southwest Greenland. Applied Geochemistry 89, 11–22.

Stockmann, G.J., Seaman, P., Balic-Zunic, T., Peternell, M., Sturkell, E., Liljebladh, B., Gyllencreutz, R., 2022. Mineral Changes to the Tufa Columns of Ikka Fjord, SW Greenland. Minerals 12 (11), 1430.

Strohm, S.B., Berghofer, S.A., Kaiser, C., Jordan, G., 2024. On the Ephemeral Occurrence of Ikaite in Aqueous Solutions between 0 and 20 °C. ACS Earth and Space Chemistry 8 (9), 1725–1736.

Strohm, S.B., Inckemann, S.E., Gao, K., Schweikert, M., Lemloh, M.-L., Schmahl, W.W., Jordan, G., 2022. On the nucleation of ikaite (CaCO3x6H2O) – A comparative study in the presence and absence of mineral surfaces. Chemical Geology 611, 121089.

Strohm, S.B., Saldi, G.D., Mavromatis, V., Schmahl, W.W., Jordan, G., 2023. A Study on Ikaite Growth in the Presence of Phosphate. Aquat Geochem 29 (4), 219–233.

Suess, E., Balzer, W., Hesse, K.F., Müller, P.J., Ungerer, C.A., Wefer, G., 1982. Calcium carbonate hexahydrate from organic-rich sediments of the antarctic shelf: precursors of glendonites. Science (New York, N.Y.) 216 (4550), 1128–1131.

Swainson, I.P., Hammond, R.P., 2001. Ikaite, CaCO3 ·6H2 O: Cold comfort for glendonites as paleothermometers. American Mineralogist 86 (11-12), 1530–1533.

Tadier, S., Rokidi, S., Rey, C., Combes, C., Koutsoukos, P.G., 2017. Crystal growth of aragonite in the presence of phosphate. Journal of Crystal Growth 458, 44–52.

Tang, C.C., Thompson, S.P., Parker, J.E., Lennie, A.R., Azough, F., Kato, K., 2009. The ikaite-to-vaterite transformation: new evidence from diffraction and imaging. J Appl Crystallogr 42 (2), 225–233.

Teng, H.H., Dove, P.M., De Yoreo, J.J., 2000. Kinetics of calcite growth: Surface processes and relationships to macroscopic rate laws. Geochimica et Cosmochimica Acta 64 (13), 2255–2266.

Tlili, M.M., Amor, M.B., Gabrielli, C., Joiret, S., Maurin, G., Rousseau, P., 2002. Characterization of CaCO3 hydrates by micro-Raman spectroscopy. Journal of Raman Spectroscopy 33 (1), 10–16.

Tollefsen, E., Balic-Zunic, T., Mörth, C.-M., Brüchert, V., Lee, C.C., Skelton, A., 2020. Ikaite nucleation at 35 °C challenges the use of glendonite as a paleotemperature indicator. Scientific reports 10 (1), 1–10.

Tollefsen, E., Stockmann, G., Skelton, A., Lundqvist, L., Sturkell, E., 2019. Secondary alteration of the Grønnedal-Ika igneous complex and the genesis of ikaite, CaCO3·6H2O, SW Greenland. Chemical Geology 510, 18–30.

Tollefsen, E., Stockmann, G., Skelton, A., Mörth, C.-M., Dupraz, C., Sturkell, E., 2018. Chemical controls on ikaite formation. Mineralogical Magazine 82 (5), 1119–1129.

Toschev, S., Milchev, A., Stoyanov, S., 1972. On some probabilistic aspects of the nucleation process. Journal of Crystal Growth 13-14, 123–127.

Trampe, E.C.L., Larsen, J.E.N., Glaring, M.A., Stougaard, P., Kühl, M., 2016. In situ Dynamics of O2, pH, Light, and Photosynthesis in Ikaite Tufa Columns (Ikka Fjord, Greenland)-A Unique Microbial Habitat. Frontiers in microbiology 7, 722.

van der Linden, F.C., Tison, J.-L., Champenois, W., Moreau, S., Carnat, G., Kotovitch, M., Fripiat, F., Deman, F., Roukaerts, A., Dehairs, F., Wauthy, S., Lourenço, A., Vivier, F., Haskell, T., Delille, B., 2020. Sea Ice CO2 Dynamics Across Seasons: Impact of Processes at the Interfaces. Journal of Geophysical Research: Oceans 125 (6).

van Driessche, A., Stawski, T.M., Kellermeier, M., 2019. Calcium sulfate precipitation pathways in natural and engineered environments. Chemical Geology 530, 119274.

Vekilov, P.G., 2010. Nucleation. Crystal Growth & Design 10 (12), 5007–5019.

Verdoes, D., Kashchiev, D., van Rosmalen, G.M., 1992. Determination of nucleation and growth rates from induction times in seeded and unseeded precipitation of calcium carbonate. Journal of Crystal Growth 118 (3-4), 401–413.

Vickers, M.L., Vickers, M., Rickaby, R.E., Wu, H., Bernasconi, S.M., Ullmann, C.V., Bohrmann, G., Spielhagen, R.F., Kassens, H., Pagh Schultz, B., Alwmark, C., Thibault, N., Korte, C., 2022. The ikaite to calcite transformation: Implications for palaeoclimate studies. Geochimica et Cosmochimica Acta 334, 201–216.

Wang, Z., Wang, J., Suess, E., Wang, G., Chen, C., Xiao, S., 2017. Silicified glendonites in the Ediacaran Doushantuo Formation (South China) and their potential paleoclimatic implications. Geology 45 (2), 115–118.

Zhong, S., Mucci, A., 1993. Calcite precipitation in seawater using a constant addition technique: A new overall reaction kinetic expression. Geochimica et Cosmochimica Acta 57 (7), 1409–1417.

Zou, Z., Bertinetti, L., Habraken, W.J.E.M., Fratzl, P., 2018. Reentrant phase transformation from crystalline ikaite to amorphous calcium carbonate. CrystEngComm 20 (21), 2902–2906.

Zou, Z., Habraken, W.J.E.M., Matveeva, G., Jensen, A.C.S., Bertinetti, L., Hood, M.A., Sun, C.-Y., Gilbert, P.U.P.A., Polishchuk, I., Pokroy, B., Mahamid, J., Politi, Y., Weiner, S., Werner, P., Bette, S., Dinnebier, R., Kolb, U., Zolotoyabko, E., Fratzl, P., 2019. A hydrated crystalline calcium carbonate phase: Calcium carbonate hemihydrate. Science 363 (6425), 396–400.